



UNIVERSITÄT  
BAYREUTH

# **Melt Synthesis, Structural, Characterization and Scaling of Swelling 2:1-Layer Silicate Materials**

Dissertation

zur Erlangung des akademischen Grades eines

Doktors der Naturwissenschaften (Dr. rer. nat) an der Fakultät für

Biologie, Chemie und Geowissenschaften der

Universität Bayreuth

vorgelegt von

Hussein Kalo

aus Aleppo (Syria)

Bayreuth

2012

# **Melt Synthesis, Structural, Characterization and Scaling of Swelling 2:1-Layer Silicate Materials**

Dissertation

zur Erlangung des akademischen Grades eines

Doktors der Naturwissenschaften (Dr. rer. nat) an der Fakultät für

Biologie, Chemie und Geowissenschaften der

Universität Bayreuth

vorgelegt von

Hussein Kalo

aus Aleppo (Syria)

Bayreuth

2012

Die vorliegende Arbeit wurde in der Zeit von März 2007 bis Mai 2012 in Bayreuth am Lehrstuhl Anorganische Chemie I unter Betreuung von Herrn Prof. Dr. Josef Breu angefertigt.

Vollständiger Abdruck der von der Fakultät für Biologie, Chemie und Geowissenschaften der Universität Bayreuth genehmigten Dissertation zur Erlangung des Akademischen Grades eines Doktors der Naturwissenschaften (Dr. rar. nat.).

Dissertation eingereicht am: 08.06.2012

Zulassung durch die Prüfungskommission: 09.08.2012

Wissenschaftliches Kolloquium:

Amtierende Dekanin:

Prof. Dr. Beate Lohnert

Prüfungsausschuss:

Prof. Dr. J. Breu (Erstgutachter)

Prof. Dr. J. Senker (Zweitgutachter)

Prof. Dr. H. Keppler

Prof. Dr. G. Papastavrou





*This thesis is dedicated to my parents  
for their love and endless support*

My sincere acknowledgement to my supervisor

**Professor Dr. Josef Breu**

for his guidance, encouragement and enthusiastic support during the course of this research program.

## **Acknowledgement**

This thesis is a cumulative result after years of research since joining Prof. Breu's group in 2007. I have worked with a large number of people who contributed in various ways to my research. I would like to take the chance to express my gratitude to all of them in my unassuming acknowledgment.

My grateful gratitude for the outstanding support and guidance goes to my supervisor Prof. Dr. Josef Breu. He was always a great source of motivation and guidance during my research.

I would also like to deeply thank Dr. Wolfgang Milius for his advice, scientific discussions, and supervision in single crystal refinement. My thanks goes to my previous coworkers; Michael Möller for studying the hydration behavior in the humidity chamber and for SEM images, and to Daniel Kunz for AFM imaging.

During my academic study period I was lucky to meet many people who helped me in different ways, in particular Dr. Micheal Schütz and Dr. Dunja Hirsemann. I would like to thank my colleagues in the laboratory; Matthias Stöter and Josef Hausner, and the entire ACI group.

Many thanks goes to the technical staff; Mr. Bernhard Putz who taught me how to operate the frequency furnace technology and to all other helpful people who provided different measurements and help, especially to Beate Bojer, Dieter Will, Sonja Lutschinger, and Lena Geiling.

My great appreciation goes to my professors back home at University of Aleppo; Nawzat Nabgaly, Abdalah Witte, Mohammad Abd AL-mattiy.

I want to express my gratitude to my family for the support and encouragement. I am grateful for the unending love and support I receive from my parents, my wife, my sisters and my brothers.

Finally, I would like to thank the ministry of higher education in Syria, University of Aleppo, for sponsoring my graduate studies.

<b>1. Summary – Zusammenfassung</b>	1
<b>2. Introduction.</b>	6
<b>2.1. Structure of clay minerals</b>	6
<b>2.2. Properties and characterization of swelling 2:1-layer silicate</b>	8
<b>2.3. Synthesis of swelling 2:1-layer silicate</b>	9
<b>2.4. Application of layer silicate</b>	11
<b>3. Synopsis</b>	12
<b>3.1. Motivation</b>	12
<b>3.2. Single crystal structure of hydrate sodium fluorohectorite</b>	13
<b>3.3. Large scale melt-synthesis of sodium-fluorohectorite</b>	16
<b>3.4. Synthesis of lithium-fluorohectorite</b>	19
<b>3.5. Synthesis and structure of hydrate sodium brittle mica</b>	22
<b>4. Bibliography</b>	24
<b>5. Individual contributions to joint publications</b>	28
<b>5.1. Appendix 1. Crystal structure of hydrate synthetic sodium-fluorohectorite</b>	30
<b>5.2. Appendix 2. Large scale melt-synthesis of sodium-fluorohectorite.</b>	55
<b>5.3. Appendix 3. Synthesis of lithium fluorohectorite</b>	63
<b>5.4. Appendix 4. Crystal structure of hydrate sodium brittle mica</b>	83
<b>6. Curriculum vitae</b>	104
<b>7. List of publication</b>	105
<b>8. Declaration/Erklärung</b>	107

## Summary – Zusammenfassung

### Summary

Melt synthesis, characterization, and refinement of single crystal structures of swelling 2:1-layer silicates were the main fundamental topics of the presented thesis. In particular, large scale syntheses of both lithium and sodium fluorohectorite were successfully achieved. Furthermore, the crystal structure of one-, and two-layer hydrate of sodium fluorohectorite and the one-layer hydrate of sodium brittle mica were thoroughly investigated and characterized in detail.

Swelling sodium fluorohectorite with good crystallinity in an ideal composition of  $\text{Na}_{0.85}[\text{Mg}_{2.15}\text{Li}_{0.85}]\text{Si}_4\text{O}_{10}\text{F}_2$  was synthesized for investigating the hydrated structure. Melt synthesis was done in closed molybdenum crucibles using pure reagents (glass with composition  $\text{Na}_2\text{O}-2\text{SiO}_2$ ,  $\text{Li}_2\text{SiO}_3$ ,  $\text{MgF}_2$ ,  $\text{MgO}$ ,  $\text{SiO}_2$ ). The crystal structures of one- and two-layer hydrate of sodium fluorohectorite were studied. The one-layer hydrate of sodium fluorohectorite (at relative humidity 45 %) showed two planes of interlayer sodium along [100]. The two-layer hydrate of sodium fluorohectorite showed sodium interlayer cations being located in the middle of the interlayer.

In addition, sodium brittle mica with a target composition  $\text{Na}_4[\text{Mg}_6]\text{Si}_4\text{Al}_4\text{O}_{20}\text{F}_4$  was successfully synthesized via melt synthesis in a gas tight molybdenum crucible and the refinement of the one-layer hydrate of sodium brittle mica was done. The synthetic sodium brittle mica swells only to the one-layer hydrate and could not be further hydrated to the two-layer hydrate.

Generally, natural swelling layer silicates (smectites) usually contain impurities such as iron oxide (pigmentation material), quartz, and carbonate. However, these impurities hinder the employment of swelling layer silicates in industry for cutting edge and advanced applications. In addition, they suffer from small particle size under 5  $\mu\text{m}$  limiting their aspect ratio. For industrial applications, pure synthetic swelling layer silicates with superior properties are highly desirable.

Therefore, a large scale synthesis of sodium fluorohectorite  $\text{Na}_{0.6}[\text{Mg}_{2.4}\text{Li}_{0.6}]\text{Si}_4\text{O}_{10}\text{F}_2$  was carried out in three steps. (i) *Synthesis of glass*, glass was used as precursor and low melting agent, the amorphous glass with composition  $\text{Na}_2\text{O}-\text{Li}_2\text{O}-6\text{SiO}_2$  was synthesized from sodium carbonate  $\text{Na}_2\text{CO}_3$ , lithium carbonate  $\text{Li}_2\text{CO}_3$ , and silicic acid  $\text{SiO}_2 \cdot n\text{H}_2\text{O}$  via melt synthesis in an open glassy carbon crucible at 1075 °C under flowing argon in a high frequency induction furnace, where the temperature was increased with a constant rate of 300°C/hr. (ii)

*dehydration and decarboxylation* of silicic acid  $\text{SiO}_2 \cdot n\text{H}_2\text{O}$  and magnesium basic carbonate  $\text{MgCO}_3 \cdot \text{Mg}(\text{OH})$  respectively at 900 °C for one hour in a corundum crucible in a chamber furnace. (iii) *Mixing and melting* the glass, the material obtained by dehydration and decarboxylation of  $\text{SiO}_2 \cdot n\text{H}_2\text{O}$  and  $\text{MgCO}_3 \cdot \text{Mg}(\text{OH})_2$  together with magnesium fluoride to achieve a composition of  $\text{Na}_{0.6}[\text{Mg}_{2.4}\text{Li}_{0.6}]\text{Si}_4\text{O}_{10}\text{F}_2$ . The total mixture was transferred into a glassy carbon crucible and melted at 1265 °C under argon for 15 min. The synthetic sodium fluorohectorite showed uniform and high intracrystalline reactivity, represented a pure phase, which was colorless and of good crystallinity.

High aspect ratio layer silicates would be an optimum functional material for future application in polymer layered silicate nanocomposites. Delamination via osmotic swelling is known in laponite-type clays. High hydration energy of the interlayer cation, such as lithium can force layer silicates to swell infinitely and delaminate. Consequently, the lithium fluorohectorite with variable layer charge was synthesized via melt synthesis in an open glassy carbon crucible in a high frequency induction furnace. The same procedure used for sodium fluorohectorite was applied for lithium fluorohectorite, where the glass with composition  $\text{Li}_2\text{O} \cdot 2\text{SiO}_2$  was prepared via reaction of lithium carbonate with silicic acid at 1200 °C for 1hr. Due to the high fugacity of lithium fluoride, excess of one mole Li and F was added via lithium silicate and magnesium fluoride respectively. The raw material of lithium fluorohectorite was melted at 1350 °C for 10 min.

The synthetic lithium fluorohectorite showed uniform intracrystalline reactivity, came in large well crystalline tactoids and completely delaminated to a single silicate layers in water. The lithium fluorohectorite behavior reveals that these materials have high potential for barrier application and flame retardancy. Furthermore, the lithium fluorohectorite was synthesized in large scale.

**Zusammenfassung:**

Das Ziel dieser Promotionsarbeit ist die Synthese, Charakterisierung und Kristallstrukturverfeinerung von quellfähigen Schichtsilikaten des 2:1 Typs. In diesem Zusammenhang wurden die Kristallstrukturen von Ein- und Zweischichthydraten eines Natriumfluorohectorits und des Einschichthydrats eines Sprödglimmers untersucht. Des Weiteren wurde in dieser Arbeit die erfolgreiche Synthese eines Lithium- und Natriumfluorohectorits im Großmaßstab entwickelt.

Um die Hydratstruktur von 2:1-Schichtsilikaten zu untersuchen, wurden hochkristalline quellfähige Natriumfluorohectorite synthetisiert. Die Natriumfluorohectorite der idealen Zusammensetzung  $\text{Na}_{0.85}[\text{Mg}_{2.15}\text{Li}_{0.85}]\text{Si}_4\text{O}_{10}\text{F}_2$  wurden mittels einer Schmelzsynthese in gasdichten Molybdäntiegeln unter Verwendung von hochreinen Edukten (Glas der Zusammensetzung  $\text{Na}_2\text{O}-2\text{SiO}_2$ ,  $\text{Li}_2\text{SiO}_3$ ,  $\text{MgF}_2$ ,  $\text{MgO}$ ,  $\text{SiO}_2$ ) hergestellt.

Die Kristallstruktur der Ein- und Zweischichthydrate der auf diese Weise erhaltenen Natriumfluorohectorite wurde genauer untersucht: In der Monohydratschicht des Natriumfluorohectorits, welche bei 45% relativer Luftfeuchtigkeit vorliegt, liegt das Zwischenschichtnatrium entlang [100] in zwei Ebenen auf unterschiedlicher Höhe. Dagegen ergab sich für das Zweischichtwasserhydrat im Natriumfluorohectorit nur eine Natriumposition in der Mitte der Zwischenschicht.

Zusätzlich wurde ein Sprödglimmer der Zielzusammensetzung  $\text{Na}_4[\text{Mg}_6]\text{Si}_4\text{Al}_4\text{O}_{20}\text{F}_4$  mittels einer Schmelzsynthese in gasdichten Molybdäntiegeln synthetisiert. Die Kristallstruktur des Einschichthydrates des Sprödglimmers wurde verfeinert. Der synthetische Sprödglimmer quoll nur bis zum Einschichthydrat an, eine weitere Quellung zum Zweischichthydrat war dagegen nicht möglich.

Im Allgemeinen enthalten natürliche quellfähige Schichtsilikate Verunreinigungen wie Eisenoxide, die Verfärbungen im Material verursachen, außerdem Quarz und Carbonate, welche den Einsatz von quellfähigen Schichtsilikaten für industrielle Anwendungen erschweren. Zusätzlich besitzen natürliche Schichtsilikate eine nachteilige geringe Partikelgröße von weniger als 5  $\mu\text{m}$ . Bis jetzt waren daher reine Schichtsilikate mit besseren Eigenschaften im größeren Maßstab nicht verfügbar.

Die Aufskalierung der Synthese des Natriumfluorohectorits  $\text{Na}_{0.6}[\text{Mg}_{2.4}\text{Li}_{0.6}]\text{Si}_4\text{O}_{10}\text{F}_2$  erfolgte in drei Schritten.

(i) Die Synthese von Glas. Glas wurde als niedrig schmelzende Vorstufe verwendet. Die amorphe Phase der Zusammensetzung  $\text{Na}_2\text{O-Li}_2\text{O-6SiO}_2$  wurde aus Natriumcarbonat  $\text{Na}_2\text{CO}_3$ , Lithiumcarbonat  $\text{LiCO}_3$  und Kieselsäure  $\text{SiO}_2 \cdot n\text{H}_2\text{O}$  mittels einer Schmelzsynthese in einem offenen Glaskohlenstofftiegel bei  $1075^\circ\text{C}$  unter Argonfluss in einem Hochfrequenzinduktionsofen mit einer Heizrate von  $300^\circ\text{C/h}$  durchgeführt.

(ii) Die Dehydrierung und Entkarbonisierung von Kieselsäure  $\text{SiO}_2 \cdot n\text{H}_2\text{O}$  und basischem Magnesiumcarbonat  $\text{MgCO}_3 \cdot \text{Mg}(\text{OH})_2$  erfolgte bei  $900^\circ\text{C}$  für eine Stunde in einem Korundtiegel im Kammerofen.

(III) Das Mischen und Schmelzen des Glases und des Produktes der Dehydrierung und Entkarbonisierung von  $\text{SiO}_2 \cdot n\text{H}_2\text{O}$  und  $\text{MgCO}_3 \cdot \text{Mg}(\text{OH})_2$  mit Magnesiumfluorid erfolgte als letzter Schritt, um das Schichtsilikat der Zusammensetzung  $\text{Na}_{0,6}[\text{Mg}_{2,4}\text{Li}_{0,6}]\text{Si}_4\text{O}_{10}\text{F}_2$  zu erhalten. Die gesamte Mischung wurde in einen Glaskohlenstofftiegel überführt und für 15 Minuten unter Argonfluss auf  $1265^\circ\text{C}$  erhitzt. Der auf diese Weise erhaltene synthetische Natriumfluorohectorit wies eine einheitliche und hohe interkristalline Reaktivität auf und lag als einphasiges, farbloses und hochkristallines Material vor.

Ein hohes Aspektverhältnis von quellfähigen Schichtsilikaten ist für viele zukünftige industrielle Anwendungen, z.B. bei deren Verwendung in Polymernanokompositen, von großer Bedeutung. Die für diesen Zweck erforderliche Exfolierung oder Delaminierung von Schichtsilikaten kann teilweise durch eine mechanische Einwirkung, bei der eine Scherung der Plättchen eintritt, erreicht werden. Eine interessante Alternative stellt hierzu die Delaminierung mittels osmotischer Quellung dar, wie sie z.B. für Laponit-artige Schichtsilikate bereits bekannt ist. Eine hohe Hydratationsenergie des Zwischenschichtkations, wie sie z.B. für Lithium vorliegt, kann ausgenutzt werden, um mittels der Hydratationsenthalpie eine osmotische Quellung und Delaminierung zu erreichen. Aus diesem Grund wurde ein Lithiumfluorohectorit mit variabler Schichtladung mittels einer Schmelzsynthese in einem offenen Glaskohlenstofftiegel mit einem Hochfrequenzofen hergestellt. Für die Herstellung des Lithiumfluorohectorits wurde ein Vorgehen, wie es bei der Synthese des Natriumfluorohectorits entwickelt wurde, eingesetzt. Das Glas mit der Zusammensetzung  $\text{Li}_2\text{O-2SiO}_2$  wurde aus der Reaktion von Lithiumcarbonat mit Kieselsäure bei  $1200^\circ\text{C}$  in einer einstündigen Reaktionszeit synthetisiert. Aufgrund der hohen Fugazität des Lithiumfluorids wurde ein Überschuss von einem Mol Li und einem Mol F verwendet, was durch Hinzufügen von zusätzlichem Lithium-haltigen Glases und durch Zugabe von



Magnesiumfluorid erreicht wurde. Das Ausgangsmaterial für die Fluorohectoritsynthese wurde schließlich bei 1350°C für 10min aufgeschmolzen.

Der synthetische Lithiumfluorohectorit zeigte wie erwartet eine vollständige Delaminierung der Silikatschichten in Wasser und wies eine einheitliche intrakristalline Reaktivität, eine hohe Taktoidgröße, sowie eine hohe Kristallinität auf.

Die interessanten Eigenschaften der Lithiumfluoridsuspension deuten auf ein hohes Potential für Barriereanwendungen und als Flammenschutzmittel hin. Aus diesem Grund wurde in dieser Arbeit die Herstellung des Lithiumfluorohectorits ebenfalls hochkaliert, wodurch auch dieses Material für eine industrielle Anwendung zugänglich gemacht wurde.

## 1. Introduction:

Clay has been known and used by human beings since antiquity. Indeed, clay has been employed in various applications since the very beginning of life on earth. It is used for many kinds of ceramics, such as porcelain, bricks, tiles, and sanitary ware. Clay is an essential constituent for plastics, paints, paper, rubber, and cosmetics. More recently clay-polymer nanocomposites were extensively studied and many products have been synthesized for different applications<sup>[1]</sup>.

### 2.1. Structure of clay minerals

Phyllosilicates (from the Greek “phyllon”: leaf, and from the Latin “silic”: flint) or layer silicates have two types of sheets, a tetrahedral sheet T, and an octahedral sheet M and these two sheets are connected by shared oxygen atoms. 1:1-layer silicates are formed by T-M sandwiches of one tetrahedral sheet T and one octahedral sheet M, 2:1-layer silicates are formed by T-M-T sandwiches whereas two tetrahedral sheets encompass the octahedral sheet. Figure 1 shows the general structure of a 2:1-layer silicate<sup>[1,2]</sup>.

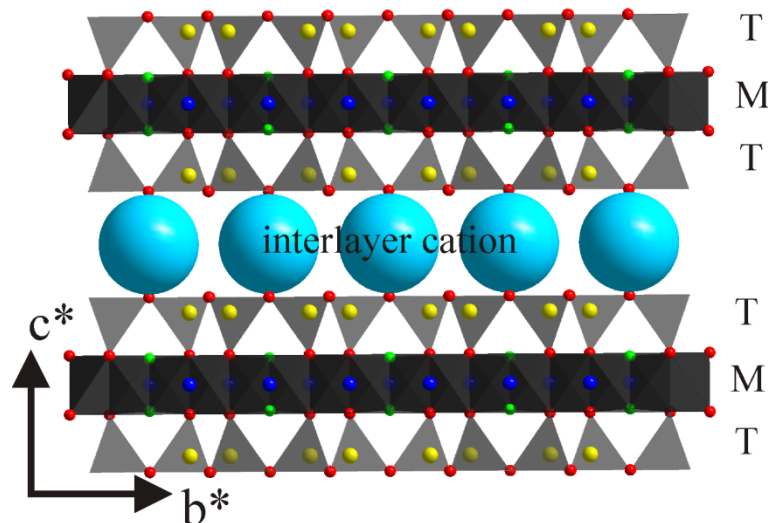


**Figure 1.** A general structure of 2:1-layer silicate

#### 2.1.1. Tetrahedral sheet

The tetrahedral sheet of layer silicates are composed of  $\text{SiO}_4^{4-}$  or  $\text{AlO}_4^{5-}$ , which are linked together by sharing three corners of the basal oxygen atoms  $\text{O}_b$ , the fourth being the apical oxygen atom  $\text{O}_a$ . Each of the basal  $\text{O}^{2-}$  connects a  $\text{Si}^{4+}$ - $\text{Si}^{4+}$  or a  $\text{Si}^{4+}$ - $\text{Al}^{3+}$  cation pair. The basal oxygen atoms form a two-dimensional lattice exhibiting hexagonal cavities as shown in Figure 2<sup>[1,2]</sup>.

### 2.1.1. Octahedral sheet

The octahedral sheet holds cations such as  $\text{Mg}^{2+}$ ,  $\text{Al}^{3+}$ ,  $\text{Ni}^{2+}$ ,  $\text{Cr}^{3+}$ ,  $\text{Fe}^{2+}$ ,  $\text{Fe}^{3+}$ ,  $\text{Cu}^{2+}$ ,  $\text{Zn}^{2+}$ ,  $\text{Ti}^{4+}$ ,  $\text{V}^{3+}$ ,  $\text{Li}^+$ ,  $\text{Co}^{2+}$ , and  $\text{Mn}^{2+}$ , where these cations are coordinated by four shared oxygen atoms, and two additional hydroxyl or fluoride groups <sup>[1]</sup>. The dimension of the unit cell depends on the type of cations in the octahedral sheet:  $\text{Al}^{3+}$  (dioctahedral 2 out of 3 octahedral sites are occupied) and  $\text{Mg}^{2+}$  (trioctahedral 3 out of 3 octahedral sites are occupied). Dioctahedral and trioctahedral layer silicate can simply be distinguished by X-ray powder diffraction, where  $d_{060} = 1.49\text{--}1.50 \text{ \AA}$  and  $d_{060} = 1.51\text{--}1.53 \text{ \AA}$  for dioctahedral and trioctahedral layer silicates, respectively <sup>[1]</sup>.

### 2.1.3 Linkage of the tetrahedral and octahedral sheets

Usually the lateral dimension of a tetrahedral sheet is larger than of an octahedral sheet, to overcome this misfit the two sheet types T and M require an adjustment in one or both sheets by the following mechanisms: (i) rotation of the tetrahedra around an axis perpendicular to the sheet with angle  $\alpha$  (ii) increasing the thickness of the tetrahedral sheet leading to a reduction of the basal area of tetrahedron (iii) flattening of the octahedral sheet <sup>[1,3,4]</sup>.

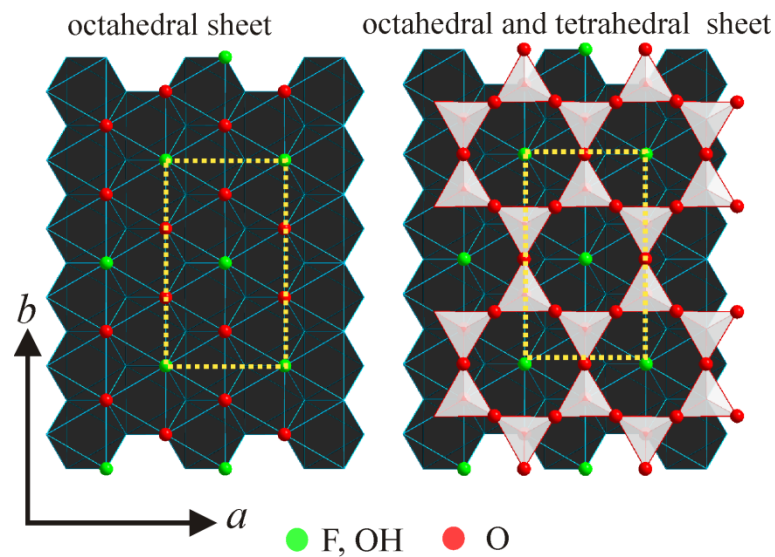


**Figure 2.** A scheme of the octahedral (trioctahedral) and tetrahedral sheet in direction  $[001]$

### 2.1.4 Interlayer cation

Due to the isomorphous substitution in the octahedral sheet and/or tetrahedral sheet a negative charge is obtained which can be balanced with interlayer cations. This charge is the one of the most important prosperities of 2:1-layer silicate type. The layer charge, in the 1:1-

layer silicate type is close to zero and varies in 2:1-layer silicates type from 0.2 in montmorillonite and hectorite to 2.0 in brittle mica per formula unit <sup>[1,4]</sup>. In Table 1 the layer charges and the ideal formulae of some types of layer silicates are presented <sup>[1]</sup>.

**Table 1.** Layer charge and the ideal formula of selected types of phyllosilicates <sup>[1]</sup>.

group name charge (per formula unit).	dioctahedral type	trioctahedral type
kaolinite – serpentine group ~ 0	kaolinite (Si <sub>2</sub> ) <sup>IV</sup> (Al <sub>2</sub> ) <sup>VI</sup> O <sub>5</sub> (OH) <sub>4</sub>	serpentine (Si <sub>2</sub> ) <sup>IV</sup> (Mg <sub>3</sub> ) <sup>VI</sup> O <sub>5</sub> (OH) <sub>4</sub>
talc-pyrophyllite group ~ 0	pyrophyllite (Si <sub>4</sub> ) <sup>IV</sup> (Al <sub>2</sub> ) <sup>VI</sup> O <sub>10</sub> (OH) <sub>2</sub>	talc (Si <sub>4</sub> ) <sup>IV</sup> (Mg <sub>3</sub> ) <sup>VI</sup> O <sub>10</sub> (OH) <sub>2</sub>
smectite group ~ 0.2-0.6	montmorillonite (Si <sub>4</sub> ) <sup>IV</sup> (Al <sub>2- y</sub> Mg <sub>y</sub> ) <sup>VI</sup> O <sub>10</sub> (OH) <sub>2</sub> , yM <sup>+</sup> ·nH <sub>2</sub> O beidellite (Si <sub>4-x</sub> Al <sub>x</sub> ) <sup>IV</sup> (Al <sub>2</sub> ) <sup>VI</sup> O <sub>10</sub> (OH) <sub>2</sub> , xM <sup>+</sup> ·nH <sub>2</sub> O	hectorite (Si <sub>4</sub> ) <sup>IV</sup> (Mg <sub>3-y</sub> Li <sub>y</sub> ) <sup>VI</sup> O <sub>10</sub> (OH) <sub>2</sub> , yM <sup>+</sup> ·nH <sub>2</sub> O saponite (Si <sub>4-x</sub> Al <sub>x</sub> ) <sup>IV</sup> (Mg <sub>3</sub> ) <sup>VI</sup> O <sub>10</sub> (OH) <sub>2</sub> , xM <sup>+</sup> ·nH <sub>2</sub> O
vermiculite group~ 0.6-0.9	vermiculite (Si <sub>4-x</sub> Al <sub>x</sub> ) <sup>IV</sup> (Al <sub>2- y</sub> Mg <sub>y</sub> ) <sup>VI</sup> O <sub>10</sub> (OH) <sub>2</sub> , (x+y)M <sup>+</sup> .	vermiculite (Si <sub>4-x</sub> Al <sub>x</sub> ) <sup>IV</sup> (Mg <sub>3-y</sub> M <sup>3+</sup> <sub>y</sub> ) <sup>VI</sup> O <sub>10</sub> (OH) <sub>2</sub> , (x-y)/2Mg <sup>2+</sup> .
true mica group ~ 0.9-1.0	muscovite (Si <sub>3</sub> Al) <sup>IV</sup> (Al <sub>2</sub> ) <sup>VI</sup> O <sub>10</sub> (OH) <sub>2</sub> , K <sup>+</sup>	phlogopite (Si <sub>3</sub> Al) <sup>IV</sup> (Mg <sub>3</sub> ) <sup>VI</sup> O <sub>10</sub> (OH) <sub>2</sub> K <sup>+</sup>

## 2.2 Swelling properties of 2:1-layer silicates

Swelling layer silicates of the 2:1 family are rigid 2-dimensional polyanions with a rich intracrystalline reactivity resulting from solvation and exchange of the interlayer cations. Depending on the water vapour pressure, the layer charge and the type of interlayer cation the 2:1-layer silicate family forms different hydration states with one-, two-, and three- or even four pseudo-layer of water molecules between silicate layers <sup>[5-8]</sup>. Whereas, the stepwise increase of the interlayer space is a characteristic of the swelling 2:1-layer silicates with interlayer cations such as sodium or lithium as shown in Figure 3.

The effect of the interlayer cation on the hydration behavior of smectites was studied by Cases et al. for alkaline-earth metals (e.g. Mg<sup>2+</sup>, Ca<sup>2+</sup>, Sr<sup>2+</sup>, and Ba<sup>2+</sup>) <sup>[9]</sup>. They observed a gradual variation of water adsorption and swelling depending on the hydration enthalpy of the cation <sup>[9]</sup>. Berend et al. have studied different alkaline metals (e.g. Li<sup>+</sup>, Na<sup>+</sup>, Rb<sup>+</sup>, and Cs<sup>+</sup>)

<sup>[10-12]</sup> as interlayer cation, where the rate of interlayer space filling increased in relation to vapour pressure.

Eric Ferrage et al. investigated the influence of layer charge and charge location on the hydration properties of smectites and they found that as the layer charge was increased, the basal spacing shifted from the two-layer hydrate to the one-layer hydrate at the same relative humidity for both montmorillonite (charge location in octahedral sheet) and beidellite (charge location in tetrahedral sheet) <sup>[13,14]</sup>.

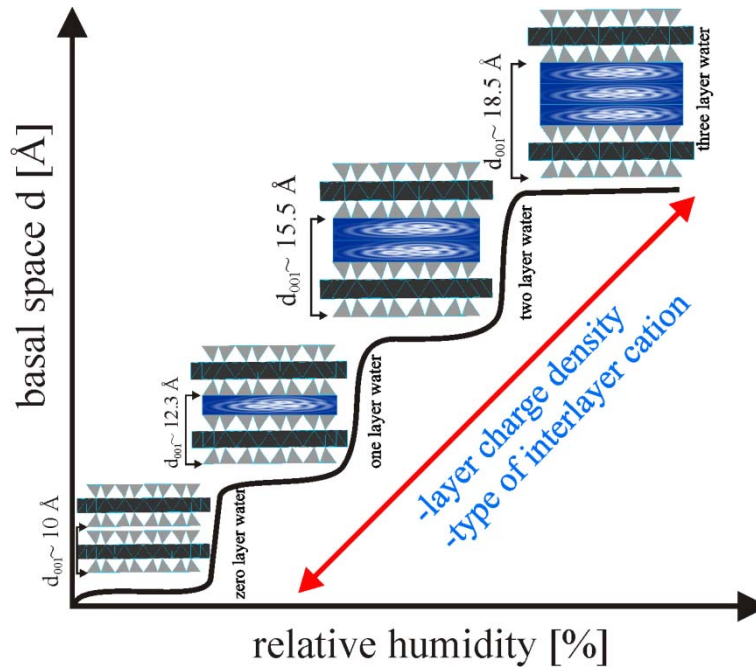


**Figure 3.** Stepwise increase of the interlayer space of 2:1-layer silicates,  $d_{001} \sim 10 \text{ \AA}$  refers to zero-hydration,  $d_{001} \sim 12.3 \text{ \AA}$  to one-layer hydrate,  $d_{001} \sim 15.5 \text{ \AA}$  to two-layer hydrate, and  $d_{001} \sim 18.5 \text{ \AA}$  to three-layer hydrate.

### 2.3. Synthesis of swelling 2:1-layer silicates

The motivation of clay synthesis is to produce highly pure material at the lowest possible temperature with remarkable properties such as homogeneity in layer charge density and high crystallinity. For preparation of synthetic clay two main paths can be used, either with a melt synthesis or by hydrothermal methods.

#### 2.3.1. Melt synthesis

The advantages of melt synthesis of layer silicates are:

- ❖ Due to substitution of  $F^-$  anions with  $OH^-$  in melt synthesis, the obtained fluoro-silicates are more stable at high temperature than hydroxi-silicates.

- ❖ Highly crystalline layer silicates can be achieved by using high temperature and slow cooling.
- ❖ The method is easier to tune for the synthesis of different layer silicates such as  $Mg^{2+}$ ,  $Fe^{2+}$ ,  $Ni^{2+}$ , and  $Co^{2+}$  rich octahedral sheets [15].
- ❖ Homogeneity in layer charge density.

Different methods are applied for the synthesis of layer silicates via the melt where the synthesis depends on the state and type of starting material such as minerals or rocks, glasses and gels. Fiore et al. has used minerals as precursor but impurities were observed in the final product. In addition, glass was used as a starting material as a source for metal and as a low flux agent [15-19].

The most used starting materials are gels, which can be prepared by one of these three methods: (i) using only organic salts like tetraethoxysilane (TEOS), tri-isopropyl aluminates, iron acetylacetonate, etc [20], (ii) using TEOS and nitrates of  $Mg^{2+}$ ,  $Al^{3+}$ , or  $Fe^{3+}$  cations and heating the gels at 800 °C for a complete dehydration [21-23], and finally (iii) using sodium meta-silicate and chloride or as sulfate anions [24]. Nevertheless, gels take longer times to dry and the dried gel show heterogeneity of the element distribution which might affect the homogeneity of the layer charge of the synthetic layer silicate.

### 2.3.2. Hydrothermal Synthesis

There are different drawbacks of using hydrothermal methods for the synthesis of layer silicates;

- ❖ Due to the hydroxyl content in synthetic layer silicates the thermal stability of is low (not more than 350 °C).
- ❖ Heterogeneity in the element distribution of the synthetic material.
- ❖ Using low temperature generates small particles
- ❖ Product suffering a high degree of stacking fault.

Commonly, the hydrothermal process requires long periods and produces a product with a small particle size [25]. For example hectorite was synthesized by Carrado et al. [26] in hydrothermal treatment using silica sol, magnesium hydroxide sol, and lithium fluoride. The mixture was treated under reflux for 2 days and the product had a maximum particle size of 1-2  $\mu m$ .

## 2.4. Application of layer silicates

Layer silicate materials are extensively used in different industrial applications such as: polymer fillers <sup>[27]</sup>, catalysis, ceramics, refractory bricks, paper, paint, in agriculture, and sensors <sup>[28]</sup>. Table 2 shows some applications of different layer silicates.

**Table. 2** Selected applications of layer silicates in industry

Layer silicates type	Industry	Use
mica	electrical industry	insulation
	paint	UV-, heat-stable, and under-water paint
vermiculite	building industry	heat insulation, sound dissipation
	packaging industry	shock proof materials, thermal protection
smectite	agriculture	soil improvement
	building industry	antifriction agents for pipe jacking and shaft sinking additions to concrete and mortar
kaolinite	paper, plastics, rubber	filler
talc	paper, plastics, rubber	filler

### 3. Synopsis

#### 3.1 Motivation

The hydrates of 2:1-layer silicates are widely employed and studied. When the structure of this type of materials was investigated typically natural clay minerals such as vermiculite were used. Studies on the one-layer hydrate demonstrated that the location of the interlayer cation is close to a one-side of the tetrahedral sheet. Other records claimed to show that the interlayer sodium cations are located in the middle of the interlayer in case of one-layer hydrate. Nevertheless, the crystal structure of one-, and two-layer of hydrate sodium fluorohectorite is still not well determined using complete single crystal X-ray diffraction data. Figuring out the hydrate structure can, however, help finding more advanced applications of swelling sodium fluorohectorite.

Additionally, sodium brittle mica with the ideal composition  $\text{Na}_4[\text{Mg}_6]\text{Si}_4\text{Al}_4\text{O}_{20}(\text{OH},\text{F})_4$  shows a swelling behavior although it has high layer charge (4 negative charge per formula unit). Recently sodium brittle mica has drawn attention of scientists due to its high cation exchange capacity (CEC). Most of previous publications concerning the synthesis of sodium brittle mica reported a synthesis procedure which produces different types of sodium brittle mica (different layer charge) and small particle size. However, the crystal structure of the one-layer hydrate of sodium brittle mica is still not well defined and an efficient synthesis procedure needs to be established.

The preparation of synthetic 2:1-layer silicates in a melt procedure produces well defined clay with much enhanced properties such as:(i) homogeneity of chemical composition and layer charge density (ii) colorless (iii) high aspect ratio (iv) large particles sizes (v) highly pure material (vi) uniform intracrystalline reactivity. The variation of interlayer chemistry gives a broad range of possible functionalizations and exfoliation via osmotic swelling. The exfoliation of layer silicates by osmotic swelling or external mechanical shear stress produces nano-platelets with extremely large aspect ratios which may be used in different applications<sup>[29,30]</sup>.

For industrial applications an economically and scalable method is highly desirable without having to accept any compromises in the final materials properties regarding aspect ratios and homogeneity of charge density. Designing a melt synthesis process of swelling 2:1-layer silicates of  $\text{Na}_{0.6}[\text{Mg}_{2.4}\text{Li}_{0.6}]\text{Si}_4\text{O}_{10}\text{F}_2$ , and lithium fluorohectorite with a perfectly uniform distribution of isomorphous substitution in an unsealed container was not previously reported.



### 3.2. Single crystal structure of hydrate of sodium fluorohectorite

Swelling probably is the most important feature of expandable 2:1-layer silicates. The dominant driving force for water uptake is the hydration enthalpy of interlayer cations that of course varies with charge density and type of interlayer cation. For true solid solution type clays where the charge density is homogenous the intercalation occurs in well defined steps as a function of water activity<sup>[31-34]</sup>. The hydrate structures of 2:1-layer silicates were studied applying different methods such as NMR spectroscopy, neutron scattering, X-ray diffraction, and computer simulation<sup>[35-38]</sup>. The computer simulation was applied to understand the hydration geometry and location of the interlayer cation in respect to the lower and upper tetrahedral sheet<sup>[10,39,39-42]</sup>. However, there is a limited number of “single crystal” refinements of hydrated phases available in the literature applying some rare occasions of semi-ordered vermiculites (Santa Olalla, Spain and Carl Moss Ranch, Llano County, Texas)<sup>[36,43]</sup>.

In order to study the structure of hydrate fluorohectorite,  $\text{Na}_{0.85}[\text{Mg}_{2.15}\text{Li}_{0.85}]\text{Si}_4\text{O}_{10}\text{F}_2$  was synthesized. The synthesis was done as described elsewhere by Breu et al.<sup>[44]</sup>, only the starting materials was changed, instead of LiF and NaF the lithium metasilicate ( $\text{Li}_2\text{SiO}_3$ ) and sodium orthosilicate ( $\text{Na}_2\text{O}\cdot 2\text{SiO}_2$ ) (glass) were used. The synthetic sodium fluorohectorite was characterized via powder X-ray diffraction PXRD, wavelength dispersive X-ray WDX and inductively coupled plasma atomic emission spectroscopy ICP-AES. The synthetic sodium fluorohectorite showed a pure phase and high crystallinity, uniform intracrystalline reactivity whereas the 001 peak of the one-layer hydrate of sodium fluorohectorite at 12.5 Å was observed as shown in Figure 4.

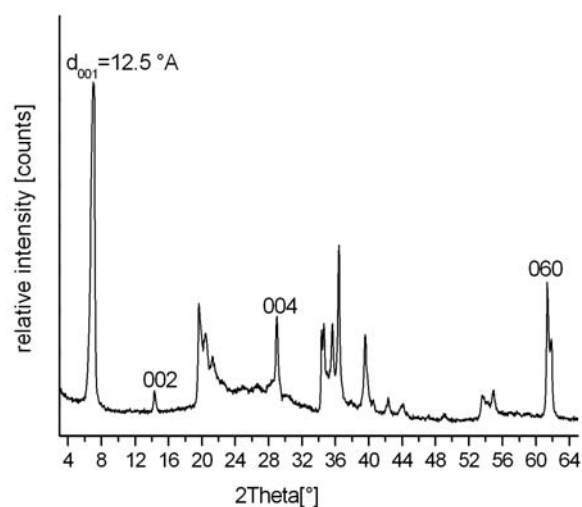


**Figure 4.** Powder X-ray diffraction pattern of one-layer hydrate of synthetic sodium fluorohectorite

Surprisingly, the PXRD of two-layer hydrate of synthetic sodium fluorohectorite showed features indicating ordered stacking, the 02 $l$  and 11 $l$  peaks observed were relatively sharp (Figure 5).

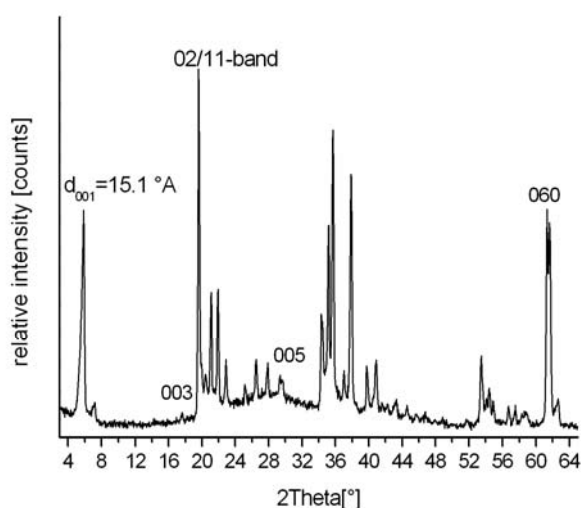


**Figure 5.** Powder X-ray diffraction pattern of the two-layer hydrate of synthetic sodium fluorohectorite

The single crystal structure refinement of the one-layer hydrate of synthetic sodium fluorohectorite showed two planes of interlayer cations (sodium) along the [100] (Figure 6A). The sodium interlayer cations are located approximately above the centre of hexagonal cavity

at the m3 site. In the case of two-layer hydrate the sodium is located in the middle of interlayer (Figure 6B). The observed distance between the oxygen of water and the basal oxygen atoms of the tetrahedral sheet was 2.90 -3.03Å Figure 7.

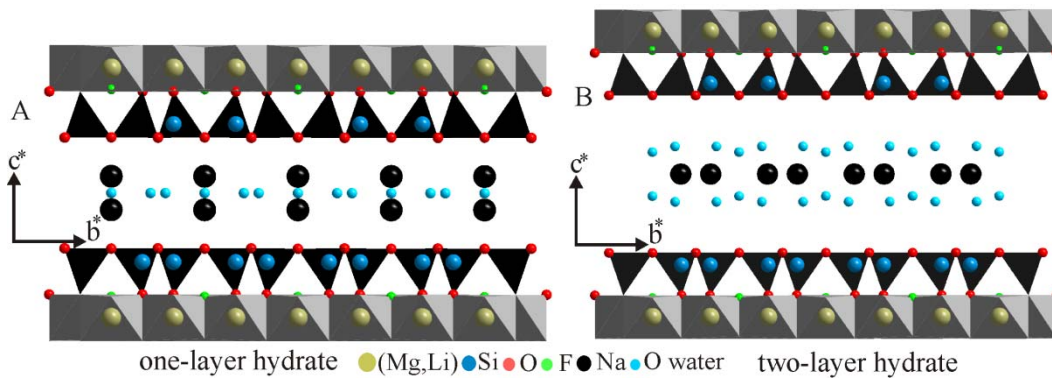


**Figure 6.** Structure of one-, and two-layer hydrate of sodium fluorohectorite projected along [100] indicating in particular the location of interlayer cations

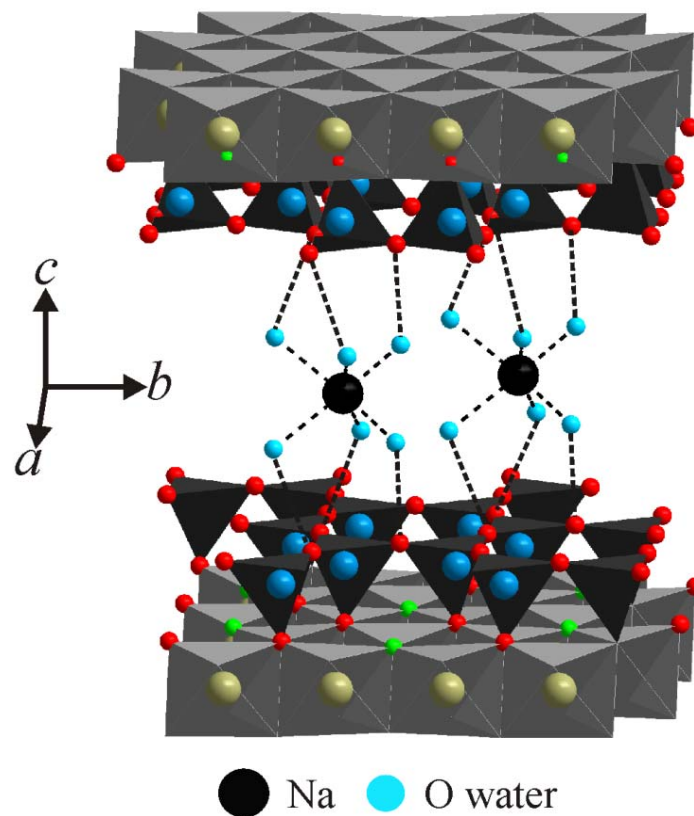


**Figure 7.** The structure of two-layer hydrate of synthetic sodium fluorohectorite present the hydrogen bonding between interlayer sodium water complex and the tetrahedral sheets fixing the stacking order.

#### Details and further discussion:

Appendix 1: Crystal structure of the hydrate of synthetic sodium-fluorohectorite.

### 3.3. Large scale melt-synthesis of sodium fluorohectorite

For the purpose of synthesizing a 2:1-layer silicate with an ideal formula  $\text{Na}_{0.6}[\text{Mg}_{2.4}\text{Li}_{0.6}]\text{Si}_4\text{O}_{10}\text{F}_2$  in a scalable commercially interesting way, melt synthesis was carried out in an open glassy carbon crucible. The synthesis procedure afforded three steps; (i) synthesis of glass with composition  $\text{Na}_2\text{O}-\text{Li}_2\text{O}-6\text{SiO}_2$  at  $1075\text{ }^\circ\text{C}$  (ii) decarboxylation and dehydration of  $\text{MgCO}_3 \cdot \text{Mg}(\text{OH})_2 \cdot x\text{H}_2\text{O}$  and silicic acid hydrate,  $\text{SiO}_2 \cdot x\text{H}_2\text{O}$  with a molar ratio of  $\text{MgO}/\text{SiO}_2 = 1.4/2.2$  (iii) mixing, grinding, and melting of 0.3 mole of the synthetic glass with  $\text{MgO}/\text{SiO}_2 = 1.4/2.2$  and 1 mole of magnesium fluoride in an open glassy carbon crucible at  $1265\text{ }^\circ\text{C}$  for 15 min. The synthesis equipment (Figure 8), including the crucible, the cooling system of the furnace, and the coil of the high frequency furnace, was developed to reproduce the materials at low cost.

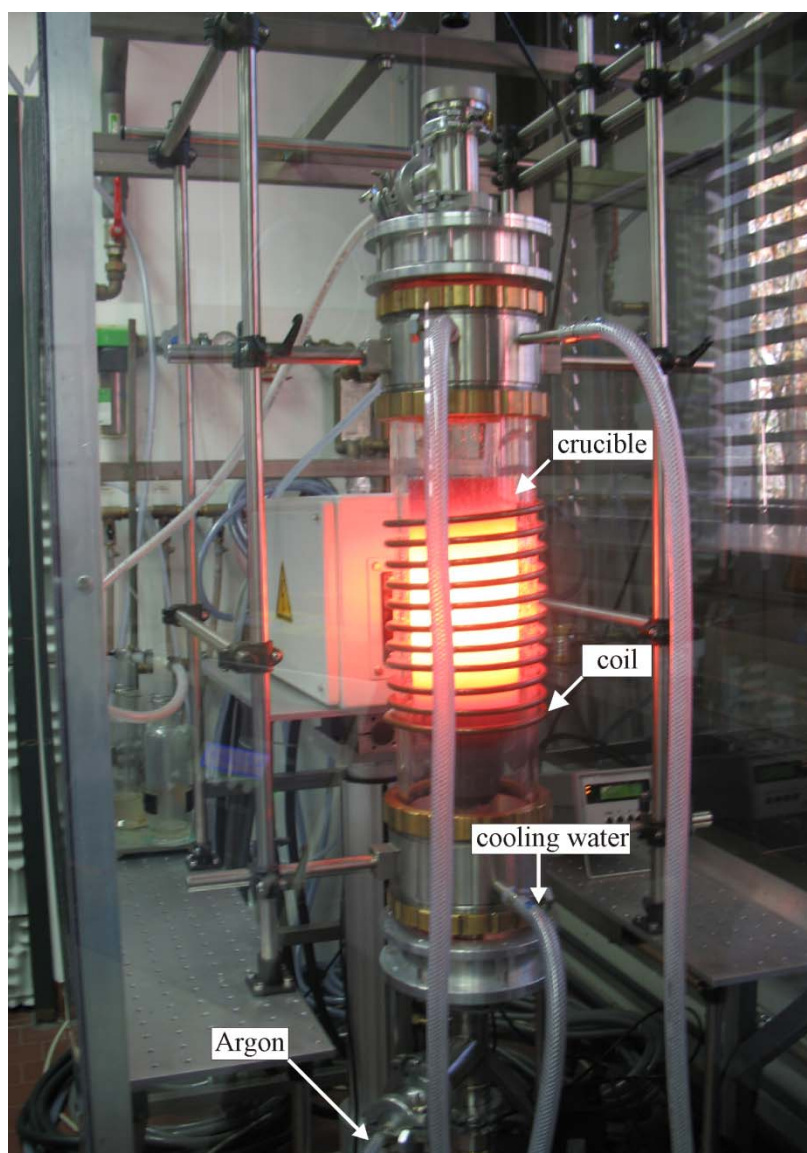


**Figure 8.** The furnace used for scaling the synthesis of the sodium fluorohectorite.

The powder X-ray diffraction of synthetic sodium fluorohectorite (Figure 9) showed uniform intracrystalline reactivity, the basal spacing at relative humidity 30 % was  $d_{001}=12.3 \text{ \AA}$ .

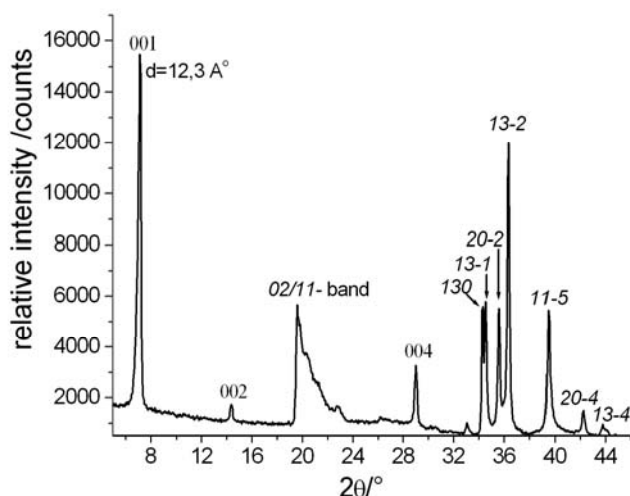


**Figure 9.** PXRD pattern of synthetic  $\text{Na}_{0.6}[\text{Mg}_{2.4}\text{Li}_{0.6}]\text{Si}_4\text{O}_{10}\text{F}_2$  (one layer hydrate,  $d_{001} = 12.3 \text{ \AA}$ ).

The sodium fluorohectorite with layer charge of 0.6 (per half formula unit) obtained, stands out for (i) phase purity as checked by X-ray powder diffraction (PXRD), (ii) a superb homogeneity of the charge density as demonstrated by the stepwise hydration behavior followed by in-situ PXRD in a humidity chamber and the Lagaly method with alkylammonium exchange <sup>[45]</sup>, (iii) a high cation exchange capacity (CEC) of 136 meq/100g as determined by the copper complex ( $[\text{Cu}(\text{trien})]^{2+}$ ) method, and finally (iv) extremely large lateral extensions with a median value of the particle size of 45  $\mu\text{m}$  as measured by static light scattering (SLS) which was confirmed by scanning electron microscopy (SEM) Figure 10.

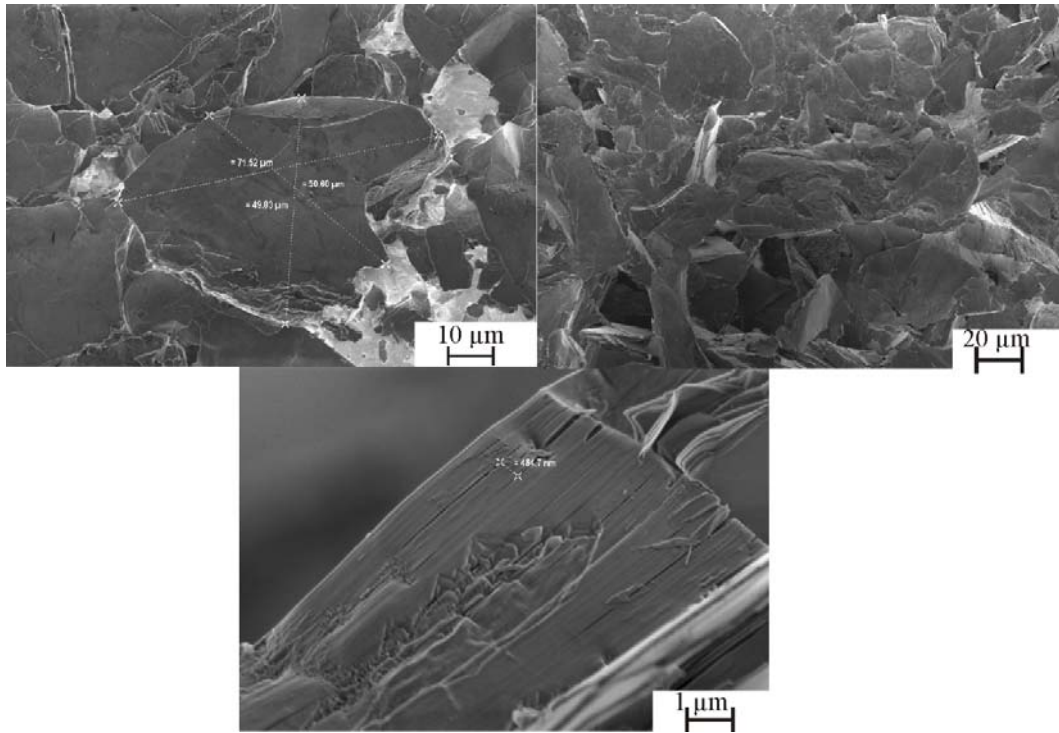


**Figure 10.** SEM images of sodium fluorohectorite with layer charge 0.6 (per formula unit) as obtained by melt synthesis

**Details and further discussion:**

Appendix 2: Large scale melt-synthesis of sodium-fluorohectorite.

### 3.4. Synthesis of lithium fluorohectorite

Previous publications have already investigated the synthesis of lithium fluorohectorite  $\text{Li}_x[\text{Mg}_{2-x}\text{Li}_x]\text{Si}_4\text{O}_{10}\text{F}_2$  (Li-hect<sub>x</sub>). Nevertheless, confirming the lithium cation as interlayer cation in the synthetic layer silicates is tricky and difficult due to many reasons including: (i) the small cationic radius of the lithium for the interlayer (ii) a phase separation in the system  $\text{MgO-Li}_2\text{O-SiO}_2$ , and (iii) fugacity of lithium compounds (using an open crucible) [46,47]. In this approach a direct melt-synthesis method was employed for the synthesis of variable layer charges of Li-hect<sub>x</sub> in the range between 0.4 to 1.0 per formula unit.

The synthesis procedure was done as described in the synthesis of sodium fluorohectorite, changing only the starting glass compositions (glass with composition  $\text{Li}_2\text{O-2SiO}_2$ ). In addition 1 mole of lithium fluoride was added to the raw material of Li-hect<sub>x</sub> in the form of lithium silicate and magnesium fluoride. The synthesis of Li-hect<sub>x</sub> ( $x= 0.4, 0.6, 0.8, 1.0$ ) was achieved at 1350 °C with a dwelling time of 10 min in an open glassy carbon crucible. The lithium fluorohectorite ( $\text{Li}_x[\text{Mg}_{2-x}\text{Li}_x]\text{Si}_4\text{O}_{10}\text{F}_2$   $x=1.0$ ) was synthesized in a large scale (1 kg).

Depending on the composition of Li-hect<sub>x</sub> the synthetic Li-hect<sub>x</sub> had considerable impurities. Less impurity were obtained in the case of high layer charges of Li-hect<sub>x</sub>. The hydration behavior of Li-hect<sub>1.0</sub> showed stepwise increasing of the basal space by increasing the relative humidity as shown in PXRD pattern in Figure 11.

By increasing the layer charge of synthetic Li-hect<sub>x</sub> we could achieve interesting features:

- ❖ Larger particle sizes.
- ❖ Higher CEC value.
- ❖ Less impurity as side product.



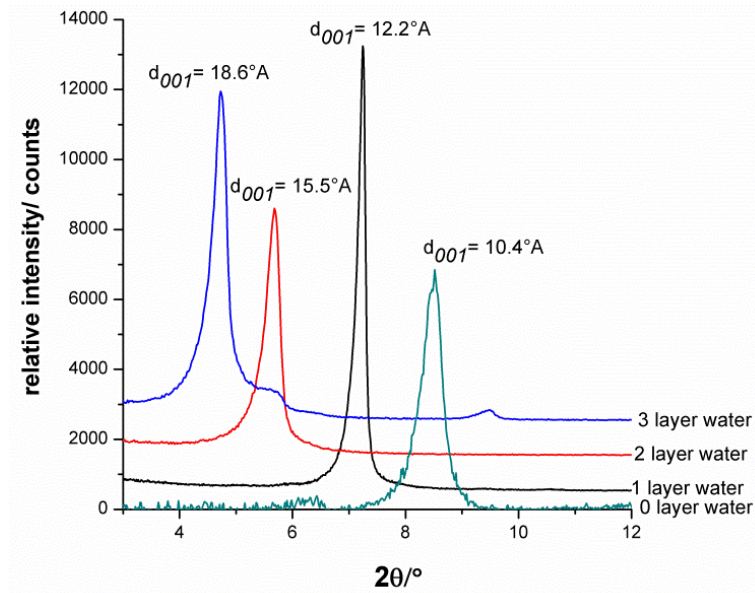


**Figure 11.** Stepwise increase of  $d_{001}$  of Li-hect<sub>1.0</sub> measured at certain relative humidity.

Figure 12 shows the PXRD pattern of Li-hect<sub>1.0</sub> suspensions. By increasing the water content the 00 $l$  peak shifted to low  $2\theta$  angle (higher  $d$  value). The  $d_{00l}$  series of Li-hect<sub>1.0</sub> suspension with a ratio of water/Li-hect<sub>x</sub> (H<sub>2</sub>O:Li-hect<sub>1.0</sub>) of (3:1) was found to be well defined ( $d_{001}$ = 70.1 Å,  $d_{002}$ = 35.2 Å, and  $d_{003}$  = 23.8 Å), in the state of H<sub>2</sub>O/Li-hect<sub>1.0</sub> ratio (5:1) the 001 peak cannot be observed, only the 002 peak can be observed at  $d_{002}$ =44 Å. By increasing water/Li-hect<sub>1.0</sub> ratio up to (10:1) we can achieve a completely delaminated state.

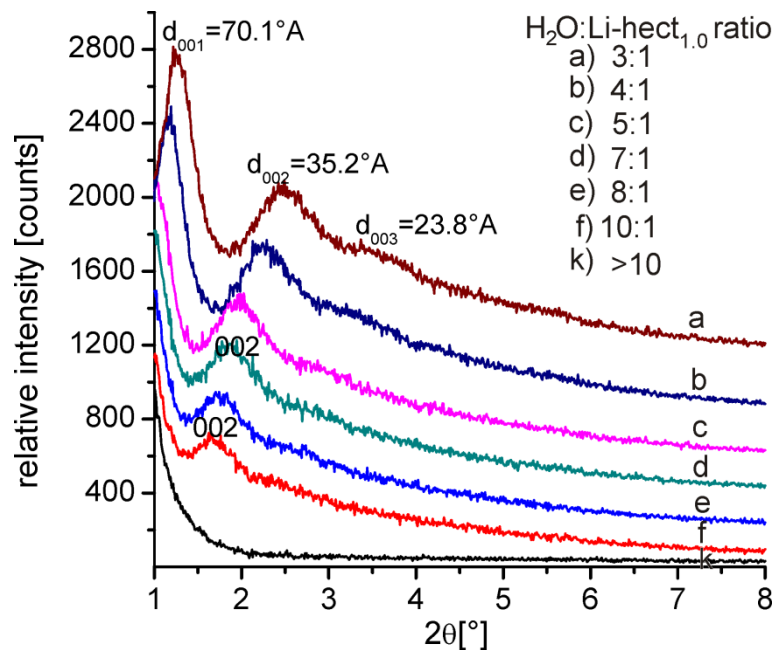


**Figure 12.** PXRD patterns of Li-hect<sub>1.0</sub> at different water: Li-hect<sub>1.0</sub> weight ratios.



Conformation of delamination can be obtained from AFM imaging as shown in Figure 13. The broad 001 peaks observed may be due various amounts of water inserting in different interlayers sequentially stacked. The low intensity of the 001 peak can be explained the thin tactoids of  $\text{Li-heckt}_{1.0}$  suspension caused by the hydration force of lithium interlayer cation.

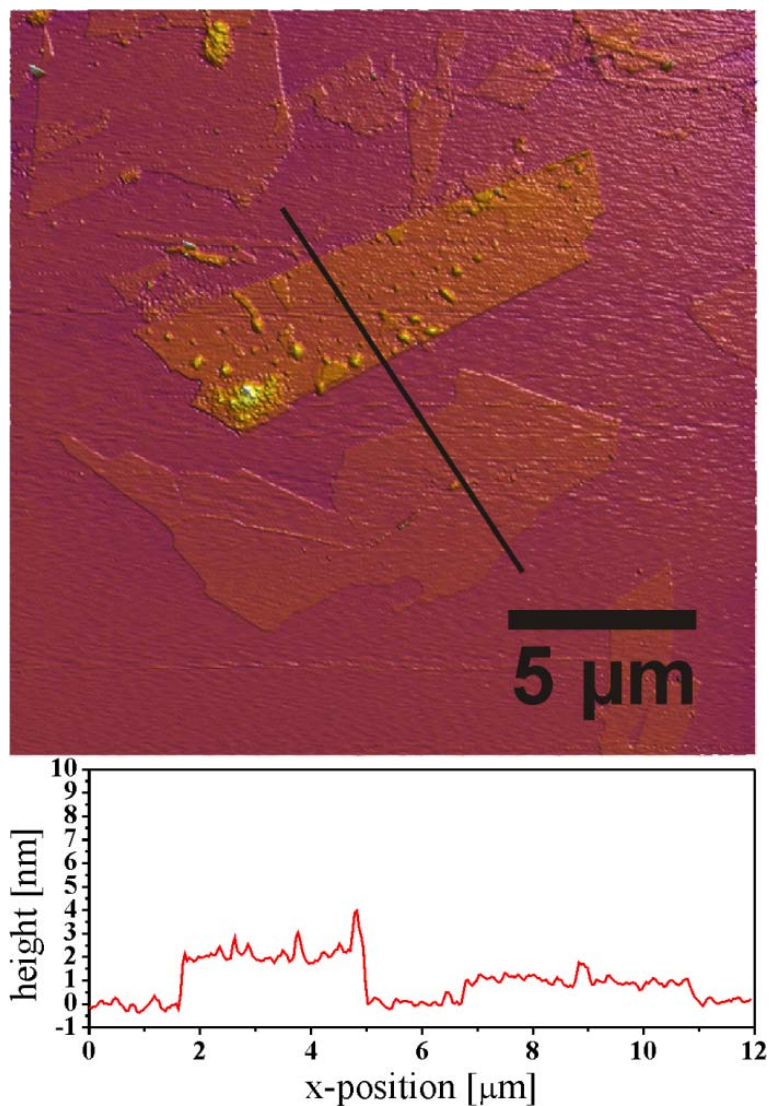


**Figure 13.** AFM image (20 X 20 μm) of synthetic  $\text{Li-heckt}_{1.0}$  viewing one- and two-layer layer silicates

**Details and further discussion:**

Appendix 3: Synthesis of lithium fluorohectorite.

### 3.5. Synthesis and structure of hydrate sodium brittle mica

Sodium brittle mica with an ideal composition  $\text{Na}_4[\text{Mg}_6]\text{Si}_4\text{Al}_4\text{O}_{20}\text{F}_4$  (4 negative charges per unit cell) shows swelling behavior and high cation exchange capacity (CEC). Recently many literature reports have described the synthesis procedure of sodium brittle mica for cation exchange applications, as the sodium brittle mica has a high theoretical CEC of 468 meq/100g<sup>[48-50]</sup>. However, those synthesis procedures yielded a material with small particle size and high impurities, even after washing with water<sup>[50]</sup>. Moreover, the crystal structure of brittle mica and one-layer hydrate brittle mica are still not well determined.

Sodium brittle mica with ideal composition  $\text{Na}_4[\text{Mg}_6]\text{Si}_4\text{Al}_4\text{O}_{20}\text{F}_4$  was synthesized in gas tight molybdenum crucible at 1750 °C<sup>[49-54]</sup>. The synthetic sodium brittle mica was characterized by means of PXRD, wavelength dispersive X-ray WDX and inductively coupled plasma atomic emission spectroscopy ICP-AES. Additionally, the crystal structure of the one-layer hydrate of sodium brittle mica was investigated. The synthesis was optimized to yield large particle sizes suitable for studying single crystals. Magnesium silicate  $\text{Mg}_2\text{SiO}_4$ <sup>[55]</sup> and sodium aluminum silicate  $\text{Na}_6\text{Al}_4\text{Si}_4\text{O}_{17}$ <sup>[56]</sup> can be identified in the PXRD pattern as side-products (Figure 14).

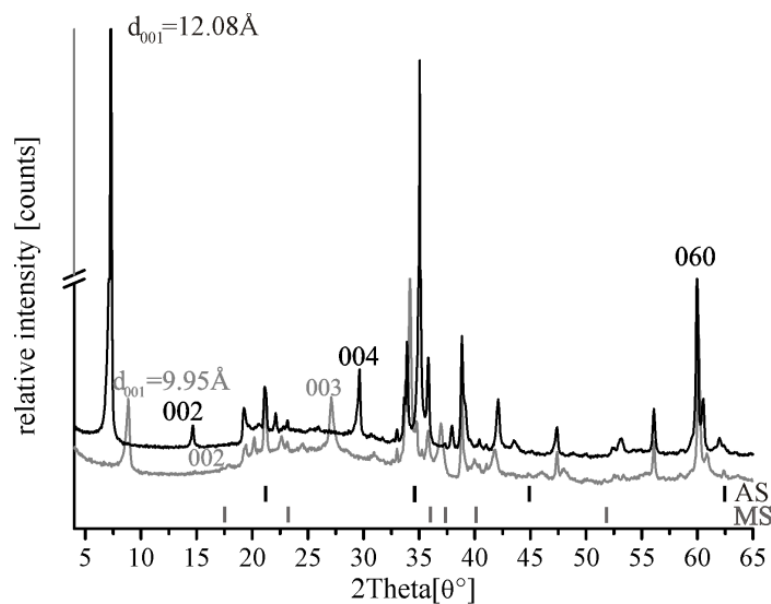


**Figure 14.** PXRD of zero-, and one-layer hydrate of sodium brittle mica. The one-layer hydrate was measured at 43% relative humidity. AS: Sodium aluminum silicate

$\text{Na}_6\text{Al}_4\text{Si}_4\text{O}_{17}$ , MS: Magnesium silicate  $\text{Mg}_2\text{SiO}_4$  (see text).

The structure of one-layer hydrate sodium brittle mica was determined and the refined structure is presented in Figure 15. The crystals are systematic six-fold twins; the three main domains are accumulated in projection [001] and the other three domains occur in projection [010] for each main domain.

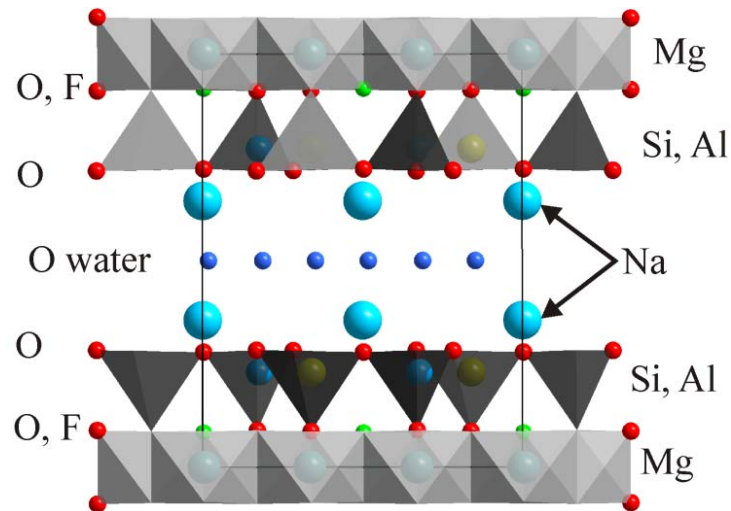


**Figure 15.** The structure of one-layer hydrate of synthetic sodium brittle mica along [100].

**Details and further discussion:**

Appendix 4: Crystal structure of hydrate sodium brittle mica.

---

#### 4. Bibliography

- [1] F. Bergaya, G. Lagaly, General Introduction: Clays, Clay Minerals, and Clay science, in *Handbook of Clay Science, Vol. 1* (Eds.: F. Bergaya, B.K.G. Theng, G. Lagaly), Elsevier, Amsterdam 2006.
- [2] J. Breu, W. Seidl, A. Stoll, Disorder in smectites in dependence of the interlayer cation, *Zeitschrift Fur Anorganische Und Allgemeine Chemie* 2003, 629, 503-515.
- [3] D. M. Moore, R. C. Reynolds, *X-Ray Diffraction and the Identification and Analysis of Clay Minerals*, Oxford University Press, Oxford 1997.
- [4] M. F. Brigatti, S. Guggenheim, Mica Crystal Chemistry and the Influence of Pressure, Temperature, and Solid Solution on Atomistic Models, *Reviews in Mineralogy and Geochemistry* 2002, 46, 1-97.
- [5] L. J. Michot, I. Bihannic, M. Pelletier, E. Rinnert, J. L. Robert, Hydration and swelling of synthetic Na-saponites: Influence of layer charge, *American Mineralogist* 2005, 90, 166-172.
- [6] P. Komadel, J. Hrobarikova, L. Smrcok, B. Koppelhuber-Bitschnau, Hydration of reduced-charge montmorillonite, *Clay Minerals* 2002, 37, 543-550.
- [7] D. Divakar, D. Manikandan, G. Kalidoss, T. Sivakumar, Hydrogenation of benzaldehyde over palladium intercalated bentonite catalysts: Kinetic studies, *Catalysis Letters* 2008, 125, 277-282.
- [8] R. P. Tenorio, M. Engelsberg, J. O. Fossum, G. J. da Silva, Intercalated Water in Synthetic Fluorhectorite Clay, *Langmuir* 2010, 26, 9703-9709.
- [9] J. M. Cases, I. Berend, M. Francois, J. P. Uriot, L. J. Michot, F. Thomas, Mechanism of adsorption and desorption of water vapor by homoionic montmorillonite .3. The  $Mg^{2+}$ ,  $Ca^{2+}$ ,  $Sr^{2+}$  and  $Ba^{2+}$  exchanged forms, *Clays and Clay Minerals* 1997, 45, 8-22.
- [10] E. S. Boek, P. V. Coveney, N. T. Skipper, Monte Carlo molecular modeling studies of hydrated Li-, Na-, and K-smectites: Understanding the role of potassium as a clay swelling inhibitor, *Journal of the American Chemical Society* 1995, 117, 12608-12617.
- [11] J. Fripiat, J. Cases, M. Francois, M. Letellier, Thermodynamic and Microdynamic Behavior of Water in Clay Suspensions and Gels, *Journal of Colloid And Interface Science* 1982, 89, 378-400.
- [12] I. Berend, J. M. Cases, M. Francois, J. P. Uriot, L. Michot, A. Masion, F. Thomas, Mechanism of Adsorption and Desorption of Water-Vapor by Homoionic Montmorillonites 2. the  $Li^+$ ,  $Na^+$ ,  $K^+$ ,  $Rb^+$  and  $Cs^+$ -Exchanged Forms, *Clays and Clay Minerals* 1995, 43, 324-336.
- [13] E. Ferrage, C. A. Kirk, G. Cressey, J. Cuadros, Dehydration of Ca-montmorillonite at the crystal scale. Part I: Structure evolution, *American Mineralogist* 2007, 92, 994-1006.
- [14] E. Ferrage, B. Lanson, B. A. Sakharov, N. Geoffroy, E. Jacquot, V. A. Drits, Investigation of dioctahedral smectite hydration properties by modeling of X-ray diffraction profiles: Influence of layer charge and charge location, *American Mineralogist* 2007, 92, 1731-1743.
- [15] Alexander, Baumgartner, Synthese, Charakterisierung und Modifizierung von Übergangsmetallhaltigen Schichtsilicaten, PhD thesis, University of Bayreuth, 2008.

- 
- [16] K. Kitajima, N. Daimon, Synthesis and Swelling Characteristics of Li-Taeniolite, *Nippon Kagaku Kaishi* 1975, 1168-1174.
- [17] K. Kitajima, Y. Shinomiya, N. Takusagawa, Synthesis and Swelling of Sr-Fluorine Micas, *Chemistry Letters* 1984, 1473-1476.
- [18] K. Kitajima, F. Koyama, N. Takusagawa, Synthesis and Swelling Properties of Fluorine Micas with Variable Layer Charges, *The Chemical Society of Japan, Bulletin* 1985, 58, 1325-1326.
- [19] S. Fiore, F. J. Huertas, F. Huertas, J. Linares, Smectite formation in rhyolitic obsidian as inferred by microscopic (SEM-TEM-AEM) investigation, *Clay Minerals* 2001, 36, 489-500.
- [20] C. R. Dekimpe, H. Kodama, R. Rivard, Hydrothermal Formation of A Kaolinite-Like Product from Noncrystalline Aluminosilicate Gels, *Clays and Clay Minerals* 1981, 29, 446-450.
- [21] A. Decarreau, D. Bonnin, D. Badautrauth, R. Couty, P. Kaiser, Synthesis and Crystallogensis of Ferric Smectite by Evolution of Si-Fe Coprecipitates in Oxidizing Conditions, *Clay Minerals* 1987, 22, 207-223.
- [22] J. T. Klopogge, L. V. Duong, R. L. Frost, A review of the synthesis and characterisation of pillared clays and related porous materials for cracking of vegetable oils to produce biofuels, *Environmental Geology* 2005, 47, 967-981.
- [23] J. T. Klopogge, R. Vogels, Hydrothermal Synthesis of Ammonium-Beidellite, *Clays and Clay Minerals* 1995, 43, 135-137.
- [24] A. Decarreau, O. Grauby, S. Petit, The actual distribution of octahedral cations in 2:1 clay minerals: Results from clay synthesis, *Applied Clay Science* 1992, 7, 147-167.
- [25] F. Bergaya, K. G. T. Benny, G. Lagaly, *Handbook of Clay Science, Developments in Clay Science*, Elsevier, Amsterdam 2006.
- [26] K. A. Carrado, L. Xu, D. M. Gregory, K. Song, S. Seifert, R. E. Botto, Crystallization of a layer silicate clay as monitored by small-angle X-ray scattering and NMR, *Chemistry of Materials* 2000, 12, 3052-3059.
- [27] L. A. Utracki, M. Sepehr, E. Boccaleri, Synthetic, layer nanoparticles for polymeric nanocomposites WNCO, *Polymers for Advanced Technologies* 2007, 18, 1-37.
- [28] C.C.Harvey, G.Lagaly, Conevtional Application , in *Handbook of Clay Sceince, Vol. 1* (Eds.: F.Bergaya, B.K.G.Theng, G.Lagaly), Elsevier, Amsterdam 2006.
- [29] A. Baumgartner, K. Sattler, J. Thun, J. Brey, A route to microporous materials through oxidative pillaring of micas, *Angewandte Chemie-International Edition In English* 2008, 47, 1640-1644.
- [30] I. Dekany, L. Turi, Z. Kiraly, CdS, TiO<sub>2</sub> and Pd-circle nanoparticles growing in the interlamellar space of montmorillonite in binary liquids, *Applied Clay Science* 1999, 15, 221-239.
- [31] N. Malikova, E. Dubois, V. Marry, B. Rotenberg, P. Turq, Dynamics in Clays - Combining Neutron Scattering and Microscopic Simulation, *Zeitschrift fur Physikalische Chemie-International Journal of Research in Physical Chemistry & Chemical Physics* 2010, 224, 153-181.

- 
- [32] M. W. Möller, U. A. Handge, D. A. Kunz, T. Lunkenbein, V. Altstadt, J. Breu, Tailoring Shear-Stiff, Mica-like Nanoplatelets, *Acs Nano* 2010, 4, 717-724.
- [33] T. J. Tambach, P. G. Bolhuis, E. J. M. Hensen, B. Smit, Hysteresis in clay swelling induced by hydrogen bonding: Accurate prediction of swelling states, *Langmuir* 2006, 22, 1223-1234.
- [34] E. Ferrage, B. Lanson, N. Malikova, A. Plancon, B. A. Sakharov, V. A. Drits, New insights on the distribution of interlayer water in bi-hydrated smectite from X-ray diffraction profile modeling of 00l reflections, *Chemistry Of Materials* 2005, 17, 3499-3512.
- [35] P. G. Slade, P. A. Stone, E. W. Radoslovich, Interlayer structures of the two-layer hydrates of Na- and Ca-vermiculites, *Clays and Clay Minerals* 1985, 33, 51-61.
- [36] H. Shirozu, S. W. Bailey, Crystal Structure of A 2-Layer Mg-Vermiculite, *American Mineralogist* 1966, 51, 1124-1143.
- [37] N. T. Skipper, A. K. Soper, J. D. C. McConnell, The Structure of Interlayer Water in Vermiculite, *Journal of Chemical Physics* 1991, 94, 5751-5760.
- [38] N. T. Skipper, A. K. Soper, M. V. Smalley, Neutron-Diffraction Study of Calcium Vermiculite - Hydration of Calcium-Ions in A Confined Environment, *Journal of Physical Chemistry* 1994, 98, 942-945.
- [39] N. T. Skipper, K. Refson, J. D. C. McConnell, Computer-Simulation of Interlayer Water in 2-1 Clays, *Journal of Chemical Physics* 1991, 94, 7434-7445.
- [40] N. T. Skipper, F. R. C. Chang, G. Sposito, Monte-Carlo Simulation of Interlayer Molecular-Structure in Swelling Clay-Minerals .1. Methodology, *Clays Clay Miner.* 1995, 43, 285-293.
- [41] F. R. C. Chang, N. T. Skipper, G. Sposito, Computer-Simulation of Interlayer Molecular-Structure in Sodium Montmorillonite Hydrates, *Langmuir* 1995, 11, 2734-2741.
- [42] N. T. Skipper, Computer simulation of aqueous pore fluids in 2 : 1 clay minerals, *Mineralogical Magazine* 1998, 62, 657-667.
- [43] A. Arguelles, M. Leoni, J. A. Blanco, C. Marcos, Semi-ordered crystalline structure of the Santa Olalla vermiculite inferred from X-ray powder diffraction, *American Mineralogist* 2010, 95, 126-134.
- [44] J. Breu, W. Seidl, A. J. Stoll, K. G. Lange, T. U. Probst, Charge homogeneity in synthetic fluorohectorite, *Chemistry Of Materials* 2001, 13, 4213-4220.
- [45] A. R. Mermut, G. Lagaly, Baseline studies of The Clay Minerals Society Source Clays: Layer-charge determination and characteristics of those minerals containing 2 : 1 layers, *Clays and Clay Minerals* 2001, 49, 393-397.
- [46] M. K. Murthy, F. A. Hummel, Phase Equilibria in the System Lithium Metasilicate - Forsterite-Silica, *Journal of the American Ceramic Society* 1955, 38, 55-63.
- [47] S. Taruta, T. Ichinose, T. Yamaguchi, K. Kitajima, Preparation of transparent lithium-mica glass-ceramics, *Journal Of Non-Crystalline Solids* 2006, 352, 5556-5563.
- [48] T. Kodama, Y. Harada, M. Ueda, K. Shimizu, K. Shuto, S. Komarneni, W. Hoffbauer, H. Schneider, Crystal-size control and characterization of Na-4-mica prepared from kaolinite, *Journal of Materials Chemistry* 2001, 11, 1222-1227.

## Bibliography

---

- [49] M. D. Alba, M. A. Castro, M. Naranjo, E. Pavon, Hydrothermal reactivity of Na-n-micas (n=2, 3, 4), *Chemistry Of Materials* 2006, 18, 2867-2872.
- [50] M. Park, D. H. Lee, C. L. Choi, S. S. Kim, K. S. Kim, J. Choi, Pure Na-4-mica: Synthesis and characterization, *Chemistry Of Materials* 2002, 14, 2582-2589.
- [51] M. Gregorkiewitz, J. A. Rausellcolom, Characterization and Properties of A New Synthetic Silicate with Highly Charged Mica-Type Layers, *American Mineralogist* 1987, 72, 515-527.
- [52] T. Kodama, S. Komarneni, Na-4-mica:  $\text{Cd}^{2+}$ ,  $\text{Ni}^{2+}$ ,  $\text{Co}^{2+}$ ,  $\text{Mn}^{2+}$  and  $\text{Zn}^{2+}$  ion exchange, *Journal of Materials Chemistry* 1999, 9, 533-539.
- [53] T. Kodama, S. Komarneni, W. Hoffbauer, H. Schneider, Na-4-mica: simplified synthesis from kaolinite, characterization and Zn, Cd, Pb, Cu and Ba uptake kinetics, *Journal of Materials Chemistry* 2000, 10, 1649-1653.
- [54] W. J. Paulus, S. Komarneni, R. Roy, Bulk Synthesis and Selective Exchange of Strontium Ions in  $\text{Na}_4\text{Mg}_6\text{Al}_4\text{Si}_4\text{O}_{20}\text{F}_4$  Mica, *Nature* 1992, 357, 571-573.
- [55] W. H. Baur, Computer-Simulated Crystal-Structures of Observed and Hypothetical  $\text{Mg}_2\text{SiO}_4$  Polymorphs of Low and High-Density, *American Mineralogist* 1972, 57, 709-&.
- [56] W. Borchert, K. Jürgen, Beiträge zur Reaktionsfähigkeit der Silikate bei niedrigen Temperaturen, *Contributions to Mineralogy and Petrology* 1947, 1, 17-30.

### **5. Individual contributions to Joint Publications:**

The publications/manuscripts, which are presented in the appendix, were obtained in cooperation with other co-workers at different departments. My contributions to each publication are specified below and the asterisk denotes the corresponding author (s).

#### **5.1- Appendix 1.**

This work was submitted to RSC Advance under the title “**Single Crystal Structure Refinement of One- and Two-layer Hydrate of Sodium-Fluorohectorite**”. By Hussein Kalo, Wolfgang Milius, Josef Breu\*.

- I have performed the synthesis, characterization, and single crystal measurement in addition to writing the manuscript.
- Dr. Wolfgang Milius performed the refinement of one-layer hydrate of sodium fluorohectorite and also contributed to the scientific discussion.
- Prof. Josef Breu contributed to the scientific discussion.

#### **5.2- Appendix 2:**

This work was published in Applied Clay Science under the title “**Large scale melt-synthesis in an open crucible of Na-fluorohectorite with superb charge homogeneity and particle size**”. By Hussein Kalo, Michael W. Möller, Mazen Ziadeh, David Dolejš, Josef Breu\*.

- I have performed the synthesis, characterization of sodium fluorohectorite, and the scaling procedure in addition to writing the manuscript.
- Michael W. Möller performed the swelling evaluation procedure in the humidity chamber.
- David Dolejš performed the thermodynamics calculation and evaluation of the phase diagram.
- Mazen Ziadeh provided language help.
- Prof. Josef Breu contributed to the scientific discussion.

#### **5.3- Appendix 3:**

This work submitted to Nanoscale under the title “**How to Maximize the Aspect Ratio of Clay Nanoplatelets**”. By Hussein Kalo, Michael W. Möller, Daniel A. Kunz, and Josef Breu\*.



- I have performed the synthesis, characterization of sodium fluorohectorite and subsequently the scaling procedure and the scientific writing.
- Michael W. Möller conducted the swelling evaluation in the humidity chamber.
- Daniel A. Kunz made the atomic force microscope AFM measurement.
- Prof. Josef Breu contributed to the scientific discussion.

#### **5.4- Appendix 4:**

This work submitted to Journal of Solid State Chemistry under the title “**Synthesis and Single Crystal Structure of the One-layer hydrate of Sodium Brittle Mica**“. By Hussein Kalo, Wolfgang Milius, Michael Bräu and Josef Breu\*.

- I have performed the synthesis, characterization, single crystal measurements and refinements, in addition to the scientific writing.
- Dr. Wolfgang Milius contributed to the refinement discussion.
- Dr. Michael Bräu contributed to the twinning discussion.
- Prof. Josef Breu contributed to the scientific discussion.

# Appendix 1

## **Single Crystal Structure Refinement of One- and Two-layer Hydrate of Sodium-Fluorohectorite**

Hussein Kalo, Wolfgang Milius, Josef Breu\*

Department of Inorganic chemistry I, University of Bayreuth, D-95440 Bayreuth, Germany

Run title: crystal structure of hydrate Sodium-Fluorohectorite

Corresponding author:

Prof. Dr. Josef Breu

Universitätsstr. 30

95440 Bayreuth

Germany

\* E-mail address: [josef.breu@uni-bayreuth.de](mailto:josef.breu@uni-bayreuth.de)

**RSC Advance, DOI: 10.1039/C2RA20457F**

## Single Crystal Structure Refinement of One- and Two-layer Hydrate of Sodium-Fluorohectorite

*Hussein Kalo, Wolfgang Milius and Josef Breu\**

Lehrstuhl für Anorganische Chemie I, Universität Bayreuth, D-95440 Bayreuth, Germany

\* josef.breu@uni-bayreuth.de

Running title: structure refinement of one- and two-layer hydrate

\* Corresponding author: Prof. Dr. Josef Breu, Phone: 0049921552531 Fax: 0049921552788

E-mail: [Josef.Breu@uni-bayreuth.de](mailto:Josef.Breu@uni-bayreuth.de)

### Abstract

Crystal structures of both, one- and two-layer hydrate of sodium fluorohectorite could be refined against single crystal data for the first time because melt synthesis yielded a sodium fluorohectorite showing little stacking disorder as compared to natural clays. In both hydrate phases, the relative shift of adjacent 2:1-layer is fixed by hydrogen-bonding between water molecules coordinated to interlayer cations and basal oxygen atoms of tetrahedral sheets encompassing the interlayer space. Despite some reminiscent diffuse scattering, a decent single crystal refinement of the semi-ordered structure of the one-layer hydrate could be achieved revealing structural details of the interlayer space for the first time. For the two-layer hydrate the structural model proposed for vermiculites could be confirmed but a different ordering pattern of interlayer  $[\text{Na}(\text{H}_2\text{O})_6]^+$  is suggested. While in the two-layer hydrate sodium cations reside at the center of the interlayer space, in the one-layer hydrate sodium is displaced from the center of the interlayer space either towards the upper or towards the lower tetrahedral sheet. This displacement allows for coordination to the hexagonal cavity on one side while the coordination sphere of sodium is completed by three coordinating water molecules on the other side. These three water molecules in turn are involved in hydrogen bonding to the opposite tetrahedral sheet.

### Introduction

Hydrated (swollen) clays of the 2:1 structure family (e.g. montmorillonite, hectorite, or vermiculite; for nomenclature of clay minerals see Martin et al.<sup>1</sup>) are among the most important industrial minerals. World production of bentonites (rocks rich in montmorillonite)

in 2006 amounted to 13,700,000 metric tons which were mostly used as rheological additives for drilling fluids and civil engineering, as foundry sand binder, and as adsorptive for instance in pet litter.<sup>2</sup> More recently, more advanced applications such as microporous hybrid materials,<sup>3,4</sup> functional films for optoelectronic packaging,<sup>5</sup> halogen-free flame retardants,<sup>6</sup> and nanofillers in composites<sup>7</sup> had been established. All these applications depend crucially on the hydration state of the clays and swelling probably is the most important feature of expandable 2:1 layered silicates.

Despite the industrial importance of hydrated clay phases and despite intensive research over decades,<sup>8-17</sup> details of the one-layer hydrate structure are under debate. This is due to two handicaps intrinsic to natural clays: Hydration is critically dependent on two factors, the hydration enthalpy of interlayer cations and the charge density. For natural 2:1-clays like montmorillonite isomorphic substitution responsible for the layer charge clusters into domains and the charge density is inhomogeneous. As a consequence of charge heterogeneity, individual interlayers in any singular clay crystal will realize different states of hydration. It is common that at a given relative humidity (r.h.) zero-, one-, and two-layer hydrates are found concomitantly in the same crystal. The random interstratification of different basal spacings renders even a 1-dimensional Fourier analysis of the electron density distribution in the interlayer space difficult.

Besides interstratification, structure solution is even more severely hampered by planar defects. Intercalated water acts as a kind of lubricant and this is why most hydrated clay phases are turbostratically disordered. Adjacent layer stacked into a crystal are randomly rotated or shifted, the phase is not fixed, a unit cell cannot be defined, and scattering is completely diffuse.

A comprehensive description of the structure of these hydrated phases would have to deliver information about the coordination of interlayer cations, the relative position/phase relationship of adjacent 2:1-layer (interlayer displacement),<sup>18</sup> and the “interaction” pattern between the interlayer species (cations and water) and the basal oxygen atoms comprising the interlayer. Although an amazingly detailed picture of the structure of the interlayer could be derived employing 1-dimensional Fourier synthesis of X-ray and neutron diffraction data, possibly in combination with NMR data and different computer simulation methods,<sup>19-22</sup> experimental evidence for interlayer displacement and specific interactions between interlayer species and the silicate layer require 3-dimensionally or at least semi-ordered “crystals” that are only little affected by planar defects (stacking disorder). There is, however,

only a limited number of “single crystal” refinements of hydrated phases available in the literature applying some rare occasions of semi-ordered vermiculites (Santa Olalla, Spain and Carl Moss Ranch, Llano County, Texas) showing significantly less stacking faults and consequently much reduced diffuse scattering.<sup>23,24</sup> In addition to remaining stacking disorder, the electron density of these natural vermiculites is, however, affected by mixed occupation of all cationic positions (octahedral, tetrahedral, and interlayer). Consequently, crystal structure refinement in all cases had to be restricted to certain classes of reflections that are least affected by the stacking disorder patterns ( $k=3n$ ). Disorder patterns and structures of two-layer hydrates of Na- and Mg-vermiculites was comprehensively discussed by Suquet and Perzerat, and de la Calle et al. applying PXRD and Weissenberg-camera single crystal data.<sup>10,11</sup> In these studies, the one-layer hydrate was found to be completely disordered and details of the interlayer structure could consequently not be resolved. The two-layer hydrate was found to be semi-ordered and a structural model of the interlayer space was deduced. Please note, that all these “single crystal” refinements used standard programs that are incapable to take diffuse scattering into account. Consequently, the information about disorder patterns hidden in the diffuse scattering is ignored and only the main structure of the 3-dimensionally ordered volume of the crystals is refined. More recently, the Rietveld refinement of a X-ray powder diffraction (PXRD) trace of semi-ordered Santa Olalla vermiculite was refined with DIFFaX+, a program that indeed also takes stacking disorder and diffuse scattering into account.<sup>25</sup>

To reduce the complexity we sought to synthesize a well ordered fluorovermiculite (vermiculite where the hydroxyl group is replaced by fluorine) of nominal composition,  $[\text{Na}_{0.85}]^{\text{inter}}[\text{Mg}_{2.15}\text{Li}_{0.85}]^{\text{oct}}[\text{Si}_4]^{\text{tet}}\text{O}_{10}\text{F}_2$ , which we prefer to refer to as highly charged fluorohectorite (Na-hect) (hectorite where the hydroxyl group is replaced by fluorine) because the material lacks the Tschermak substitution typical for vermiculites. Fortunately, for this synthetic Na-hect stacking disorder and thus diffuse scattering are indeed reduced to a level that allows a full crystal structure refinement applying all  $hkl$  reflections delivering full structural details for both, the one-layer and the two-layer hydrates.

## Experimental Section

The fluorohectorite used, was synthesized via melt synthesis.<sup>16,26,27</sup> The high purity reagents (in total ~4 g) of  $\text{SiO}_2$  (Merck, fine granular, calcined),  $\text{MgF}_2$  (chempur, 99.99%),  $\text{MgO}$  (alfa aesar 99.95 %),  $\text{Li}_2\text{SiO}_3$  (alfa aesar 99.95 %), and  $\text{Na}_2\text{O}\cdot 2\text{SiO}_2$ -glass were weighed into a molybdenum crucible in an Ar atmosphere in accordance with a stoichiometric composition

of  $[\text{Na}_{0.85}]^{\text{inter}}[\text{Mg}_{2.15}\text{Li}_{0.85}]^{\text{oct}}[\text{Si}_4]^{\text{tet}}\text{O}_{10}\text{F}_2$  (target composition).  $\text{Na}_2\text{O}-2\text{SiO}_2$ -glass has been produced by melting  $\text{Na}_2\text{CO}_3$  (Aldrich, 99.9%) and  $\text{SiO}_2$  (Merck, fine granular, calcined) in a 1:2 molar ratio at 1050 °C for 10 h to ensure complete release of carbon dioxide. The molybdenum crucible was sealed so as to be gas tight using the procedure described elsewhere.<sup>28</sup> The crucible was heated in a graphite furnace (Graphit HT-1900, Linn High Therm) for the synthesis. To prevent inhomogeneity of the product owing to gravity segregation in the melt, the crucible was positioned horizontally in the furnace and rotated at 50 rpm. The crucible was heated from room temperature (RT) to 1750 °C (20 °C min<sup>-1</sup>), left at 1750 °C for 1 h, then cooled to 1450 °C with a cooling rate of 50 °C min<sup>-1</sup>, followed by a low cooling rate of 3 °C min<sup>-1</sup> from 1450 °C to 800 °C, and finally it was quenched by switching off the power. The crucible was opened under Ar atmosphere and the synthetic Na-hect was stored in a Glovebox.

PXRD patterns of zero-, one-, and two-layer hydrate of synthetic Na-hect were measured using a STOE Stadi P powder diffractometer (transmission geometry,  $\text{CuK}\alpha_1$  radiation ( $\lambda = 1.54059$  Å), Ge monochromator, linear position sensitive scintillation detector). The measurement was done in sealed glass capillaries in order to fix r.h. and to minimize texture effects. For zero-layer hydrate Na-hect, the capillary was filled and closed in the Glovebox. For the one- layer hydrate the synthetic Na-hect was exposed to water vapour at 43% r.h. ( $\text{K}_2\text{CO}_3$  saturated solution). The equilibrated sample was quickly transferred into a capillary which was sealed with grease for PXRD measuring. For the two-layer hydrate the synthetic Na-hect was filled into a capillary which was still open at both ends. Then the capillary was filled with distilled water by immersing one end of the capillary into water. After two weeks of equilibration, the capillary was sealed at both ends and the PXRD pattern was recorded.

The single crystal X-ray data of one- and two- layer hydrate of synthetic Na-hect were collected for selected crystals showing a minimum of diffuse streaks. In order to minimize dynamics of interlayer water and to fix the water content, data were collected at 173 K on a STOE IPDS diffractometer with graphite monochromated  $\text{MoK}\alpha_1$  radiation ( $\lambda = 0.71073$  Å) using crystals of appr. 0.25 mm x 0.20 mm x 0.02 mm in size in 320 frames (0.5° step per frame, 30 min per frame). Prior to mounting, the single crystals were equilibrated at appropriate r.h. as described above for the PXRD measurements. Further details of the data collection and structure refinement are given in Table 1. The composition of the synthetic Na-hect was determined by wavelength dispersive X-ray spectroscopy (WDX) on a Joel JXA 8200 spectrometer, with acceleration voltage 15 kV, and beam spot diameter 1  $\mu\text{m}$ , which

was calibrated against certified mineral standards (Si - andradite  $\text{Ca}_3\text{Fe}_2\text{Si}_3\text{O}_{12}$ , Mg- synthetic Enstatit  $\text{Mg}_2[\text{Si}_2\text{O}_6]$ , O - silicon dioxide  $\text{SiO}_2$ , F - fluorite  $\text{CaF}_2$ , Na - albite  $\text{NaAlSi}_3\text{O}_8$ ). The counting time was 20 s at the peak position and 10 s on each side of the peak position. For microprobe analysis, the very same crystal that has been used for X-ray data collection was fixed in resin on a glass slide and coated with carbon. Because of the incapability of this method to determine the lithium content, the composition of the synthetic layered silicate was normalized to  $\text{Si}_{4.00}$ . The lithium content was confirmed independently for the bulk material by inductively coupled plasma atomic emission spectroscopy (ICP-AES), where for Li determination two samples of about 20 mg of dry synthetic Na-hect were weighed into a clean Teflon flask of 150 mL volume. After addition of 1.5 mL 30 wt. % HCl (Merck), 0.5 mL of 85 wt. %  $\text{H}_3\text{PO}_4$ , 0.5 mL 65 wt. %  $\text{HNO}_3$  (Merck) and 1 mL of 48 wt. %  $\text{HBF}_4$  (Merck) the sample was digested in a MLS 1200 Mega microwave digestion apparatus for 6.5 min and heated at 600W (MLS GmbH, Mikrowellen-Labor-Systeme, Leutkirch, Germany). The closed sample container was cooled to room temperature and the clear solution was diluted to 100 mL in a volumetric flask.

The water content of both hydrates was determined gravimetrically. Approximately 100 mg of equilibrated one- and two-layer hydrate samples were dried at 250 °C at reduced pressure ( $2.2 \cdot 10^{-2}$  mbar) for 24 h. The weight loss during drying was attributed to interlayer water.

The cation exchange capacity (CEC) of synthetic Na-hect was determined by the barium chloride method. For this, 0.2 g of synthetic Na-hect were suspended in 25 mL of distilled water, 25 mL of 1 M barium chloride solution were added. The mixture was shaken overnight and then centrifuged, and the supernatant solution was collected. To ensure complete exchange of sodium, the cation exchange was repeated two times. The  $\text{Na}^+$  content of the collected solutions was determined by Atomic Absorption Spectroscopy (AAS). Additionally, the CEC was crosschecked by analyzing the Ba-exchanged Na-hect for its Ba-content by ICP-AES after microwave digestion as described for the determination of the Li-content.

## Results and Discussion

### Synthesis of a phase pure Na-hect

(Fig. 1) shows the PXRD pattern of zero-, one-, and two-layer hydrate (0WL, 1WL, and 2WL, respectively) of synthetic Na-hect. No crystalline impurities could be detected.

The 1WL showed uniform intercrystalline reactivity as indicated by a rational  $00l$  series (variation coefficient = 0.33%)<sup>29</sup> and a basal spacing of  $d_{001} = 12.5 \text{ \AA}$ . Due to overlap, we were only able to unambiguously determine the positions of the  $00l$ -series where  $l_{\max} = 5$  in case of zero-layer hydrate and one layer hydrate, and  $l_{\max} = 8$  in case of the two-layer hydrate. While the 1WL is uniformly hydrated, at the 2WL state some crystals remain in the 1WL state. The  $00l$  series (variation coefficient = 0.42%) of the 2WL phase is nevertheless rational suggesting a uniform swelling behavior within a single crystal while some crystals are less reactive for whatever reason. The 2WL gives a basal spacing of  $d_{001} = 15.1 \text{ \AA}$ . Judging by the number of peaks detectable in the diffraction pattern, in particular at the diffraction angle ( $20\text{--}23^\circ 2\theta$ ) where the  $02/11$  band appears, it became quite obvious that the stacking disorder decreased significantly with increasing hydration. Please note that PXRD samples an average of the bulk material and even a view peak maxima superimposed on an asymmetric  $\lambda$ -shaped  $hk$  band might already indicate that a few (semi-)ordered single crystals are present. In any case, the 2WL can be indexed without problems ( $a = 5.2310 \text{ \AA}$ ,  $b = 9.0681 \text{ \AA}$ ,  $c = 15.0307 \text{ \AA}$ , and  $\beta = 97.12^\circ$ ). Good quality crystals with little diffuse scattering can also quite easily be found for the 2WL. The disorder-order transition upon hydration is reversible. We therefore tried to improve the stacking order for 1WL by repeatedly cycling between 1WL and 2WL but the crystallinity as judged by the PXRD trace could not be improved. Nevertheless, by screening a large number of 1WL crystals we succeeded in identifying individual crystals with much reduced diffuse scattering. In agreement with previous observations for non-hydrated  $[\text{Na}_{0.5}]^{\text{inter}}[\text{Mg}_{2.5}\text{Li}_{0.5}]^{\text{oct}}[\text{Si}_4]^{\text{tet}}\text{O}_{10}\text{F}_2$  which is also heavily disordered,<sup>30</sup> for 0WL, however, all crystals checked were highly disordered and therefore no structure refinement was attempted.

The chemical composition of synthetic Na-hect was determined by WDX to be  $[\text{Na}_{0.7}]^{\text{inter}}[\text{Mg}_{2.3}\text{Li}_{0.7}]^{\text{oct}}[\text{Si}_4]^{\text{tet}}\text{O}_{10}\text{F}_2$ . Following digestion of the material and applying ICP-AES, the contents of  $\text{Na}^+$ ,  $\text{Li}^+$ , and  $\text{Mg}^{2+}$  were  $0.73 \pm 0.05$ ,  $0.72 \pm 0.02$ , and  $2.25 \pm 0.04$ , respectively. The CEC of synthetic Na-hect as determined via  $\text{Na}^+$  in the supernatant after  $\text{Ba}^{2+}$  exchange was  $1.85 \text{ meq.g}^{-1}$ . The CEC calculated from the Ba-content of Ba-hect was  $1.75 \text{ meq.g}^{-1}$ . These values are in close agreement with theoretical values calculated from the chemical formula as determined by WDX ( $1.81 \text{ meq.g}^{-1}$ ).



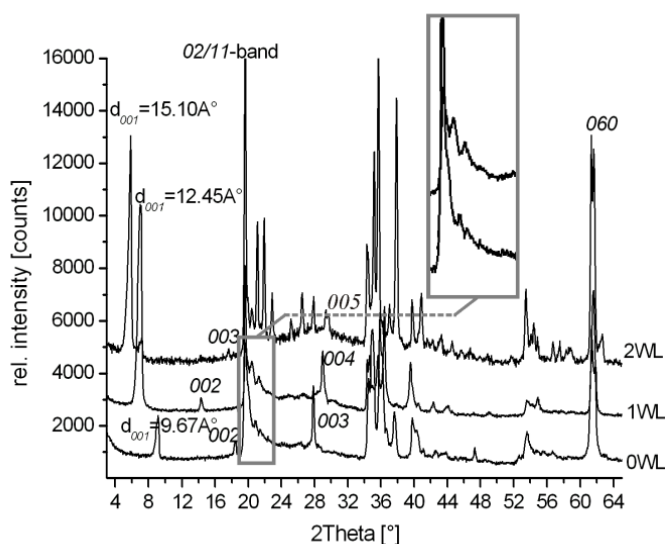


**Fig. 1** Powder X-ray diffraction pattern of zero- (0WL,  $d_{001}=9.67 \text{ \AA}$ ), one- (1WL,  $d_{001}=12.45 \text{ \AA}$ ), and two-layer hydrate (2WL,  $d_{001}=15.10 \text{ \AA}$ ) of synthetic sodium fluorohectorite.

The  $\text{H}_2\text{O}/\text{Na}$  molar ratio as determined gravimetrically was 3.2 and 5.6 for the 1WL and 2WL, respectively. The value for the 2WL was significantly higher than what has been reported by Beyer and von Reichenbach<sup>31</sup> who have used a phlogopite with a layer charge per formula unit (p.f.u.) of  $x = 0.98$ . They pointed out that for the 2WL the interlayer space is densely packed with a ratio of  $\text{H}_2\text{O}/\text{Na} = 4$  and therefore no additional water could be possibly accommodated in the interlayer space. Please note that we synthesized a much lower layer charge of  $x = 0.7$  p.f.u. as indicated by microprobe analysis. Since the interlayer space is expected to be still densely packed, unoccupied Na-positions will yield voids to accommodate additional water.

### Single crystal structure refinement

Details of the single crystal structure refinements together with experimental details of 1WL and 2WL of synthetic Na-hect are included in Table 1. A standard single crystal refinement program was applied that is not capable of handling diffuse (non-Bragg) scattering. As in earlier work, diffuse scattering had to be ignored but refinement was performed against the complete data set. Further information about the structure refinement can be requested from Fachinformationszentrum Karlsruhe, Gesellschaft für wissenschaftlich-technische Information mbH, D-76344 Eggenstein-Leopoldshafen, Germany, by indicating the deposition numbers CSD-424706 and CSD-424707 For 1WL and 2WL hydrate, respectively. (Email: [crysdata@fiz-karlsruhe.de](mailto:crysdata@fiz-karlsruhe.de)).

The quality of the data sets as indicated by the  $R_{\text{int}}$  values is satisfactory for this class of materials since due to the diffuse scattering; the integration profiles of affected reflections are ill-defined which consequently leads to somewhat higher  $R_{\text{int}}$  values. The structures could be solved without problems applying direct methods as implemented in SHELXTL 5.1 (Bruker AXS).<sup>32</sup> For both hydrates, the refinement of the substructure of the 2:1 layer also was straight forward and atomic displacement parameters (ADP) could even be refined anisotropically. This underlines the good quality of the data sets. Occupancies of interlayer cation and water were freely refined. The water content as obtained by the refinement is somewhat lower than values determined by gravimetric analysis. From the occupation factors obtained in the refinement the following compositions could be calculated:  $[\text{Na}_{0.7} \cdot 2.1\text{H}_2\text{O}]^{\text{inter}}[\text{Mg}_{2.2}\text{Li}_{0.8}]^{\text{oct}}[\text{Si}_4]^{\text{tet}}\text{O}_{10}\text{F}_2$  and  $[\text{Na}_{0.7} \cdot 4\text{H}_2\text{O}]^{\text{inter}}[\text{Mg}_{2.2}\text{Li}_{0.8}]^{\text{oct}}[\text{Si}_4]^{\text{tet}}\text{O}_{10}\text{F}_2$  for 1WL and 2WL, respectively). Most likely this is due to the residual disorder and diffuse scattering (see **Fig. S1, S2**).

As might have been expected, interlayer water and cations were trickier to be located and refined. Na-sites could, however, be identified by looking for a sensible coordination environment. In both 1WL and 2WL alternative positions with partial occupation were identified. As pointed out earlier, unoccupied Na-sites are generally expected to be filled by additional water molecules. However, given the complexity of the refinement, we did not attempt concomitant refinement of partially occupied water on Na-sites. Despite these difficulties, for 2WL a stable refinement was possible without restraining or even constraining atomic distances and bond angles between interlayer constituents for 2WL structure as done by Beyer and von Reichenbach.<sup>31</sup> For 1WL all water molecules coordinating to sodium could be identified in the difference Fourier map, however, for stable refinement the distances between water molecules and between water and sodium had to be restrained applying DFIX. Please note, that the refinements were not restricted to selected classes of reflections that are less affected by stacking faults, but all reflections have been used. Given this, the quality of the refinement as indicated by R values of around 11 % is very reliable.

### Structure of 1WL and 2WL hydrate

The crystal structure of 1WL and 2WL in projection along  $a$  are represented in (**Fig. 2**). There is an longstanding dispute in the literature about the position of the interlayer cations in the 1WL. Some authors suggest it to reside on the central plane of the interlayer.<sup>33,34</sup>

Computer simulations of 1WL support this view.<sup>35,36</sup> Some other authors claimed that the interlayer cations are displaced from the center towards tetrahedral sheets.<sup>14,37</sup>

Our refinement clearly showed that in the 1WL Na<sup>+</sup> interlayer cations are not residing in the middle of the interlammellar space but are displaced towards the tetrahedral sheet enclosing the interlayer space. Displacement towards upper or lower tetrahedral sheet are of course degenerate and consequently two alternative sites with differing  $z$  values for Na<sup>+</sup> could be identified during refinement. These alternative Na<sup>+</sup> sites can be clearly spotted in the Fourier map (Fo-map:  $F(\text{obs})$  Fourier with phases from  $F(\text{calc})$ ) of the interlayer space (see **Fig. S3**). For 1WL the central plane of the interlayer space is occupied by water molecules which are coordinating to the interlayer cations (see below).

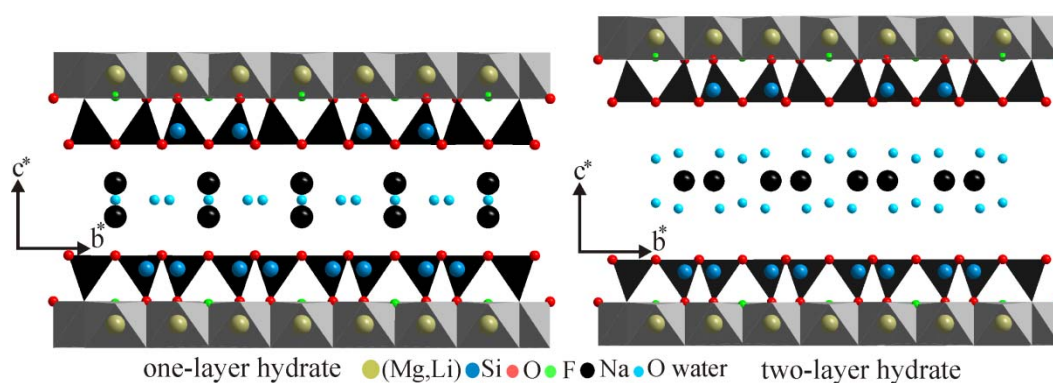


**Fig. 2** Structure of 1WL and 2WL of Na-hect projected along  $a^*$  indicating in particular the location of interlayer cations.

Although the close proximity of the origin of charge in saponites certainly will influence the location of interlayer cations, we still would like to compare the  $z$ -positions of these cations and the interlayer water coordinated to them as recently published by Ferrage et al.<sup>38</sup> for a high layer charge saponite ( $[\text{Na}_x]^{\text{inter}}[\text{Mg}_6]^{\text{oct}}[\text{Si}_{4-x}\text{Al}_x]^{\text{tet}}\text{O}_{10}(\text{OH})_2$ ,  $x=0.7$ ). For the 1WL Ferrage et al. found a strong dependence of the Na-location on the forcefield applied in the modelling study. For the S/S-FF-forcefield38 the Na-sites were well located and were found to be displaced approx.  $\pm 0.8$  Å from the central plane of water molecules which is in close agreement with 0.815 Å found in our refinement. For the 2WL Ferrage et al., with all forcefields, applied found a smaller part of Na displaced from the central plane of the interlayer space which most is related to the tetrahedral substitution.<sup>38</sup> The distance between the main Na-site at the central plane and the two water layers above and below reported by Ferrage et al. is around 1.5 Å. Our refinement of the single crystal data gave, however, significantly shorter distances along  $z$  of 1.32 Å and 1.37 Å. It is difficult to judge whether

these differences are due to the different type of clay and charge pattern or whether it indeed would suggest that the forcefield parameters applied would have to be further refined. Part of the difference can certainly also be attributed to the different temperatures that the data were collected at.

**Table 1** Crystallographic data and details of the single crystal structure refinements of 1WL and 2WL of synthetic Na-hect

Crystal data	
Formula unit $[\text{Na}_{0.7} \cdot x\text{H}_2\text{O}]^{\text{inter}}[\text{Mg}_{2.3}\text{Li}_{0.7}]^{\text{oct}}[\text{Si}_4]^{\text{tet}}\text{O}_{10}\text{F}_2$	
Formula weight = 387.22 (g/mole) (without interlayer water)	
MoK $\alpha$ radiation ( $\lambda = 0.71073 \text{ \AA}$ ) graphite monochromator	
T = 173 K	
1WL	2WL
$a = 5.2434(10) \text{ \AA}$	$a = 5.2432(10) \text{ \AA}$
$b = 9.0891(18) \text{ \AA}$	$b = 9.0870(18) \text{ \AA}$
$c = 12.165(2) \text{ \AA}$	$c = 15.064(3) \text{ \AA}$
$\beta = 93.92(3)^\circ$	$\beta = 96.42(3)^\circ$
$V = 578.4(2) \text{ \AA}^3$	$V = 713.2(2) \text{ \AA}^3$
Monoclinic. C2/m (No. 12)	Monoclinic. C2/m (No. 12)
Z = 2	Z = 2
Plate colorless	Plate colorless
0.25mm x 0.20mm x 0.02mm	0.25mm x 0.20mm x 0.02mm
Data collection	
STOE IPDS I diffractometer	
Completeness of $2\theta = 0.98$	Completeness of $2\theta = 0.98$
2006 measured reflections	2477 measured reflections
597 independent reflections	734 independent reflections
384 reflections with $I > 2\sigma(I)$	426 reflections with $I > 2\sigma(I)$
$R_{\text{int}} = 0.181$	$R_{\text{int}} = 0.226$
$\theta_{\text{max}} = 25.90^\circ$	$\theta_{\text{max}} = 25.93^\circ$
$\theta_{\text{min}} = 3.36^\circ$	$\theta_{\text{min}} = 2.72^\circ$
$h = -5 \rightarrow 6$	$h = -5 \rightarrow 6$
$k = -11 \rightarrow 10$	$k = -10 \rightarrow 10$
$l = -14 \rightarrow 14$	$l = -18 \rightarrow 18$
Refinement applying SHELXTL 5.1 (Bruker AXS).	
Refinement on $F^2$	Refinement on $F^2$
$R[F^2 > 2\sigma(F^2)] = 0.109$	$R[F^2 > 2\sigma(F^2)] = 0.1150$
$wR(F^2) = 0.2881$	$wR(F^2) = 0.2787$
$S = 1.110$	$S = 1.042$
$w = 1/[\sigma^2(F_o^2) + (0.20000P)^2 + 0.000P]$ where $P = (F_o^2 + 2 F_c^2)/3$	$w = 1/[\sigma^2(F_o^2) + (0.20000P)^2 + 0.000P]$ where $P = (F_o^2 + 2 F_c^2)/3$
$\Delta \rho_{\text{max}} = 1.58 \text{ e\AA}^{-3}$	$\Delta \rho_{\text{max}} = 1.12 \text{ e\AA}^{-3}$
$\Delta \rho_{\text{min}} = -0.71 \text{ e\AA}^{-3}$	$\Delta \rho_{\text{min}} = -0.76 \text{ e\AA}^{-3}$
61 parameters	73 parameters

Contrary to the 1WL, for the 2WL the interlayer cations reside at the central plane of the interlayer space as has been suggested by others<sup>23,31</sup> before and also supported by the Fo-map of the interlayer space (see **Fig. S4**).

The relative position of lower and upper tetrahedral sheet encompassing the interlayer region (stacking order) as viewed along  $c^*$  is presented in (**Fig. 3A**) and (**Fig. 3B**) for 2WL and 1WL, respectively. The observed location of sodium cations for 1WL and 2WL relative to the lower tetrahedral sheet is depicted in (**Fig. 4**). For 2WL upper and lower hexagonal cavity are stacked face to face. Contrary to mica structures where this arrangement is assured by interlayer cations in the center intruding into the hexagonal cavities on both sides, the cavities are not occupied by interlayer cations in the 2WL structure. Instead, the  $\text{Na}^+$  resides above the tetrahedrons (see also (**Fig. S4**)).

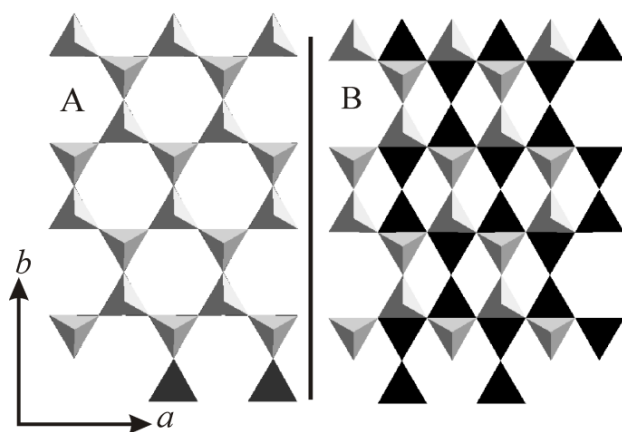


**Fig. 3** Comparison of the relative position of lower (black) and upper (grey) tetrahedral sheet encompassing the interlayer region (stacking order) as viewed along  $c^*$ : 2WL (A) and 1WL (B).

As pointed out by Beyer and von Reichenbach<sup>31</sup> two sets of  $\text{Na}^+$  sites depicted as m1 and m2 in (**Fig. 4A**) exist. With a charge density of  $x = 1.0$  p.f.u. only half of these possible  $\text{Na}^+$  sites are occupied, with  $x = 0.7$  p.f.u., as we found for Na-hect, even less than half are occupied. Not surprisingly, structure refinement results in an equal statistical occupation of both sites, m1 and m2 as is also obvious from the Fo-map (see **Fig. S5**). Beyer and von Reichenbach<sup>31</sup> have proposed that m1 and m2 sites are concomitantly occupied in the same interlayer space resulting in zig-zag-chains of edge-sharing octahedral running along  $a$ . Beyer and von Reichenbach<sup>31</sup> had to propose this ordering pattern in order to match octahedral coordination of  $\text{Na}^+$  interlayer cations with a  $\text{H}_2\text{O}/\text{Na}$  molar ratio of only 4. While this motif is widespread for  $\mu$ -hydroxy-bridges we are not aware of other examples of  $\mu$ -aquo-bridges of  $\text{Na}^+$

in the literature. Moreover, we determined a  $\text{H}_2\text{O}/\text{Na}$  molar ratio of close to six allowing to propose isolated  $[\text{Na}(\text{H}_2\text{O})_6]^+$ . We therefore suggest that the electron density seen in the X-ray experiment is interpreted in an alternative way: For any individual interlayer space, either purely m1 or purely m2 sites are occupied and m1 and m2 interlayers are stacked randomly with equal probability.

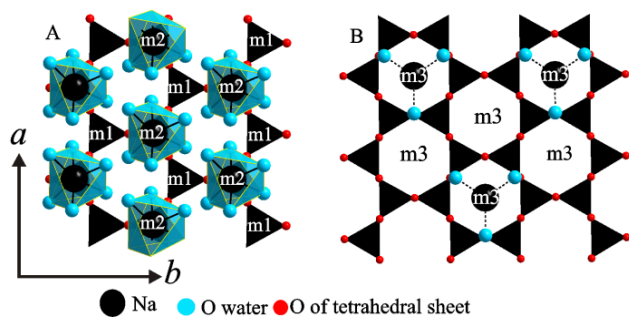


**Fig. 4** Position of hydrated  $\text{Na}^+$  interlayer cations relative to lower hexagonal cavity; A: 2WL hydrate the position m1 and m2, B: 1WL hydrate position m3 along  $c^*$  projection. Please note that non-occupied m3 sites host water molecules coordinated to  $\text{Na}^+$  in contact with the upper tetrahedral sheet.

This packing pattern of  $[\text{Na}(\text{H}_2\text{O})_6]^+$  complex cations is shown in (**Fig. 4A**). Each  $\text{Na}^+$  in the interlayer is coordinated by six oxygen of water ( $\text{O}_w$ ) (the average of  $\text{Na}-\text{O}_w$  bond length 2.45 Å). The coordinating oxygen atoms are located in two slightly corrugated planes above and below the plane of  $\text{Na}^+$  (**Fig. 2**). As pointed out by Beyer and von Reichenbach,<sup>31</sup> with  $x = 1.0$  p.f.u. two densely packed planes of interlayer water result (**Fig. S6**). However, with  $x = 0.7$  p.f.u., some  $\text{Na}^+$  sites are not occupied and the then non-coordinated water molecules are expected to relax. This might explain why Ferrage et al.<sup>15</sup> had to apply a Gaussian-shaped distribution in their 1-dimensional Fourier synthesis. Similarly, Argülles et al.<sup>25</sup> introduced interstitial, non-coordinated water sites.

The stacking order of adjacent 2:1 layer is assured by well defined hydrogen bonding motifs between interlayer  $[\text{Na}(\text{H}_2\text{O})_6]^+$  and the silicate layers. Each coordinated water molecule is able to connect to one basal oxygen atom of the tetrahedral sheet via hydrogen bonding (**Fig. 5**). The distance between the two oxygen atoms connected by hydrogen bonding was 2.90 - 3.03 Å.

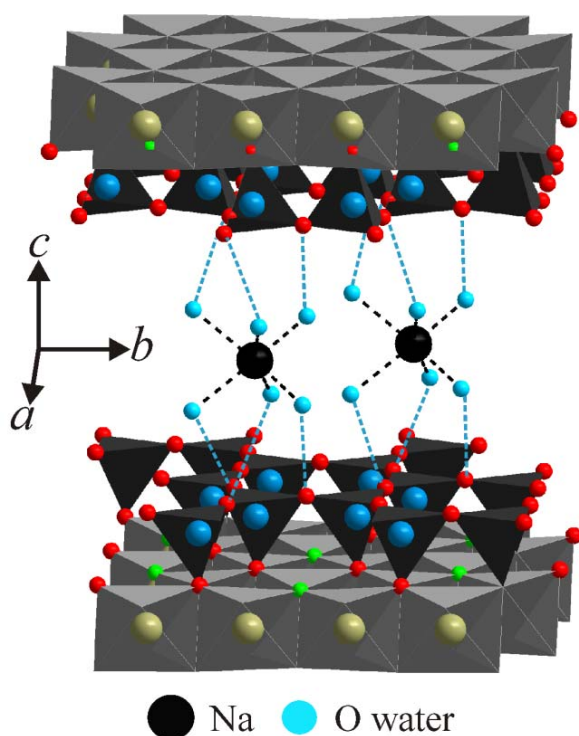


**Fig. 5** Hydrogen bonding between interlayer  $[\text{Na}(\text{H}_2\text{O})_6]^+$  and tetrahedral sheets fixing the stacking order in 2WL Na-hect.

The stacking order puts the basal oxygen atoms of the two tetrahedral sheets encompassing the interlayer space on top of each other. In order to allow for concomitant connection of the octahedral interlayer species to both sides of the interlayer space, the two triangles of oxygen atoms forming  $[\text{Na}(\text{H}_2\text{O})_6]^+$  need to be rotated relative to the triangle of the basal oxygens of the tetrahedral sheets.

As was already obvious from the PXRD trace, the 1WL suffers more severely from stacking faults as compared to the 2WL. This is in line with observations for vermiculite where the 1WL material has been labeled disordered.<sup>39</sup> Consequently, the knowledge of interlayer structures is much more limited as compared to the 2WL. However, as shown in the inset of (**Fig. 1**), some comparatively sharp symmetric reflections are superimposed on the asymmetric  $\lambda$ -shaped 11/02-band indicating that the bulk material also contained a view much better ordered crystals. Applying these maxima a unit cell could be indexed and refined even for the 1WL ( $a= 5.2430 \text{ \AA}$ ,  $b= 9.0851 \text{ \AA}$ ,  $c=12.2150 \text{ \AA}$ ,  $\beta=94.24^\circ$ ). By screening a large number of crystals, we were able to identify relatively well ordered individuals that allowed a single crystal structure refinement. The unit cell found for this single crystal is in close agreement with the one refined from PXRD. As became already obvious from the metric of the unit cell the stacking order found for Na-hect differed significantly from what has been

reported for the 1WL of vermiculite.<sup>39</sup> While these authors report a monoclinic angle of  $90^\circ$ , we get  $\beta = 93.92(3)^\circ$  clearly indicating that the relative position of tetrahedral sheets encompassing the interlayer space was different (**Fig. 3B**). The hexagonal cavities are not arranged opposite of each other but are shifted by  $2.62 \text{ \AA}$  relative to each other corresponding to an interlayer displacement of  $a/2$ .  $\text{Na}^+$  occupies m3 positions (**Fig. 4B**). As will be explained next, this shifting is required for the coordination of the interlayer cation by basal oxygen atoms of the two tetrahedral sheets encompassing the interlayer space.

In total 4  $\text{Na}^+$  sites, all partially occupied ( $\approx 0.35$ ) are located in the unit cell. Clearly, some of the distances to water sites are too short to be occupied concomitantly in the same interlayer space. It would not be expected that ordering of interlayer species in a particular interlayer space influences the ordering in adjacent interlayer spaces. However, the X-ray beam averages within the coherence length over all possible positions and the electron density is artificially superimposed into an average interlayer space. A tentative assignment of superimposed electron densities into an ordering pattern that makes sense chemically is attempted in the following (**Fig. 6**): The coordination observed for  $\text{Na}^+$  is unusual. It involves both basal oxygen atoms of the tetrahedral sheet and interlayer water. In the direction of the displacement of the interlayer cation towards the tetrahedral sheet,  $\text{Na}^+$  resides above the hexagonal cavity and is coordinated by 6 basal oxygens with distances ranging between  $3.22 \text{ \AA}$  and  $3.24 \text{ \AA}$ . On the opposite side of the interlayer region a single siloxan bridge is located at a rather long distance of  $3.52 \text{ \AA}$  which was therefore not regarded to be part of the coordination sphere. The coordination of  $\text{Na}^+$  is rather completed by water molecules residing at the central plane resulting in 9-fold coordination ( $[\text{Na}(\text{O}_b)_6(\text{H}_2\text{O})_3]^+$ ). In (**Fig. 6**) we choose the three closest water ( $2.45\text{-}2.55 \text{ \AA}$ ) positions to be coordinated. These three oxygen atoms are involved in hydrogen bonding to basal oxygens ( $2.72\text{-}3.60 \text{ \AA}$ ). While this interaction pattern explains why the interlayer space is bridged in a well defined mode resulting in the interlayer displacement of  $a/2$ , some arbitrariness remains in the assignment due to the many alternative oxygen positions generated by the four alternative  $\text{Na}^+$  sites clearly visible in the Fo-map of 1WL (**Fig. S3**). Also, it was not clear whether indeed adjacent upper and lower  $\text{Na}^+$  sites are occupied concomitantly in the same interlayer or whether these alternate sites are rather segregated into different interlayer spaces.



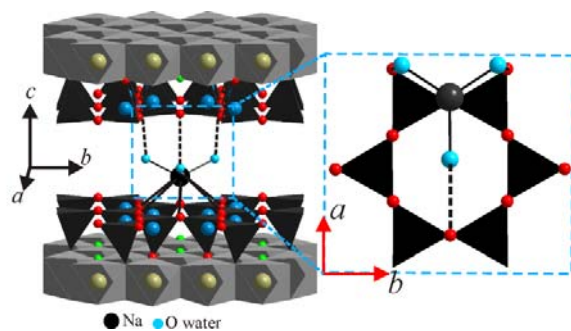


**Fig. 6** Tentative coordination of interlayer  $\text{Na}^+$  and connecting mode of adjacent silicate layers for 1WL of Na-hect.

### Disorder mode of 1WL Na-hect

As has been pointed out in the literature, stacking faults may significantly alter properties and in consequence applications of clays.<sup>40,41</sup> Therefore, we briefly focus on the diffuse scattering containing the information on such disorder modes. As pointed before, the 2WL structure is only little effected by disorder and only little diffuse scattering is apparent in the reciprocal lattice (**Fig. S1, S2**). In agreement with the shape of the PXRD traces (**Fig. 1**), in the reciprocal lattice of 1WL diffuse scattering is much more prominent as compared to the 2WL. Moreover, only some  $hk$ -rods are affected by the disorder while others only show sharp Bragg reflections, suggesting that the disorder patterns are commensurate with the lattice (for comparison see (**Fig.1**) in Slade and Stone<sup>42</sup>). Clearly, 1WL represents a semi-ordered structure. The most prominent semi-ordered stacking is observed for micas where  $\pm b/3$  shifts occur frequently and reflections with  $k=3n$  remain sharp. Please note that tetrahedral rotation for the synthetic Na-hect is close to zero generating an ideal hexagonal pseudo-symmetry for interlayer species. Therefore, disorder modes will be available that are not feasible for vermiculites.<sup>24,25</sup>

In 1WL a different disorder mode was realized as clearly indicated by the distribution of diffuse scattering in the reciprocal lattice space:  $02l$ ,  $42l$ ,  $24l$ ,  $06l$ , and  $46l$  are diffuse, while  $22l$ ,  $62l$ ,  $04l$ ,  $44l$ , and  $26l$  are sharp. As shown in (**Fig. 7**), translations of the upper layer by combinations of  $\pm a/4$  and  $\pm b/4$  create the same environment for the interlayer cations suggesting that random shifts of that type will generate energetically degenerate modes of stacking. This degeneracy in turn is responsible for the stacking disorder observed.

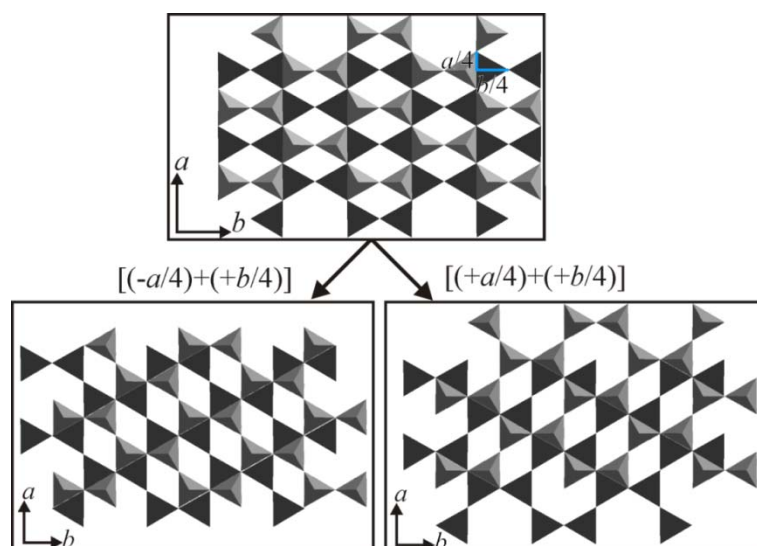


**Fig. 7** Illustration of energetically degenerate stacking modes for semi-ordered 1WL explaining the observed diffuse scattering. Translation of upper tetrahedral sheet (grey) relative to lower tetrahedral sheet (black) with  $[+a/4] + (+b/4)$  or  $[-a/4] + (+b/4)$  provide a similar environment for interlayer species.

### Conclusion

By melt synthesis swelling Na-hect could be synthesized that upon hydration converts to semi-ordered (1WL) and ordered (2WL) hydrates. The significant reduction of stacking faults in these synthetic hydrates allowed for the first time to solve the structure of the one-layer hydrate. The interlayer cations reside off the central plane in a 9-fold coordination of 6 basal oxygen atoms and three water molecules. The stacking order is determined by hydrogen bonding of the latter to the second tetrahedral sheet. For the two-layer hydrate structures proposed for vermiculites in the literature were in large confirmed. However, modifications in details like ordering of alternative sites for  $[\text{Na}(\text{H}_2\text{O})_6]^+$  were suggested.

### Acknowledgements

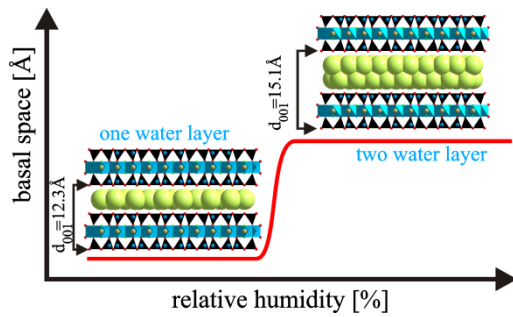
The authors thank the Bayerisches Geoinstitut, Bayreuth, Germany, for the WDX measurement. This work was supported financially by the graduate school ‘Structure, Reactivity and Properties of Oxide Materials’ within the Elitenetzwerk Bayern, the Deutsche Forschungsgemeinschaft (SFB 840), and the University of Aleppo.

- 1 R. T. Martin, S. W. Bailey, D. D. Eberl, D. S. Fanning, S. Guggenheim, H. Kodama, D. R. Pevear, J. Srodon and F. J. Wicks, *Clays Clay Miner.*, 1991, **39**, 333-335.
- 2 D. D. Eisenhour and R. K. Brown, *Elements*, 2009, **5**, 83-88.
- 3 A. Baumgartner, K. Sattler, J. Thun and J. Breu, *Angew. Chem. Int. Ed.*, 2008, **47**, 1640-1644.
- 4 M. Stöcker, W. Seidl, L. Seyfarth, J. Senker and J. Breu, *Chem. Commun.*, 2008, 629-631.
- 5 M. W. Möller, T. Lunkenbein, H. Kalo, M. Schieder, D. A. Kunz and J. Breu, *Adv. Mater.*, 2010, **22**, 5245-5249.
- 6 M. R. Schutz, H. Kalo, T. Lunkenbein, A. H. Groschel, A. H. E. Muller, C. A. Wilkie and J. Breu, *J. Mater. Chem.*, 2011, **21**, 12110-12116.
- 7 M. W. Möller, D. Hirsemann, F. Haarmann, J. Senker and J. Breu, *Chem. Mater.*, 2010, **22**, 186-196.
- 8 J. F. Alcover and L. Gatineau, *Clay Miner.*, 1980, **15**, 193-203.
- 9 J. F. Alcover and L. Gatineau, *Clay Miner.*, 1980, **15**, 25-35.
- 10 H. Suquet and H. Pezerat, *Clays Clay Miner.*, 1987, **35**, 353-362.
- 11 C. Delacalle, H. Suquet and C. H. Pons, *Clays Clay Miner.*, 1988, **36**, 481-490.
- 12 N. Malikova, E. Dubois, V. Marry, B. Rotenberg and P. Turq, *Z. Phys. Chem.*, 2010, **224**, 153-181.
- 13 M. W. Möller, U. A. Handge, D. A. Kunz, T. Lunkenbein, V. Altstadt and J. Breu, *Acs Nano*, 2010, **4**, 717-724.
- 14 T. J. Tambach, P. G. Bolhuis, E. J. M. Hensen and B. Smit, *Langmuir*, 2006, **22**, 1223-1234.
- 15 E. Ferrage, B. Lanson, N. Malikova, A. Plancon, B. A. Sakharov and V. A. Drits, *Chem. Mater.*, 2005, **17**, 3499-3512.
- 16 H. Kalo, M. W. Möller, M. Ziadeh, D. Dolej and J. Breu, *Appl. Clay Sci.*, 2010, **48**, 39-45.
- 17 V. Marry, E. Dubois, N. Malikova, S. Durand-Vidal, S. Longeville and J. Breu, *Environ. Sci. Technol.*, 2011, **45**, 2850-2855.

- 18 S. Guggenheim, J. M. Adams, F. Bergaya, M. F. Brigatti, V. A. Drits, M. L. L. Formoso, E. Galan, T. Kogure, H. Stanjek and J. W. Stucki, *Clays Clay Miner.*, 2009, **57**, 134-135.
- 19 N. T. Skipper, K. Refson and J. D. C. McConnell, *J. Chem. Phys.*, 1991, **94**, 7434-7445.
- 20 F. R. C. Chang, N. T. Skipper and G. Sposito, *Langmuir*, 1995, **11**, 2734-2741.
- 21 E. S. Boek, P. V. Coveney and N. T. Skipper, *J. Am. Chem. Soc.*, 1995, **117**, 12608-12617.
- 22 N. T. Skipper, F. R. C. Chang and G. Sposito, *Clays Clay Miner.*, 1995, **43**, 285-293.
- 23 P. G. Slade, P. A. Stone and E. W. Radoslovich, *Clays Clay Miner.*, 1985, **33**, 51-61.
- 24 H. Shirozu and S. W. Bailey, *Amer. Mineral.*, 1966, **51**, 1124-1143.
- 25 A. Arguelles, M. Leoni, J. A. Blanco and C. Marcos, *Amer. Mineral.*, 2010, **95**, 126-134.
- 26 K. Kitajima, F. Koyama and N. Takusagawa, *Bull. Chem. Soc. Jpn.*, 1985, **58**, 1325-1326.
- 27 M. Stöcker, L. Seyfarth, D. Hirsemann, J. Senker and J. Breu, *Appl. Clay Sci.*, 2010, **48**, 146-153.
- 28 J. Breu, W. Seidl, A. J. Stoll, K. G. Lange and T. U. Probst, *Chem. Mater.*, 2001, **13**, 4213-4220.
- 29 S. W. Bailey, *Amer. Mineral.*, 1982, **67**, 394-398.
- 30 J. Breu, W. Seidl and A. Stoll, *Z. Anorg. Allg. Chem.*, 2003, **629**, 503-515.
- 31 J. Beyer and H. G. von Reichenbach, *Clay Miner.*, 2002, **37**, 157-168.
- 32 G. M. Sheldrick, *Acta Crystallogr. A*, 2008, **64**, 112-122.
- 33 C. Delacalle and H. Suquet, *Rev. Mineral.*, 1988, **19**, 455-496.
- 34 C. Delacalle, A. Plancon, C. H. Pons, J. Dubernat, H. Suquet and H. Pezerat, *Clay Miner.*, 1984, **19**, 563-578.
- 35 A. Berghout, D. Tunega and A. Zaoui, *Clays Clay Miner.*, 2010, **58**, 174-187.
- 36 N. T. Skipper, A. K. Soper and J. D. C. McConnell, *J. Chem. Phys.*, 1991, **94**, 5751-5760.
- 37 R. P. Tenorio, M. Engelsberg, J. O. Fossum and G. J. da Silva, *Langmuir*, 2010, **26**, 9703-9709.
- 38 E. Ferrage, B. A. Sakharov, L. J. Michot, A. Delville, A. Bauer, B. Lanson, S. Grangeon, G. Frapper, M. Jimenez-Ruiz and G. J. Cuello, *J. Phys. Chem. C*, 2011, **115**, 1867-1881.

- 39 C. Delacalle, H. Suquet and H. Pezerat, *Clay Miner.*, 1985, **20**, 221-230.
- 40 A. Plancon, *Clay Miner.*, 2001, **36**, 1-14.
- 41 T. Kogure, J. Elzea-Kogel, C. T. Johnston and D. L. Bish, *Clays Clay Miner.*, 2010, **58**, 62-71.
- 42 P. G. Slade and P. A. Stone, *Clays Clay Miner.*, 1984, **32**, 223-226.

**TOC:** Melt synthesis yielded a highly charged swelling sodium fluorohectorite showing little stacking disorder as compared to natural clays. This allowed to refine for the first time both, the crystal structures of one- and two-layer hydrate of sodium fluorohectorite.



## Supporting Information:

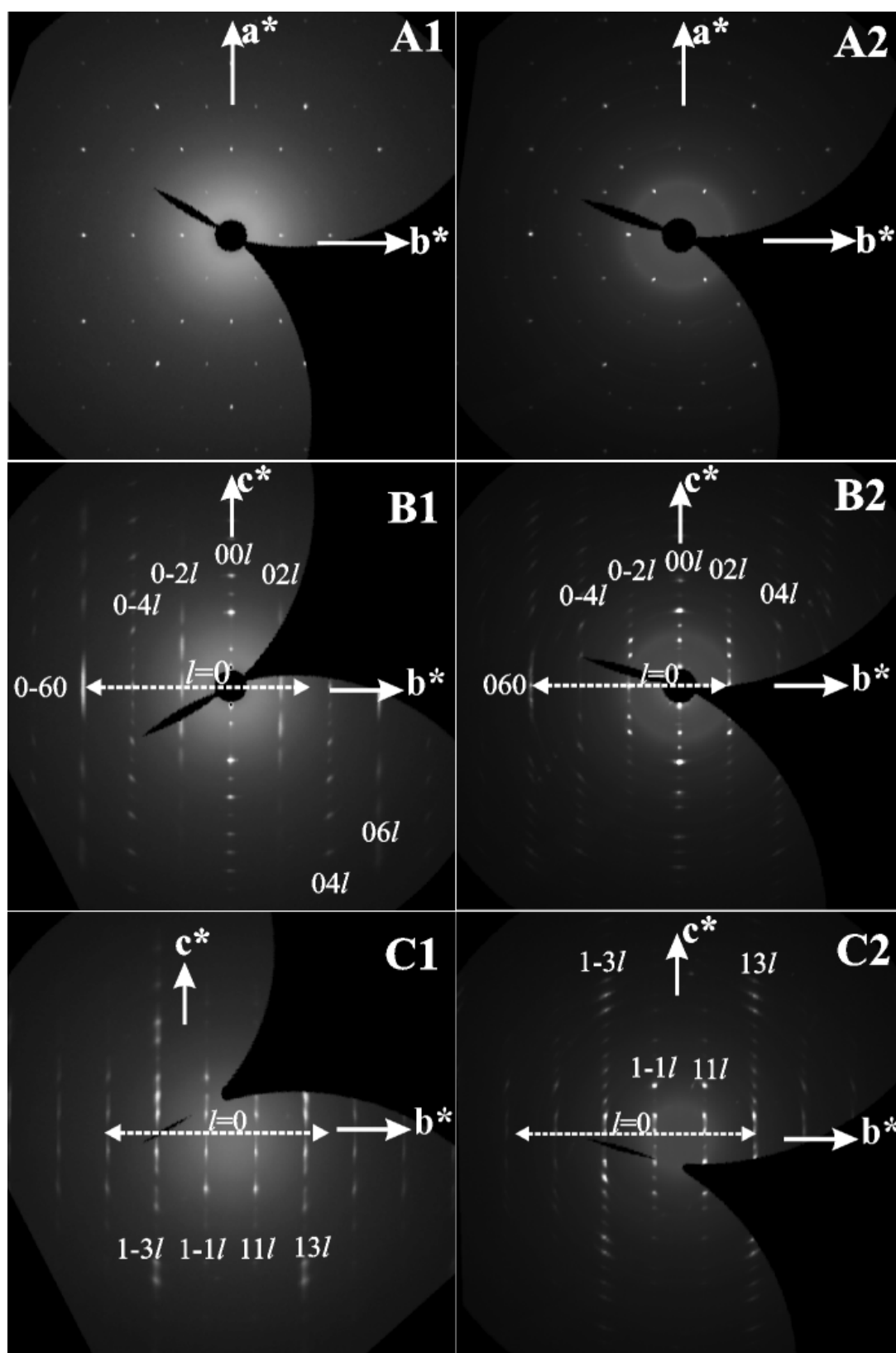


**Fig. S1** Reciprocal lattice space of 1WL (A1, B1, C1) and 2WL (A2, B2, C2) hydrate. The images of  $kh0$ ,  $0kl$  and  $lkl$  planes were created using the X-area software from STOE.

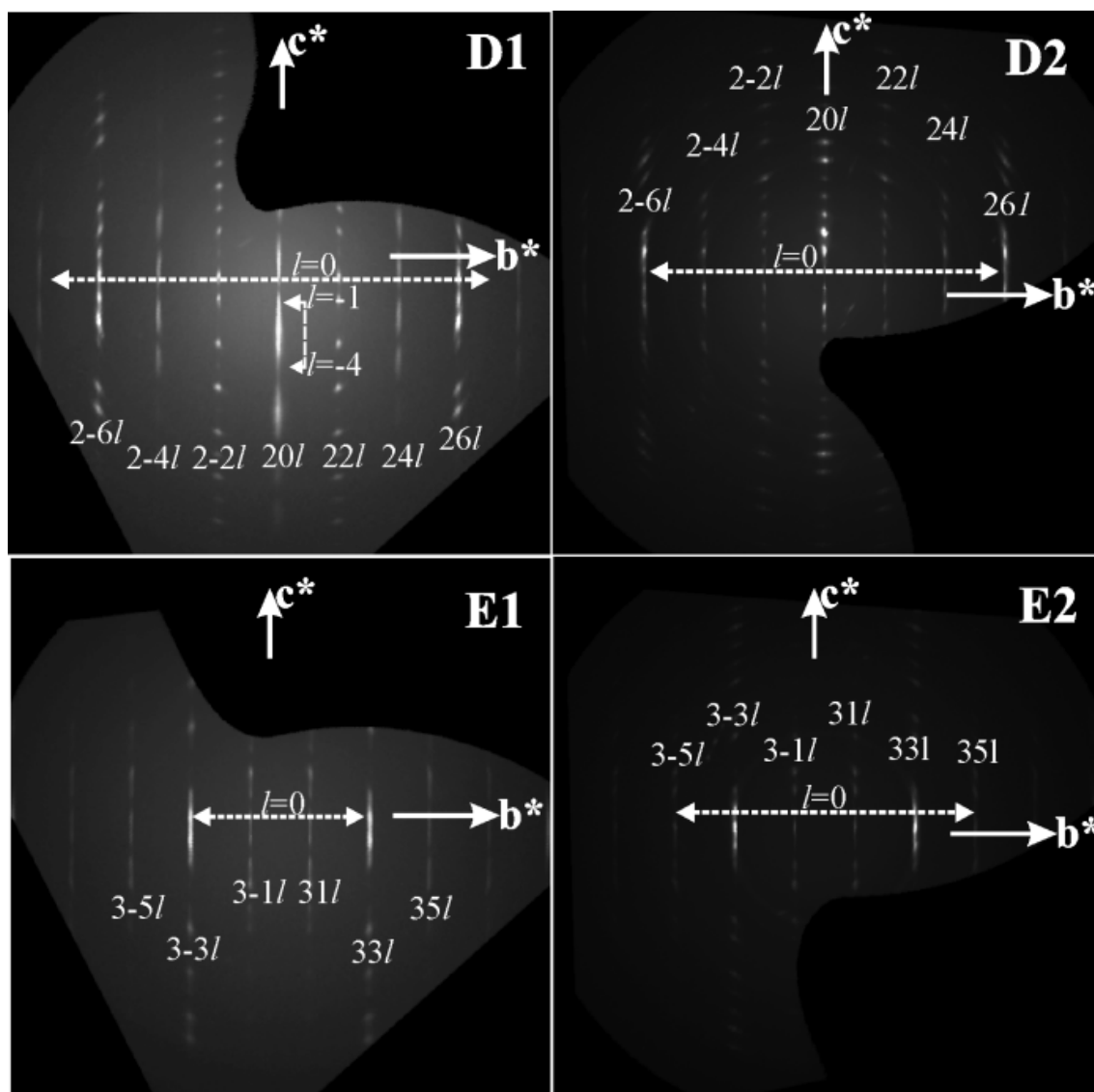


**Fig. S2** Reciprocal lattice space of 1WL (D1, E1) and 2WL (D2, E2) hydrate. The images of  $2hl$  and  $3kl$  planes were created using the X-area software from STOE.



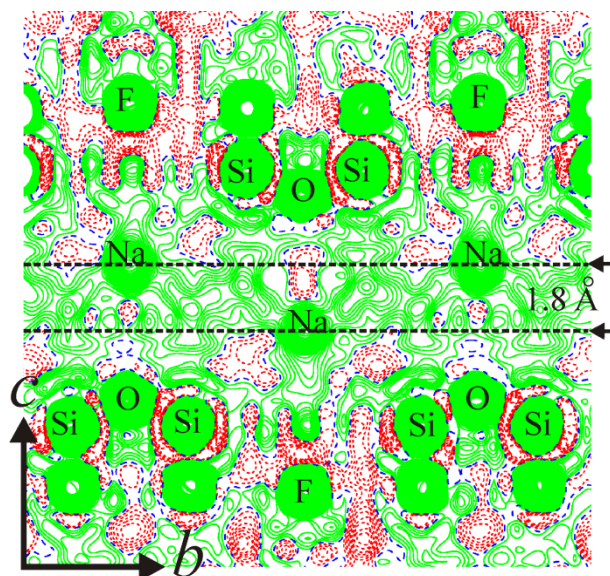


**Fig. S3** Fo-map of 1WL of Na-hect projected along  $a$ . Prominent electron density peaks are labeled.

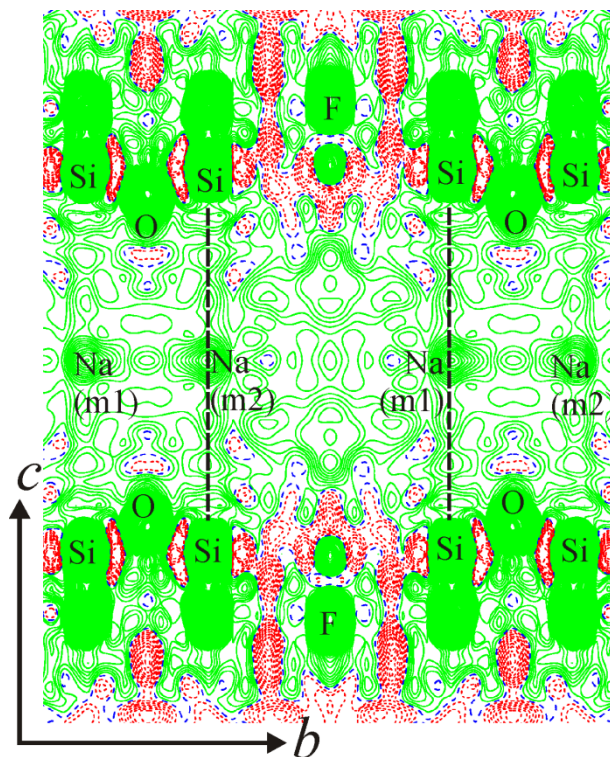


**Fig. S4** Fo-map of 2WL of Na-hect projected along  $a$ . Prominent electron density peaks are labeled.

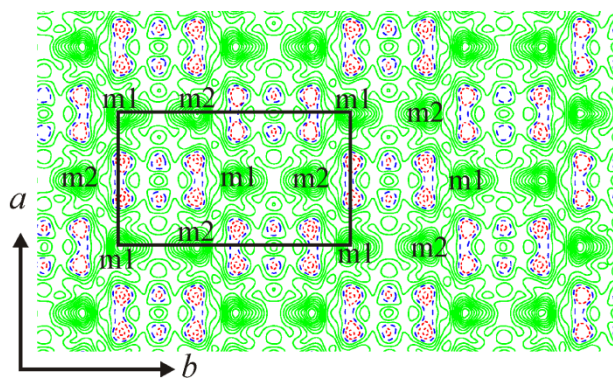


**Fig. S5** Fo-map of the  $ab$ -plane at  $z = 7\text{\AA}$  of 2WL of Na-hect. Note the equal electron density at m1 and m2 sites.

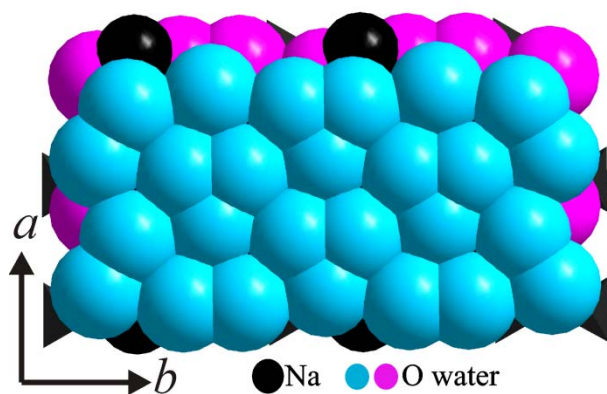


**Fig. S6** CPK representation of the interlayer space underlining the densely packed arrangement of interlayer water.

## Appendix 2

### **Large scale melt-synthesis in an open crucible of Na-fluorohectorite with superb charge homogeneity and particle size**

Hussein Kalo<sup>a</sup>, Michael W. Möller<sup>a</sup>, Mazen Ziadeh<sup>a</sup>, David Dolejš<sup>b</sup>, Josef Breu<sup>a,\*</sup>

<sup>a</sup> Lehrstuhl für Anorganische Chemie I, Universität Bayreuth, 95440 Bayreuth, Germany

<sup>b</sup> Bayerisches Geoinstitut, Universität Bayreuth, 95440 Bayreuth, Germany

\* Corresponding author. Tel.: +49921552530; fax: +49921552788.

E-mail address: josef.breu@uni-bayreuth.de (Prof. Dr. J. Breu)

**Published in Applied Clay Science, 2010, 48, 1-2, 39-45.**



# Large scale melt synthesis in an open crucible of Na-fluorohectorite with superb charge homogeneity and particle size<sup>☆</sup>

Hussein Kalo<sup>a</sup>, Michael W. Möller<sup>a</sup>, Mazen Ziadeh<sup>a</sup>, David Dolejš<sup>b</sup>, Josef Breu<sup>a,\*</sup>

<sup>a</sup> Lehrstuhl für Anorganische Chemie I, Universität Bayreuth, 95440 Bayreuth, Germany

<sup>b</sup> Bayerisches Geoinstitut, Universität Bayreuth, 95440 Bayreuth, Germany

## ARTICLE INFO

### Article history:

Received 14 July 2009

Received in revised form 28 September 2009

Accepted 11 November 2009

Available online 26 November 2009

### Keywords:

Fluorohectorite

Melt synthesis

Large scale synthesis

Charge homogeneity

## ABSTRACT

Sodium fluorohectorite  $\text{Na}_{0.6}[\text{Mg}_{2.4}\text{Li}_{0.6}]\text{Si}_4\text{O}_{10}\text{F}_2$  was synthesized from the melt in an open glassy carbon crucible at 1265 °C under argon flow. A glass ( $\text{Na}_2\text{O}-\text{Li}_2\text{O}-\text{SiO}_2$ ) precursor was used as a fluxing agent in order to maintain a low vapor pressure of volatile fluorides and sustain a low silica activity, which inhibits the formation of silicon fluoride gases and promotes the fluorine solubility in the melt. To minimize the loss of volatile fluorine compounds the pre-synthesized alkali silicate glass was heated together with additional raw materials needed in a high frequency induction furnace rapidly from 800 °C up to 1265 °C and then kept at this temperature for a short period of time (15 min). The synthesis method can easily be scaled to batches larger than 1 kg. The  $\text{Na}_{0.6}$ -fluorohectorite obtained stands out by (i) phase purity as checked by X-ray powder diffraction (PXRD), (ii) a superb homogeneity of the charge density as demonstrated by stepwise hydration behavior followed by in-situ PXRD in a humidity chamber and the Lagaly method with alkylammonium exchange (Mermut and Lagaly, 2001), (iii) a high cation exchange capacity (CEC) of 136 meq/100 g as determined by the copper complex ( $[\text{Cu}(\text{trien})]^{2+}$ ) method, and (iv) extreme lateral extensions with a median value of the particle size of 45  $\mu\text{m}$  as measured by static laser light scattering (SLS) which was confirmed by scanning electron microscopy (SEM).

© 2009 Elsevier B.V. All rights reserved.

## 1. Introduction

Swelling layered silicates of the 2:1 family are rigid 2-dimensional polyanions with a rich intracrystalline reactivity resulting, among other factors, from solvation and exchange of interlayer cations. This diverse chemistry of the interlamellar space gives way to a broad range of possible functionalization (Dekany et al., 1999; Baumgartner et al., 2008, 2009) and to exfoliation via osmotic swelling (Lagaly and Gardolinsky, 2005). This anisotropic top down by exfoliation, where only the height of the particles is reduced, delivers nano-platelets with extremely large aspect ratios which for instance may be used in gas barrier applications (Pinnavaia et al., 2006; Tetsuka et al., 2007). On one hand, for such applications the intracrystalline reactivity should be uniform over various length scales of the material, from domain to domain within a single lamellae, from one lamellae to the next lamellae within a tactoid, and finally from tactoid to tactoid. On the other hand, this lamellar 2:1-structure is extremely tolerant to chemical substitutions, which lead to a variety of solid solutions over wide ranges of composition.

For natural and some synthetic materials produced at low temperatures it has been established that the charge density is rather inhomogeneous, hence the intracrystalline reactivity is expected to be

non-uniform (Decarreau et al., 1992; Lagaly, 1995; Muller et al., 1997). Monte Carlo simulations of the order–disorder behavior of octahedral sheets of phyllosilicate lamellae confirm that for most compositions, the octahedral cations are short-range ordered, that is, the layers exhibit charge inhomogeneities at low temperatures (Palin et al., 2004). Although this short range order has been found to highly depend on the nature of the cation, temperatures often exceeding 1000 K are necessary to achieve a disordered solid solution with a homogenous charge density.

For a synthesis of swelling 2:1-layered silicate with a perfectly uniform distribution of isomorphous substitution one needs to consider the following issues: (i) at high temperatures, which are essential to ensure a true solid solution, the hydroxyl-containing members can only be synthesized in a closed system at elevated water pressure; (ii) compositional or temperature gradients may induce charge density inhomogeneities and ought to be minimized; (iii) also melts with the composition of fluorine-bearing end members will evolve volatile fluorides at temperatures >800 °C. This limits the reaction time available; (iv) among various binary alkali and alkali-earth silica systems, the  $\text{MgO}-\text{SiO}_2$  system displays the highest critical temperature of liquid–liquid immiscibility (>2000 °C, (McGahay and Tomozawa, 1989)) which further increases in the presence of fluorine (Markis et al., 1981). Therefore, besides gradients caused by evaporation, liquid–liquid miscibility gaps may be another source of inhomogeneity.

<sup>☆</sup> Dedicated to Prof. Hans-Jörg Deiseroth on the occasion of his 65th birthday.

\* Corresponding author. Tel.: +49 921552530; fax: +49 921552788.  
E-mail address: [josef.breu@uni-bayreuth.de](mailto:josef.breu@uni-bayreuth.de) (J. Breu).



With respect to these constraints, we have previously published a successful melt synthesis of fluorohectorites in gas-tight molybdenum crucibles that were rotated in a horizontal position during synthesis to assure mechanical mixing (Breu et al., 2001). The fluorohectorites obtained have a superb, so far unknown charge homogeneity as reflected by a well defined stepwise hydration behavior (Malikova et al., 2007). Major drawbacks of this method are, however, the cost of the non-reusable crucibles, the strict limitations in batch sizes due to the gas-tight sealing by lid welding, and the necessity of using highly pure anhydrous chemicals.

Commercially available materials in turn are of inferior quality mainly in respect to tactoid size, phase purity and/or charge homogeneity: Somasif™ is a synthetic clay manufactured by CBC Co. Ltd. that has a general formula  $(\text{Na})_{2x}(\text{Mg})_{3-x}(\text{Si}_4\text{O}_{10})(\text{F}_x\text{OH}_{1-a})_2$  where  $0.15 < x < 0.5$  and  $0.8 < a < 1.0$ . Somasif™ is a mixture of swelling fluorohectorite and non-swelling mica containing 0.1 wt.% Fe as additional impurity. Laponite is hydrothermally synthesized material from Laporte (Laporte industries, Ltd., UK) with the chemical formula  $\text{Na}_{0.66}(\text{Mg}_{5.34}\text{Li}_{0.66})\text{Si}_8\text{O}_{20}(\text{OH})_4$  (Utracki et al., 2007). This product has impurities that dissolve in water (Kaviratna et al., 1996) and the average particle size is reported to be as small as 0.02  $\mu\text{m}$ . Another material, named “swelling mica”,  $\text{NaMg}_{2.5}\text{Si}_4\text{O}_{10}\text{F}_2$ , is available from Topy (Topy Industries Ltd., Japan) and is prepared via a melt synthesis method. This product contains 20% cristobalite (Klapyta et al., 2001) and has a maximum particle size of 12  $\mu\text{m}$  (<http://www.topy.co.jp>). Some of  $\text{Na}^+$  is, however, non-exchangeable (Soma, et al. 1990, Tateyama et al., 1992) which indicates significant inhomogeneities.

For technical applications an economically prized and scalable method is desirable without having to accept compromises in materials properties in respect to aspect ratios or homogeneity of charge density. Designing a melt synthesis process of swelling 2:1-layer silicates with a perfectly uniform distribution of isomorphous substitution in an unsealed container remains, however, a challenging task. The synthesis process has to be carefully optimized for the choice of starting materials, reaction time and temperature settings. During this optimization matching of thermodynamic modeling of liquidus equilibria with the conditions of the synthesis process was essential.

Here we report a new simplified procedure for preparation of phase pure sodium fluorohectorite using temperature and reaction time as low and short as possible in an unsealed glassy carbon crucible. The material obtained, displays a uniform intracrystalline reactivity and high aspect ratios.

## 2. Experimental section

### 2.1. Preparation of $\text{Na}_{0.6}$ -fluorohectorite $\text{Na}_{0.6}[\text{Mg}_{2.4}\text{Li}_{0.6}]\text{Si}_4\text{O}_{10}\text{F}_2$

We have typically synthesized batches of 50 g  $\text{Na}_{0.6}$ -fluorohectorite; upscaling to batches larger than 1 kg proved to be feasible without additional problems. The synthesis involves three steps.

#### 2.1.1. Step 1

A glass with the composition  $\text{Na}_2\text{Li}_2\text{Si}_6\text{O}_{14}$  was prepared from 2.87 g  $\text{Li}_2\text{CO}_3$  ( $\geq 99.0\%$ , Merck), 4.11 g  $\text{Na}_2\text{CO}_3$  ( $\geq 99.5\%$ , Fluka) and 15.19 g silicic acid hydrate,  $\text{SiO}_2 \cdot x\text{H}_2\text{O}$  ( $\geq 99.0\%$ , Fluka) as a source for silicon dioxide. The mixture was ground and heated in a conic glassy carbon crucible ( $d = 85$  mm,  $b = 75$  mm,  $h = 130$  mm and 3 mm thick; HTW Hochtemperatur-Werkstoffe GmbH) at a rate of 300 °C/h up to 1075 °C to achieve melting. An argon flow was applied to prevent the oxidation of the crucible. The final temperature of 1075 °C was maintained for 1 h to evolve  $\text{CO}_2$  from the melt.

#### 2.1.2. Step 2

16.97 g basic magnesium carbonate,  $\text{MgCO}_3 \cdot \text{Mg}(\text{OH})_2 \cdot x\text{H}_2\text{O}$  (42.07% MgO, Acros) and 18.57 g silicic acid hydrate,  $\text{SiO}_2 \cdot x\text{H}_2\text{O}$  ( $\geq 99.0\%$ , Fluka) were used as additional sources for MgO and  $\text{SiO}_2$ .

The mixture of basic magnesium carbonate and silicic acid hydrate ( $M^*$ ) with a molar ratio of  $\text{MgO}/\text{SiO}_2 = 1.4/2.2$  was heated up to 900 °C for 1 h at a heating rate of 300 °C/h to achieve decarbonation and dehydration of the chemicals.

#### 2.1.3. Step 3

The synthetic glass  $\text{Na}_2\text{Li}_2\text{Si}_6\text{O}_{14}$  was combined with the devolatilized mixture  $M^*$  and an additional amount of 8.06 g  $\text{MgF}_2$  ( $>97\%$ , Fluka) was added to bring the total composition to the desired stoichiometry of the  $\text{Na}_{0.6}$ -fluorohectorite. For homogenization this mixture was ground in a ball mill for 30 min. The fine powder was directly transferred into a glassy carbon crucible, which was heated in a high radio-frequency induction furnace. The temperature was rapidly increased to 800 °C, maintained there for 5 min, then it was again increased rapidly to 1265 °C at which temperature the sample was held for 10–15 min. The melt was then quenched by switching off the power supply and it was allowed to cool inside the furnace to room temperature. Again, the melting steps were performed under an argon stream to prevent the oxidation of the crucible.

## 2.2. Characterization

Phase identification of the synthesized  $\text{Na}_{0.6}$ -fluorohectorite was performed by PXRD. The chemical composition was analyzed using wavelength dispersive X-ray fluorescence analysis (WD-XRF), inductively coupled plasma atomic emission spectrometry (ICP-AES) and atomic absorption spectroscopy (AAS). The CEC was determined applying the copper complex ( $[\text{Cu}(\text{trien})]^{2+}$ ) method (Ammann et al., 2005) and by exchange with barium chloride (Ruhlicke and Niederbudde, 1985; Mermut and Lagaly, 2001). The particle size distribution was measured by static laser light scattering (SLS) (Perez-Rodriguez et al., 2002).

### 2.2.1. Powder X-ray diffraction

The PXRD pattern of the one-layer hydrate of  $\text{Na}_{0.6}$ -fluorohectorite was obtained in transmission mode on a STOE Stadi powder diffractometer using  $\text{Cu K}\alpha_1$  radiation. To minimize texture effects, the sample was placed in a Lindemann glass capillary. The PXRD patterns of alkylammonium exchanged fluorohectorites were obtained in reflection mode on a PANalytical Xpert Pro equipped with a X'Celerator Scientific RTMS detector and using  $\text{Cu K}\alpha$  radiation. The samples were placed on flat glass holders. In-situ water desorption measurements were obtained in reflection mode on the same diffractometer using an Anton Paar temperature humidity chamber driven by a VTI Corp. RH-200 humidity generator.

### 2.2.2. Chemical analysis

Analysis of the synthesized  $\text{Na}_{0.6}$ -fluorohectorite was performed by AAS, ICP-AES, and WD-XRF. For the AAS and ICP-AES analyses, a 20 mg sample was weighed into a clean Teflon flask of 150 mL volume. After addition of 1.5 mL 30 wt.% HCl (Merck), 0.5 mL of 85 wt.%  $\text{H}_3\text{PO}_4$ , 0.5 mL 65 wt.%  $\text{HNO}_3$  (Merck) and 1 mL of 48 wt.%  $\text{HBF}_4$  (Merck) the sample was digested in a MLS 1200 Mega microwave digestion apparatus for 6.5 min and heated at 600 W (MLS GmbH, Mikrowellen-Labor-Systeme, Leutkirch, Germany). The closed sample container was cooled to room temperature and the clear solution was diluted to 100 mL in a volumetric flask. WD-XRF analysis was performed using borate glass discs (1.25 g sample + 5 g Spectroflux SF110A, Johnson Matthey Chemicals Ltd.) on a Joel JXA 8200 spectrometer, which was calibrated against certified mineral standards (Si – andradite  $\text{Ca}_3\text{Fe}_2\text{Si}_3\text{O}_{12}$ , O –  $\text{SiO}_2$ , F – fluorite  $\text{CaF}_2$ , Na – albite  $\text{NaAlSi}_3\text{O}_8$ ).

### 2.2.3. Cation exchange capacity

An amount of 0.2 g of synthetic  $\text{Na}_{0.6}$ -fluorohectorite dried at 110 °C for 24 h was dispersed in 100 mL distilled water (pH adjusted to 7) and was then shaken overnight. In the copper complex method,

10 mL of the suspension was transferred into a 25 mL centrifuge tube and 10 mL  $[\text{Cu}(\text{trine})]^{2+}$  was added. The sample was shaken for 24 h and then centrifuged, 3 mL of supernatant was transferred into a cuvette and the absorption was measured using monochromatic light with  $\lambda = 577$  nm. For the potential CEC using the barium chloride method 50 mL of the suspension was mixed with 50 mL of 1 M  $\text{BaCl}_2 \cdot 2\text{H}_2\text{O}$  solution, the mixture was shaken for 1 h, then centrifuged. The supernatant was discarded, and two additional exchange cycles were performed using 50 mL of barium chloride solution to ensure a complete exchange. The solid Ba-fluorohectorite was transferred into a 200 mL Erlenmeyer flask and 50 mL of 1 M ammonium acetate solution (to replace the exchanged  $\text{Ba}^{2+}$  cation) was added, shaken for 1 h, then centrifuged, and the procedure was repeated three times with the supernatant being collected in each cycle. The  $\text{Ba}^{2+}$  concentration was measured using the AAS method.

#### 2.2.4. Cation exchange with alkylammonium

Quantitative alkylammonium exchange was performed by standard published procedures (Lagaly, 1981 and 1994). The amines ( $\text{C}_n\text{H}_{2n+1}\text{NH}_2$ ;  $n = 3-9$ ; Aldrich) were converted to formates by neutralisation with formic acid (Lagaly, 1994).

#### 2.2.5. Particle size and shape

The particle size distribution was obtained from aqueous dispersion on a Retsch Horiba LA-950 SLS instrument with the same suspension as used for the CEC measurements. The refractive index of the solid phase was hereby set to a value of 1.5. SEM images were taken on a LEO 1530 FE-SEM at an operating voltage of 5 kV using an in-lens detection mode. Specimens were prepared by dripping a diluted aqueous sodium fluorohectorite dispersion onto a freshly cleaned silicon wafer. After drying, the samples were sputtered with a 2 nm platinum layer prior the measurements.

### 3. Results and discussion

#### 3.1. Thermodynamic modeling of liquidus equilibria

During synthesis, the reaction conditions must be carefully optimized in order to minimize the loss of volatile fluorine components. The essential factors determining fluorine loss are (i) low melting temperatures to maintain low vapor pressure of fluoride gaseous species, and (ii) low silica activity, which inhibits the formation of gaseous  $\text{SiF}_4$  and promotes the fluorine solubility in the melt. Therefore, we first evaluated the melting equilibrium in the system  $\text{Li}_2\text{O}-\text{Na}_2\text{O}-\text{MgO}-\text{SiO}_2$ . Phase diagram sections were calculated by Gibbs energy minimization using an internally consistent thermodynamic database for solid and liquid oxide phases (Pelton et al., 1989; Bale et al., 2002). The mixing properties of the silicate melt were described by the quasichemical model (Pelton and Blander, 1986). In this approach, thermodynamic properties in binary subsystems are defined by ordering of the nearest cation neighbors, e.g.,



The Gibbs energy of mixing in the melt,  $\Delta G_{\text{mix}}$ , consists of configurational and ordering contributions as follows:

$$\Delta G_{\text{mix}} = \Delta H_{\text{ord}} - T(\Delta S_{\text{ord}} + \Delta S_{\text{cfg}}), \quad (2)$$

where  $\Delta H_{\text{ord}}$  and  $\Delta S_{\text{ord}}$  are the standard equilibrium enthalpy and entropy, respectively, for equilibrium (1), and  $\Delta S_{\text{cfg}}$  is the configurational entropy resulting from mixing of cation-oxygen bonds in the framework of a one-dimensional Ising model. Optimized thermodynamic properties for  $\text{Na}_2\text{O}-\text{SiO}_2$  and  $\text{MgO}-\text{SiO}_2$  subsystems (Wu et al., 1993a, b) were employed in the present study.

The pseudoternary system  $\text{NaLiO}-\text{MgO}-\text{SiO}_2$  is characterized by large stability fields of  $\text{MgO}$ ,  $\text{Mg}_2\text{SiO}_4$ ,  $\text{MgSiO}_3$  and  $\text{SiO}_2$ , which extend over a broad temperature interval from 600 to 2800 °C (Fig. 1). The low-temperature (<700 °C) melting region is located along the alkali-silica join at  $\text{NaLiO}/\text{SiO}_2 = 0.8$  to 2. Liquidus surfaces of forsterite, enstatite and  $\text{SiO}_2$  polymorphs emanate from the low-temperature melting region and reach the final bulk composition near 1550 °C (Fig. 2). Consequently, the synthesis of  $\text{Na}_{0.6}[\text{Mg}_{2.4}\text{Li}_{0.6}]\text{Si}_4\text{O}_{10}\text{F}_2$  has been performed in three separate steps: (i) melting of alkali silicate composition ( $\text{NaLiSi}_3\text{O}_7$ ) at comparatively low temperature. The low  $(\text{Na} + \text{Li})/\text{Si}$  ratio = 2/3 would ensure increased solubility of fluorine in the silicate melt (Anfilogov et al., 1979; Shaw, 2004) whereas the low activity of silica inhibits fluorine vaporization as gaseous  $\text{SiF}_4$ ; (ii) decarbonation and dehydration of basic magnesium carbonate and silicic acid hydrate. Finally, (iii)  $\text{MgF}_2$ ,  $\text{MgO}$  and  $\text{SiO}_2$  are dissolved in the melt at 1265 °C. In contrast to the slow dissolution rate of  $\text{SiO}_2$  (Willgallis, 1969), rapid interaction of  $\text{MgF}_2$  and  $\text{MgO}$  with alkali-rich and  $\text{SiO}_2$ -poor melt provides a fluxing effect and it decreases the activity of silica, and this way it minimizes the volatile loss of fluorine components.

The mixed alkali silicate ( $\text{Li}_2\text{O}-\text{Na}_2\text{O}-\text{SiO}_2$ ) shows an advanced ability for glass formation as compared to alkali silicates ( $\text{Li}_2\text{O}-\text{SiO}_2$ ,  $\text{Na}_2\text{O}-\text{SiO}_2$ ) (Ota et al., 1995). Two distinct glass compositions ( $\text{Na}_2\text{Li}_2\text{Si}_4\text{O}_{10}$ ,  $\text{Na}_2\text{Li}_2\text{Si}_6\text{O}_{14}$ ) were initially tested as sources for sodium, lithium, and silicon and low melting flux. The  $\text{Na}_2\text{Li}_2\text{Si}_4\text{O}_{10}$  glass gave Na-fluorohectorite as primary phase, and silicon dioxide and protoamphibole as secondary phases during melt synthesis. The  $\text{Na}_2\text{Li}_2\text{Si}_6\text{O}_{14}$  glass did not produce any secondary phases. The formation of secondary  $\text{SiO}_2$  with  $\text{Na}_2\text{Li}_2\text{Si}_4\text{O}_{10}$  glass is probably related to local supersaturation due to the protoamphibole nucleation.

During the dissolution of the additional silicon dioxide the viscosity will increase (Fig. 2). Therefore, the starting materials were ground carefully to assure compositional homogeneity. These precautions help minimize the loss of volatile compounds, especially with increasing duration of dwelling at 1265 °C. The minimum duration of dwelling at 1265 °C necessary to produce a homogenous melt was determined experimentally by PXRD analysis of samples taken at different locations of the regulus. Due to a vigorous convection induced by the high frequency heating, only 15 min is sufficient to achieve the compositional homogeneity.

Nevertheless, when aiming at a desired final composition corresponding to a certain CEC of the synthetic Na-fluorohectorite, even minor vapor losses have to be balanced by adjusting the composition of the reacting material. The correction was determined iteratively. By starting with the ideal initial composition

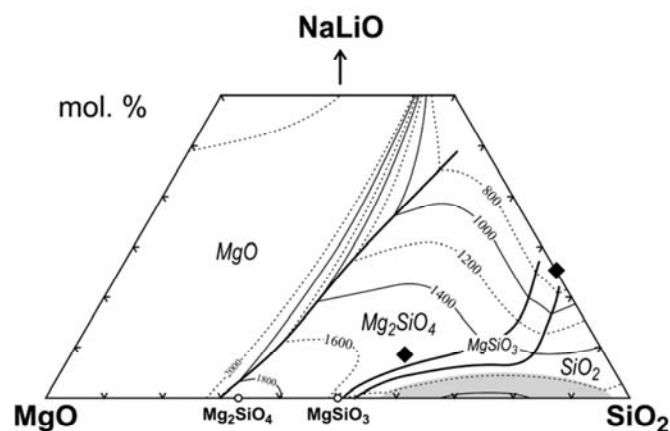


Fig. 1. Polythermal liquidus projection of the system  $\text{NaLiO}-\text{MgO}-\text{SiO}_2$  at 1 bar. The gray area indicates liquid-liquid immiscibility near the  $\text{MgO}-\text{SiO}_2$  join. The initial and final melt compositions are indicated by solid diamonds, respectively. Isotherms are labeled in °C.



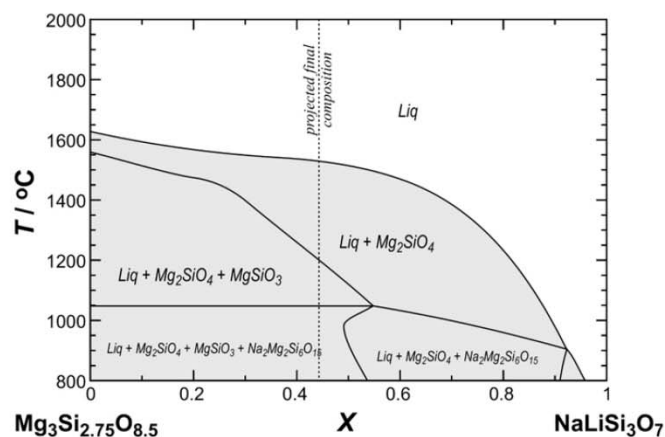


Fig. 2. Pseudobinary phase diagram section Mg<sub>3</sub>Si<sub>2.75</sub>O<sub>8.5</sub>–NaLiSi<sub>3</sub>O<sub>7</sub> at 1 bar illustrating rapid increase in the liquidus temperature as MgO and SiO<sub>2</sub> are added to the initial alkali silicate composition.

Na<sub>0.6</sub>[Mg<sub>2.4</sub>Li<sub>0.6</sub>]Si<sub>4</sub>O<sub>10</sub>F<sub>2</sub>, the mass loss during melt synthesis was determined by AAS of the experimental products. From the nominal composition, about 0.1 mol NaF and 0.2 mol LiF volatilized. Therefore, additional amounts of NaF and LiF were added in the final step to balance for the loss of fluorides. The chemical composition of the final product determined by WD-XRF was Na<sub>0.57</sub>[Mg<sub>2.41</sub>Li<sub>0.59</sub>]Si<sub>4</sub>O<sub>10</sub>F<sub>2</sub>, with standard errors for Na ± 0.01, Mg ± 0.01 and Si ± 0.02. Since this method cannot determine the Li concentration, the composition was normalized to Si<sub>4.00</sub> and to 22 negative charges according to fulfill the stoichiometry of Si<sub>4.00</sub>O<sub>10</sub>F<sub>2</sub>. The lithium cation contents were verified by AAS and ICP-AES analyses that gave 0.62 mol Na, 0.55 mol Li and 2.41 mol Mg.

It is noteworthy that the minimum mixing time and the magnitude of volatile loss are both dependent on the crucible geometry. Other geometries will require adjustments of the heating rates, the duration of dwelling, and the surplus amounts of LiF and NaF added.

### 3.2. X-ray diffraction analysis

The synthetic Na<sub>0.6</sub>-fluorohectorite is highly swelling. It spontaneously absorbs air moisture to form a monolayer hydrate (1 WL, ~2 H<sub>2</sub>O per formula unit (p.f.u.)) at ambient conditions (approximately 40% relative humidity). The X-ray diffractogram did not show any detectable crystalline byproduct. No amorphous background was obvious in the diffraction traces recorded in reflection mode. Given that a glass was used as a starting material, the presence of an amorphous phase cannot be ruled out completely. However, it is expected that such glass relics would not have the composition identical to that of crystalline hectorite. We have checked carefully by SEM in backscattering mode but were unable to detect any element contrast. Therefore, it appears unlikely that glass may coexist with the Na<sub>0.6</sub>-fluorohectorite.

Fig. 3 shows the powder diffraction pattern of the one-layer hydrate of Na<sub>0.6</sub>-fluorohectorite. The sharp 001 peak at 2θ = 7.14° (d = 12.3 Å) is narrow and has a high intensity indicating very thick tactoids. The 00l series is perfectly rational (coefficient of variation = 0.33), which is a strong indication of a very uniform intracrystalline reactivity. Please note, that even slight heterogeneities would immediately lead to random interstratifications of differently hydrated interlayers at any given relative humidity. At ambient conditions all interlamellar spaces are hydrated to the same level and there is no sign of statistical interstratification of different hydration states which would be common in natural smectites due to charge inhomogeneities.

While natural smectites are stacked turbostratically with random phase relationships between consecutive lamellae in a tactoid only, the planar defects in this highly charged synthetic Na<sub>0.6</sub>-fluorohectorite are substantially minimized. The 02/11-band at 2θ = 19.5 to 22.8°

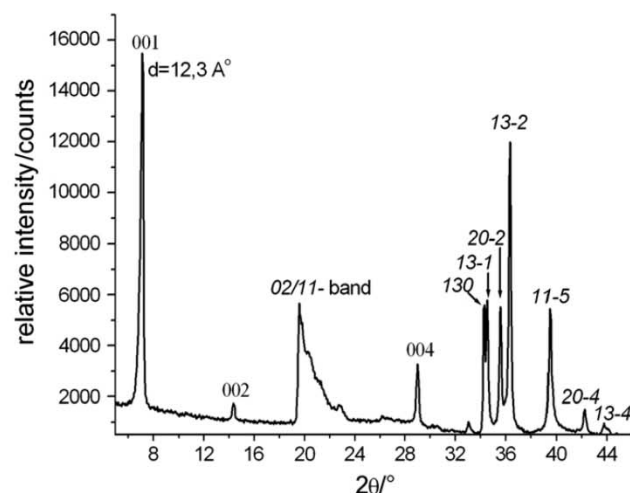


Fig. 3. PXRD profile of synthetic Na<sub>0.6</sub>[Mg<sub>2.4</sub>Li<sub>0.6</sub>]Si<sub>4</sub>O<sub>10</sub>F<sub>2</sub> (one-layer hydrate, d<sub>001</sub> = 12.3 Å).

still shows basically a λ-shape, although some shoulders become obvious. Sharp symmetric reflections are observed in the region of the 13/20-band and could be indexed (a = 5.21 Å, b = 9.08 Å, c = 12.39 Å, β = 98.9°). This diffraction pattern would be consistent with either n × 120° rotational or ± b/3 translational disorder (Breu et al., 2002). A detailed analysis is beyond the scope of this paper. Interestingly, Na<sub>0.6</sub>[Mg<sub>2.4</sub>Li<sub>0.6</sub>]Si<sub>4</sub>O<sub>10</sub>F<sub>2</sub> appears to be much less disordered than Na<sub>0.5</sub>[Mg<sub>2.5</sub>Li<sub>0.5</sub>]Si<sub>4</sub>O<sub>10</sub>F<sub>2</sub> published previously (Breu et al., 2001) suggesting that the disorder is substantially affected even by minor changes in the density of interlayer cations.

### 3.3. CEC determination

A satisfactory agreement was obtained between CEC values which were obtained using the copper complex method and the barium chloride method (potential CEC). Using the copper complex method, the measured CEC value was 136 meq/100 g and exceeded that determined by the barium chloride method (125 meq/100 g). The photometric copper complex method is more facile to perform and does not require filtration or any additional steps that might lead to a loss of exchangeable cations from the solution as compared to laborious filtration and washing steps that are required in the barium chloride method. The theoretical CEC calculated from the structural formula of Na<sub>0.6</sub>[Mg<sub>2.4</sub>Li<sub>0.6</sub>]Si<sub>4</sub>O<sub>10</sub>F<sub>2</sub> is 155 meq/100 g. The discrepancy of the experimental vs. the theoretical CEC values is attributed to the influence of layer edges that represent stoichiometric defects. It should be noted that the melt synthesis is anhydrous and consequently all tangling bonds at the edges will initially be saturated by Na<sup>+</sup>. Upon immersion into water these will be hydrolysed.

### 3.4. Homogeneity of the charge density

As pointed out in the introduction, the charge density homogeneity is a crucial property of swelling 2:1-layered silicates. We explored the homogeneity indirectly by investigating two intercalation reactions, which are sensitive to the charge density: (i) swelling with water as a function of the relative humidity (Ferrage et al., 2005, 2007; Oueslati et al., 2007; Tenorio et al., 2008), and (ii) cation exchange by alkylammonium cations of increasing chain length (Mermut and Lagaly, 2001).

#### 3.4.1. Hydration behavior

Fig. 4 illustrates the basal spacing of the 001-reflection recorded at 25 °C by PXRD as a function of relative humidity (r. h.). At high r. h., the 2 WL-hydrate (d = 15.0 Å) is the major swelling phase in addition to very



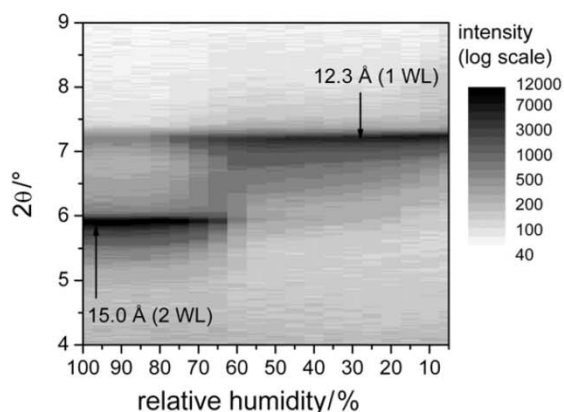


Fig. 4. Evolution of the 001 reflection of  $\text{Na}_{0.6}$ -fluorohectorite as a function of relative humidity (r. h.) at 25 °C. The humidity was decreased stepwise in 5% intervals. The sample was maintained 30 min at each r. h. value to assure equilibration.

small amounts of the 1 WL-hydrate ( $d = 12.3 \text{ \AA}$ ). Even with longer equilibration times at 100% r. h., the small amount of the 1 WL-hydrate remained constant indicating that a small volume fraction of the tactoids does indeed show an intracrystalline reactivity that differs significantly from the major phase. This might be explained by the unavoidable gradients in composition when working in an open system. At r. h. less than 75% the major swelling phase also dehydrates and converts into the 1 WL-hydrate. The transition is rather sharp indicating that all interlamellar spaces in a given tactoid display a similar intracrystalline reactivity. The range of r. h. where randomly interstratified tactoids are observed (as indicated by  $d$ -values differing from 15.0 Å or 12.3 Å) is very narrow.

### 3.4.2. Cation exchange with alkylammonium

As a final and possibly more sensitive test of the charge density homogeneity a layer charge determination according to Lagaly and Weiss was attempted. The area of an alkylammonium ion can be estimated to be  $1.27 \times 4.5 \times n + 14 \text{ (\AA}^2\text{)}$  (Lagaly and Weiss, 1971). Taking the unit cell size for the  $\text{Na}_{0.6}$ -fluorohectorite ( $ab = 47.3 \text{ \AA}^2$ ), the critical chain length expected for a layer charge of  $x = 0.6$  will be  $n = 4$ . Thus, starting with  $n = 5$  the charge density can only be satisfied by forming some bilayers. Note that since  $n$  is an integer number only the limits of the charge density can be estimated with this method.

For natural smectites the transition from the monolayer to the bilayer plateau is not sharp but instead a smooth transition for a range of intermediate chain lengths  $n$  is observed. Furthermore, the pronounced non-integrality of basal reflections in natural smectites indicates a random interstratification of differently expanded interlayer spaces. This is explained by the heterogeneity of charge densities in natural smectites (Lagaly, 1994). Such transitional chain lengths will still produce some monolayers for interlayers with lower cation densities while more highly charged interlayers already have to occur in the form of bilayers at the given  $n$ . The crystal is then composed of 13.4 Å and 17.6 Å layers in a random sequence. The ratio between these two will increase with  $n$  and the observed, apparent basal spacing, averaged by the X-ray diffraction, will migrate over the transition range until eventually only bilayers are present and give rise to sharp integral  $00l$  reflections again. With the help of charge migration curves the migration of the basal peak can be translated into a charge distribution histogram (Lagaly, 1981, 1994).

The patterns observed for both,  $\text{Na}_{0.5}[\text{Mg}_{2.5}\text{Li}_{0.5}]\text{Si}_4\text{O}_{10}\text{F}_2$  synthesized in a closed crucible (Breu et al., 2001) and for  $\text{Na}_{0.6}[\text{Mg}_{2.4}\text{Li}_{0.6}]\text{Si}_4\text{O}_{10}\text{F}_2$  synthesized in an open system (this work) upon cation exchange with alkylammonium are rather different from those of natural smectites. Fig. 5 shows PXRD pattern of the synthetic  $\text{Na}_{0.6}$ -fluorohectorite after complete exchange with alkylammonium cations of increasing chain

length. With  $\text{C}_3$  a sharp peak at  $d_{001} = 13.2 \text{ \AA}$  is observed in agreement with a flat arrangement of monolayers. While based on the average charge density the critical chain length is expected to be  $\text{C}_4$ , the experiment already showed some bilayers suggesting that some interlamellar spaces have a charge density of  $>0.64$  p.f.u. However, instead of a smooth shift of the apparent  $d$ -spacing due to random interstratification, three maxima at 13.2, 13.5 and 14.7 Å were observed. The first and the most intense peak refers to a monolayer arrangement. The second and the weakest peak is related to a random interstratification (R0) of mono- and bilayer arrangements. The remaining reflection may be interpreted as the 002-reflection of interstratified materials with Reichweite 1 (R1) and a probability ratio of mono- to bilayer larger than 1. This tendency to form ordered interstratified materials is underlined by the observation of a superstructure reflection at approximately 31–32 Å for  $\text{C}_6$ ,  $\text{C}_7$ , and  $\text{C}_8$ . Finally,  $\text{C}_9$  gives a single peak with a basal spacing corresponding to a pure bilayer arrangement (17.5 Å). To guide the eye, we have included a dot-dashed line in Fig. 5 at the ideal position ( $d = 15.35 \text{ \AA}$ ) expected for the 002-superstructure reflex of the perfectly ordered interstratification of mono- and bilayers (R1, probability 0.5).

A detailed analysis and complete description of these mixed-layer intercalation compounds require not only the identification of the types of layers involved, but also the proportions of each, and the type of order or lack thereof in the stacking sequence of monolayers and bilayers. While this certainly is beyond the scope of this paper, a qualitative holistic comparison of the evolution of PXRD profiles with increasing chain length ( $\text{C}_4$ – $\text{C}_8$ ) with the traces recorded for the previously published  $\text{Na}_{0.5}[\text{Mg}_{2.5}\text{Li}_{0.5}]\text{Si}_4\text{O}_{10}\text{F}_2$  synthesized in a closed crucible (Breu et al., 2001) is still very instructive (compare Fig. 10 in Breu et al., 2001). It can safely be stated here that for the intermediate chain lengths ( $\text{C}_4$ – $\text{C}_8$ ) fewer peaks are observed with smaller half widths for the material synthesized in closed crucible. Also, the intensity of the superreflection at 31–32 Å is higher for this material. All these observations are consistent with a somewhat lower charge homogeneity of the  $\text{Na}_{0.6}[\text{Mg}_{2.4}\text{Li}_{0.6}]\text{Si}_4\text{O}_{10}\text{F}_2$  synthesized in an open crucible. This would be expected as a consequence of the gradients in composition inherent from the synthesis in an open system. In summary, both types of intracrystalline reactions applied to test charge homogeneity show that the material synthesized in an open crucible is slightly less homogeneous as compared to the material synthesised in a closed crucible. Nevertheless, when comparing the intracrystalline reactivity with natural smectites or materials synthesized at low temperatures

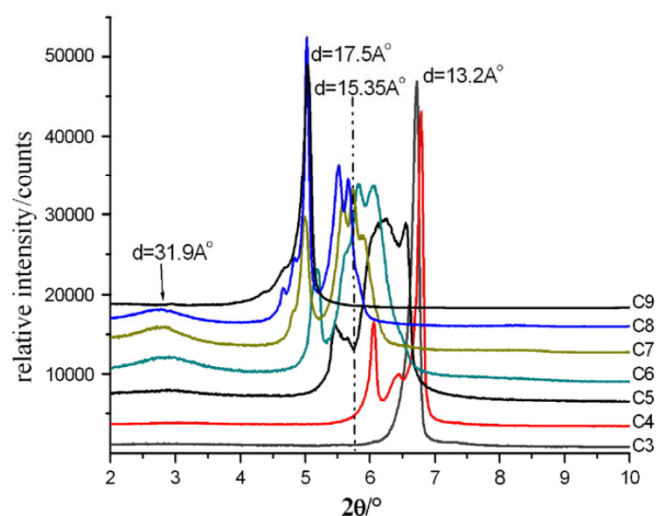


Fig. 5. Evolution of the PXRD profiles with increasing chain length ( $\text{C}_3$ – $\text{C}_9$ ) upon alkylammonium exchange of synthetic  $\text{Na}_{0.6}$ -fluorohectorite. The dot-dashed line at  $d = 15.35 \text{ \AA}$  represents the ideal position expected for the 002 superreflection of the perfectly ordered interstratification of mono- and bilayers (R1, probability 0.5).



(<200 °C),  $\text{Na}_{0.6}[\text{Mg}_{2.4}\text{Li}_{0.6}]\text{Si}_4\text{O}_{10}\text{F}_2$  obtained from the melt in an open crucible is by far superior in terms of homogeneity of charge density.

### 3.5. Particle size distribution

Clay minerals are characterized by small particle size (Meunier, 2006). Particle size increases with increasing layer charge (Taruta et al., 2005). Fig. 6 shows the particle size distribution of the synthesized  $\text{Na}_{0.6}[\text{Mg}_{2.4}\text{Li}_{0.6}]\text{Si}_4\text{O}_{10}\text{F}_2$  as measured by SLS after dispersion in water. The median of particle size distribution was found to be 45  $\mu\text{m}$ . SEM images (Fig. 7) showed typical lateral extensions of the tactoids between 10 and 15  $\mu\text{m}$ . This is very large even in the light of the high charge density of 0.6 p.f.u. The difference between values determined by SLS and SEM most likely is due to aggregates which could not be completely disaggregated by the short ultrasonic treatment applied prior to SLS.

### 3.6. Comparison with commercial synthetic smectites

To highlight the superiority of this sophisticated novel melt synthesis we briefly compare the material obtained with the commercially available competitors. Our synthetic sodium fluorohectorite is a pure phase, it displays superb charge homogeneity, and at the same time it shows large particle sizes (10–15  $\mu\text{m}$ ). As discussed in the Introduction, all available commercial materials (somasif, laponite, and swelling mica) are thus inferior in respect to this unique combination of high phase purity, homogeneity of the charge density and thus uniformity of intracrystalline reactivity, and large particle size.

## 4. Conclusions

$\text{Na}_{0.6}$ -fluorohectorite was successfully synthesized in an open glassy carbon crucible by a melt-assisted reaction. The method may easily be scaled to large quantities. Preliminary experiments show that the composition of the materials can also be adjusted easily to vary the layer charge from 0.4 to 0.7.

At the temperatures required to generate a homogenous melt, the loss of volatile fluoride components cannot be completely avoided in an open system, leading to unavoidable gradients in composition. Despite this gradient, the materials showed a superb homogeneity of the charge density as suggested by a uniform intracrystalline reactivity. The key factors for the resulting homogeneity are: (i) thermodynamic modeling of liquidus equilibria in the system  $\text{Li}_2\text{O}-\text{Na}_2\text{O}-\text{MgO}-\text{SiO}_2$  helped identify low melting glass compositions that at the same time display

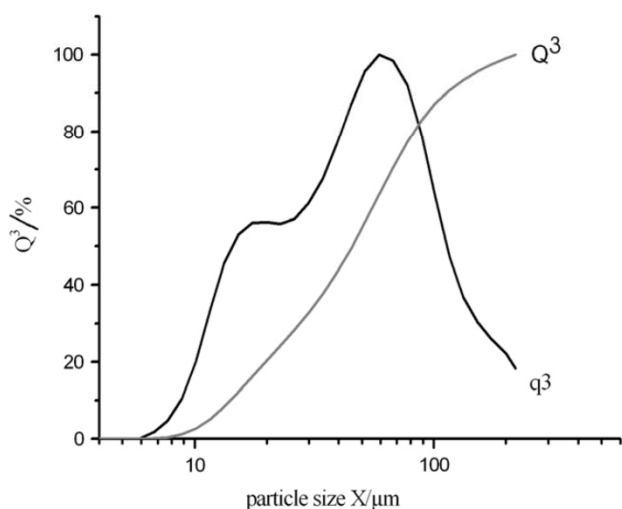


Fig. 6. Particle size distribution of the  $\text{Na}_{0.6}$ -fluorohectorite as analyzed by SLS following ultrasonic treatment for 1 min.

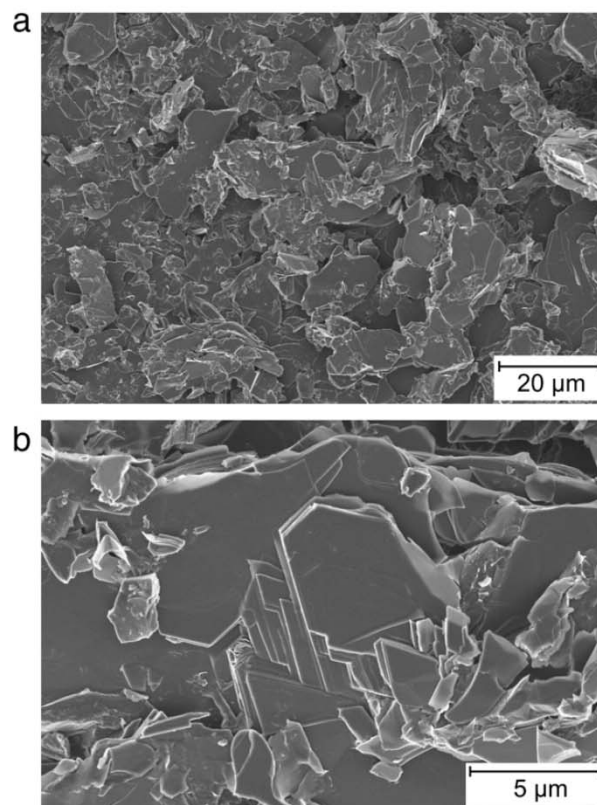


Fig. 7. Representative SEM micrographs of the synthesized  $\text{Na}_{0.6}$ -fluorohectorite.

a low silica activity, which inhibits the formation of gaseous  $\text{SiF}_4$  and promotes the fluorine solubility in the melt; (ii) effective high frequency heating assures high heating rates and efficient mixing by convection which allows to minimize the duration of dwelling at 1265 °C to 15 min. The applied temperature not only produces a homogeneous melt but a crystallization from high temperature leads to a true solid solution with isomorphous substitution, which is a prerequisite for charge homogeneity. The fast crystallization within a few minutes produces large tactoids and no impurities like  $\text{SiO}_2$  or amphiboles are observed.

### Acknowledgments

We are grateful to Lutful Arefin (Fraunhofer Institut für Silicatforschung, Würzburg) for his help with the thermodynamic modeling data and to Detlef Krauß (Bayerisches Geoinstitut, Universität Bayreuth) for his assistance with electron microprobe analyses. This work was financially supported by the graduate school “Structure, Reactivity and Properties of Oxide Materials” within the Elitenetzwerk Bayern and the Deutsche Forschungsgemeinschaft (SFB 840).

### References

- Ammann, L., Bergaya, F., Lagaly, G., 2005. Determination of the cation exchange capacity of clays with copper complexes revisited. *Clay Minerals* 40, 441–453.
- Anfilogov, V.N., Bragina, G.I., Bobylev, I.B., Zyuzeva, N.A., 1979. Fluorine and chlorine structural position in silicate melt. *Geokhimiya* 1, 30–36.
- Bale, C., Chartrand, P., Degterov, S.A., Eriksson, G., Hack, K., Ben Mahfoud, R., Melancon, J., Pelton, A.D., Petersen, S., 2002. FactSage thermochemical software and databases. *Calphad-Computer Coupling of Phase Diagrams and Thermochemistry* 26 (2), 189–228.
- Baumgartner, A., Sattler, K., Thun, J., Breu, J., 2008. A route to microporous materials through oxidative pillaring of micas. *Angewandte Chemie-International Edition* 47 (9), 1640–1644.
- Baumgartner, A., Wagner, F.E., Herling, M., Breu, J., 2009. Towards a tunable pore size utilizing oxidative pillaring of the mica ferrous tainiolite. *Microporous and Mesoporous Materials* 123 (1–3), 253–259.
- Breu, J., Seidl, W., Stoll, A.J., Lange, K.G., Probst, T.U., 2001. Charge homogeneity in synthetic fluorohectorite. *Chemistry of Materials* 13, 4213–4220.

- Breu, J., Seidl, W., Stoll, A., 2002. Fehlordnung bei Smectiten in Abhängigkeit vom Zwischenschichtkation. *Zeitschrift für Anorganische und Allgemeine Chemie* 629, 503–515.
- Decarreau, A., Grauby, O., Petit, S., 1992. The actual distribution of octahedral cations in 2:1 clay minerals: results from clay synthesis. *Applied Clay Science* 7 (1–3), 147–167.
- Dekany, I., Turi, L., Kiraly, Z., 1999. CdS, TiO<sub>2</sub> and Pd-circle nanoparticles growing in the interlamellar space of montmorillonite in binary liquids. *Applied Clay Science* 15 (1–2), 221–239.
- Ferrage, E., Lanson, B., Malikova, N., Plancon, A., Sakharov, B.A., Drits, V.A., 2005. New insights on the distribution of interlayer water in bi-hydrated smectite from X-ray diffraction profile modeling of 001 reflections. *Chemistry of Materials* 17 (13), 3499–3512.
- Ferrage, E., Lanson, B., Sakharov, B.A., Geoffroy, N., Jacquot, E., Drits, V.A., 2007. Investigation of dioctahedral smectite hydration properties by modeling of X-ray diffraction profiles: influence of layer charge and charge location. *American Mineralogist* 92, 1731–1743.
- Kaviratna, P.D., Pinnavaia, Thomas J., Schroeder, P.A., 1996. Dielectric properties of smectite clays. *Journal of Physics and Chemistry of Solids* 57 (12), 1897–1906.
- Klapayta, Z., Fujita, T., Iyi, N., 2001. Adsorption of dodecyl- and octadecyltrimethylammonium ions on a smectite and synthetic micas. *Applied Clay Science* 19 (1–6), 5–10.
- Lagaly, G., 1981. Characterization of clays by organic compounds. *Clay Minerals* 16, 1–21.
- Lagaly, G., 1994. Layer charge determination by alkylammonium ions. In: Mermut, A.R. (Ed.), *Layer Charge Characteristics of 2:1 Silicate Clay Minerals*. Clay Mineral Society, pp. 1–46.
- Lagaly, G., 1995. Surface and interlayer reactions: bentonites as adsorbents. In: Churchman, G.J., Fitzpatrick, R.W., Eggleton, R.A. (Eds.), *Clays Controlling the Environment*. CSIRO publishing, Melbourne, pp. 137–144.
- Lagaly, G., Gardolinsky, J.E.F.C., 2005. Grafted organic derivatives of kaolinite: II. Intercalation of primary n-alkylamines and delamination. *Clay Minerals* 40 (4), 547–556.
- Lagaly, G., Weiss, A., 1971. Anordnung und Orientierung kationischer Tenside auf Silicatoberflächen. *Kolloid-Zeitschrift und Zeitschrift für Polymere* 243, 48–55.
- Malikova, N., Cadene, A., Dubois, E., Marry, V., Durand-Vidal, S., Turq, P., Breu, J., Longeville, S., Zanotti, J.M., 2007. Water diffusion in a synthetic hectorite clay studied by quasi-elastic neutron scattering. *Journal of Physical Chemistry C* 111 (47), 17603–17611.
- Markis, J.H., Clemens, K., Tomozawa, M., 1981. Effect of fluorine on the phase separation of Na<sub>2</sub>O–SiO<sub>2</sub> glasses. *Journal of the American Ceramic Society* 64, C20.
- McGahay, V., Tomozawa, M., 1989. The origin of phase separation in silicate melts and glasses. *Journal of Non-Crystalline Solids* 109, 27–34.
- Mermut, A.R., Lagaly, G., 2001. Baseline studies of the Clay Minerals Society Source Clays: layer-charge determination and characteristics of those minerals containing 2:1 layers. *Clays and Clay Minerals* 49 (5), 393–397.
- Meunier, A., 2006. Why are clay minerals small? *Clay Minerals* 41 (2), 551–566.
- Muller, F., Besson, G., Manceau, A., Drits, V.A., 1997. Distribution of isomorphous cations within octahedral sheets in montmorillonite from Camp-Bertaux. *Physics and Chemistry of Minerals* 24 (3), 159–166.
- Ota, R., Wakasugi, T., Kawamura, W., Tuchiya, B., Fukunaga, J., 1995. Glass formation and crystallization in Li<sub>2</sub>O–Na<sub>2</sub>O–K<sub>2</sub>O–SiO<sub>2</sub>. *Journal of Non-Crystalline Solids* 188 (1–2), 136–146.
- Oueslati, W., Karmous, M.S., Rhaïem, H., Lanson, B., Amara, A.B.H., 2007. Effect of interlayer cation and relative humidity on the hydration properties of a dioctahedral smectite. *Zeitschrift für Kristallographie* 26, 417–422.
- Palin, E.J., Dove, M.T., Hernandez-Laguna, A., Sainz-Diaz, C.I., 2004. A computational investigation of the Al/Fe/Mg order-disorder behavior in the dioctahedral sheet of phyllosilicates. *American Mineralogist* 89 (1), 164–175.
- Pelton, A.D., Blander, M., 1986. Thermodynamic analysis of ordered liquid solutions by a modified quasi-chemical approach – application to silicate slags. *Metallurgical Transactions B-Process Metallurgy* 17 (4), 805–815.
- Pelton, A.D., Thompson, W.T., Bale, C.W., Eriksson, G., 1989. FactSage thermochemical database for calculations in materials chemistry at high-temperatures. *High Temperature Science* 26, 231–250.
- Perez-Rodriguez, J.L., Carrera, F., Poyato, J., Perez-Maqueda, L.A., 2002. Sonication as a tool for preparing nanometric vermiculite particles. *Nanotechnology* 13 (3), 382–387.
- Pinnavaia, T.J., Park, I., LeBaron, P.C., Triantafyllidis, K.S., 2006. Epoxy clay fabric film composites with unprecedented oxygen barrier properties. *Chemistry of Materials* 18, 4393–4398.
- Ruhlicke, G., Niederbudde, E.A., 1985. Determination of layer-charge density of expandable 2:1 clay minerals in soils and loess sediments using the alkylammonium method. *Clay Minerals* 20 (3), 291–300.
- Shaw, C.S.J., 2004. Mechanisms and rates of quartz dissolution in melts in the CMAS (CaO–MgO–Al<sub>2</sub>O<sub>3</sub>–SiO<sub>2</sub>) system. *Contributions to Mineralogy and Petrology* 148 (2), 180–200.
- Soma, M., Tanaka, A., Seyama, H., Hayashi, S., Hayamizu, K., 1990. Bonding states of sodium in tetrasilicic sodium fluor mica. *Clay Science* 8, 1–8.
- Taruta, Seiichi, Obara, Ryo, Takusagawa, Nobuo, Kitajima, Kunio, 2005. Effect of layer charge on chemical and physical properties of synthetic K-fluorine micas. *Journal of Materials Science* 40 (21), 5597–5602.
- Tateyama, H., Nishimura, S., Tsunematsu, K., Jinnai, K., Adachi, Y., Kimura, M., 1992. Synthesis of expandable fluorine mica from talc. *Clays and Clay Minerals* 40 (2), 180–185.
- Tenorio, R.P., Alme, L.R., Engelsberg, M., Fossum, J.O., Hallwass, F., 2008. Geometry and dynamics of intercalated water in Na-fluorhectorite clay hydrates. *Journal of Physical Chemistry C* 112 (2), 575–580.
- Tetsuka, H., Ebina, T., Nanjo, H., Mizukami, F., 2007. Highly transparent flexible clay films modified with organic polymer: structural characterization and intercalation properties. *Journal of Materials Chemistry* 17 (33), 3545–3550.
- Utracki, L.A., Sepehr, M., Boccaleri, E., 2007. Synthetic, layered nanoparticles for polymeric nanocomposites WNCO. *Polymers for Advanced Technologies* 18 (1), 1–37.
- Willgallis, A., 1969. Beitrag zum System SiO<sub>2</sub>–Na<sub>2</sub>O–NaF. *Glastechnische Berichte* 42, 506–509.
- Wu, P., Eriksson, G., Pelton, A.D., 1993a. Optimization of the thermodynamic properties and phase diagrams of the Na<sub>2</sub>O–SiO<sub>2</sub> and K<sub>2</sub>O–SiO<sub>2</sub> systems. *Journal of the American Ceramic Society* 76 (8), 2059–2064.
- Wu, P., Eriksson, G., Pelton, A.D., Blander, M., 1993b. Prediction of the thermodynamic properties and phase diagrams of silicate systems – evaluation of the FeO–MgO–SiO<sub>2</sub> system. *ISIJ International* 33 (1), 26–35.

# Appendix 3

## How to Maximize the Aspect Ratio of Clay Nanoplatelets

Hussein Kalo<sup>†</sup>, Michael W. Möller<sup>†</sup>, Daniel A. Kunz<sup>†</sup> and Josef Breu<sup>†\*</sup>

<sup>†</sup>Lehrstuhl für Anorganische Chemie I, University of Bayreuth, D-95440 Bayreuth, Germany

\* Corresponding author: Prof. Dr. Josef Breu, Phone: 0049921552531 Fax: 0049921552788

E-mail: [Josef.Breu@uni-bayreuth.de](mailto:Josef.Breu@uni-bayreuth.de)

Nanoscale, DOI: 10.1039/C2NR31322G

## How to Maximize the Aspect Ratio of Clay Nanoplatelets

Hussein Kalo, Michael W. Möller, Daniel A. Kunz, and Josef Breu\*

Lehrstuhl für Anorganische Chemie I, University of Bayreuth, D-95440 Bayreuth, Germany

\* Corresponding author: Prof. Dr. Josef Breu, Phone: 0049921552531 Fax: 0049921552788

E-mail: [Josef.Breu@uni-bayreuth.de](mailto:Josef.Breu@uni-bayreuth.de)

### Abstract

Melt-synthesis yielded Lithium-fluorohectorite (Li-hect<sub>x</sub>) with variable layer charge ( $x = 0.4, 0.6, 0.8, 1.0$ ). Counter intuitively, both tactoid diameter and intracrystalline reactivity increased concomitantly with increasing layer charge. This way hectorites with very large diameters were obtained ( $d_{50\%} = 48 \mu\text{m}$ ) that nevertheless still spontaneously delaminate when immersed into water and nano-platelets with huge aspect ratios ( $> 10000$ ) are formed. Melt-synthesis of Li-hect<sub>x</sub> has been performed in an open glassy carbon crucible allowing for easy scaling to batches of 500g. These unprecedented huge aspect ratio fillers promise great potential for flame retardants and barrier applications.

**Keywords:** Li-fluorohectorite, high aspect ratio, spontaneous delamination, barrier filler, osmotic swelling.



## 1. Introduction

Aspect ratio of fillers is the key factor in improving properties of polymer nanocomposites.<sup>1-3</sup> Fortunately, for clays the intracrystalline reactivity allows for extensive variation of properties and functions post synthesis.<sup>4-7</sup> For instance the ionic conductivity may be optimized for battery applications,<sup>8</sup> the mechanical properties of clay platelets may be tuned by controlled exfoliation,<sup>9</sup> or aspect ratios may be maximized via osmotic swelling.<sup>10</sup> Exfoliation into thinner tactoids or delamination into singular 2:1-lamellae represents an anisotropic top-down process (Figure 1a) that delivers nano-platelets with large aspect ratios  $\alpha$ , which for instance may be used in gas barrier applications.<sup>11,12</sup> Exfoliation may be triggered by applying mechanical force (platelets are sheared apart), which, however, concomitantly always will induce some breakage of tactoids.<sup>3</sup> Aspect ratios will thus only increase during mechanical agitation if shearing wins over breakage (Figure 1b). Due to comparatively high hydration enthalpies of selected interlayer cations, for 2:1 clay minerals spontaneous delamination via osmotic swelling represents an attractive alternative to mechanical force for maximizing the aspect ratio. Numerous publications focused on the influence of interlayer cations such as  $\text{Li}^+$ ,  $\text{Na}^+$ ,  $\text{K}^+$ ,  $\text{Mg}^{2+}$ ,  $\text{Ca}^{2+}$ ,  $\text{Sr}^{2+}$ , and  $\text{Ba}^{2+}$  on the hydration behaviour of swelling layered silicates,<sup>13,14</sup> and usually the highest degree of hydration was observed with  $\text{Li}^+$ . In that line, commercially available synthetic Li-hectorites (laponite-type clays) are well known for spontaneous delamination. Unfortunately, hydrothermal synthesis of these laponites yields very small tactoids (< 30 nm in diameter) and therefore even complete delamination delivers only mediocre aspect ratios. Therefore, these materials are very good rheological additives because the number of independent particles per mass is high and edge-face interactions are dominant interparticle interactions in suspension triggering gelling. Their performance as fillers is however dreadful because of the low maximum aspect ratios (< 30). For high aspect ratio nano-platelets, the diameter of tactoids have first to be significantly increased (Figure 1c) followed by a maximization of  $\alpha$  by delamination (Figure 1d).

We have previously shown that melt synthesis yields Na-hectorites with large tactoid sizes.<sup>15,16</sup> While these Na-hectorites easily desagglomerated and exfoliated in platelets of some 10 nm thickness, this material did not spontaneously delaminate. Na-hectorites can of course easily be converted to Li-heck by repeated exchange with  $\text{Li}^+$  and this way the swelling in water can be improved. This ion exchange is, however, time consuming and we therefore sought after a direct access to Li-heck.

High temperature synthesis of clays with interlayer  $\text{Li}^+$  is, however, difficult. The small ionic radius of  $\text{Li}^+$  hampers the synthesis of Li-mica as mentioned by Taruta S. et al.<sup>17</sup> Furthermore, phase segregation in the melt of the ternary system  $\text{Li}_2\text{O-SiO}_2\text{-MgO}$  represents a severe problem for homogeneity.<sup>18</sup> The melt separates into two phases, one is enriched in network modifier ( $\text{Mg}^{2+}$  and  $\text{Li}^+$ ) and the other phase is enriched in silica. Generally, phase segregation in silicate melts is fostered by increasing ionic potentials ( $Z/r$ ) ( $Z$  stands for the valence and  $r$  is radius) of the network modifier, i.e. the problem eases in the series  $\text{Mg}^{2+} > \text{Li}^+ > \text{Na}^+ > \text{K}^+ > \text{Cs}^+$ .<sup>19-23</sup> Additionally, it is known that fluoride in alkali silica melts increases the immiscibility gap and decreases the viscosity of the silicate melt.<sup>24,25</sup> Gibbs et al. have studied the system  $\text{Li}_2\text{O-MgO-MgF}_2\text{-SiO}_2$  within the temperature range of 1350 to 1450 °C and identified a mixture of layered silicate and protoamphibole.<sup>26</sup> Following work by Barrer and Jones, Corning Glass, Inc. company synthesized Li-hect in the 1970s with a chemical composition of  $[\text{Li}_{0.56}]^{\text{inter}}[\text{Mg}_{2.44}\text{Li}_{0.56}]^{\text{oct}}[\text{Si}_4]^{\text{tet}}\text{O}_{10}\text{F}_2$  and a cation exchange capacity of 122 meq/100g.<sup>27</sup> Unfortunately, this material is not available any longer. Eitel et al. have proven the advantage of  $\text{MgF}_2$  to synthesize mica in solid state reactions at high temperatures between 1100 and 1350 °C,<sup>28</sup> and the disadvantage of open melt-synthesis methods (evaporation of volatile precursors). In summary of the literature, it was clear that synthesis of Li-fluorohectorite cannot be expected to be straight forward.

The type of starting materials, their chemical composition, the melt temperature of the eutectic, heating program/temperature gradients are the main variables to be optimized. Here we demonstrate an undemanding method for the synthesis of variable layer charge Li-hect<sub>x</sub> with  $x$  being in the range 0.4 to 1.0 per formula unit (p.f.u.). The composition of starting materials was optimized to achieve high silica activity while decreasing the fugacity of volatile compounds and minimizing reaction temperature and time. To avoid the nucleation of the protoamphibole side-phase, short reaction times and precursors composed of lithium rich silicates and magnesium fluoride were used. Our ultimate goal, however, was to obtain high aspect ratio nano-platelets by spontaneous delamination in water. The challenge we are tackling in this paper is therefore to maximize the lateral dimension of the tactoids during synthesis while keeping the intracrystalline reactivity sufficiently high to foster spontaneous delamination by osmotic swelling post synthesis. As long as the latter is provided, the anisotropic top-down will deliver nanoplatelets of huge aspect ratio. Therefore, we studied the swelling behavior of the synthesized Li-hect<sub>x</sub> as a function of varying layer charge.

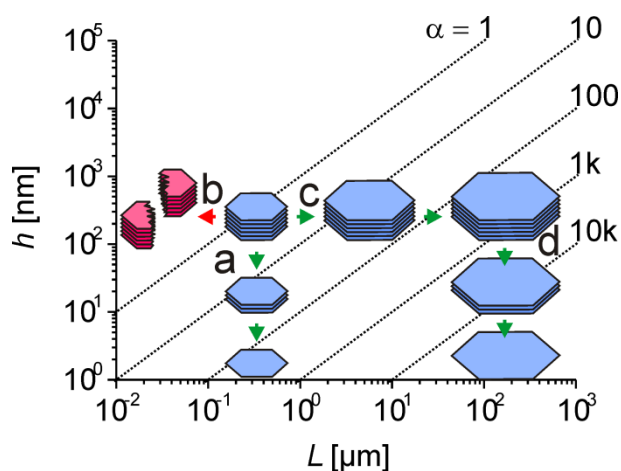


**Figure 1.** Scheme of possible mechanisms that influence the aspect ratio  $\alpha$  of a clay platelet. The reduction of the platelet height  $h$  by exfoliation/delamination (a) increases  $\alpha$  while fracture (b) decreases  $\alpha$  respectively. Enlargement of the diameter  $L$  achieved by advancing synthesis conditions (c) followed by complete delamination (d) gives access to ultra-high aspect ratios. The dotted lines mark decadal isopleths of  $\alpha$ .

## 2. Experimental section

**Synthesis of lithium fluorohectorite.** The synthesis of Li-hect<sub>x</sub> was performed in three steps, for each layer charge initially 3 g were synthesized. The synthesis of Li-hect<sub>x</sub> with nominal layer charge  $x=1.0$  p.f.u. was finally scaled to 500 g per batch:

Step 1. Synthesis of the glass precursor. 50 g of glass with composition  $\text{Li}_2\text{O}-2\text{SiO}_2$  was prepared from 24.62 g  $\text{Li}_2\text{CO}_3$  ( $\geq 99.0\%$ , Merck), and 43.50 g silicic acid hydrate,  $\text{SiO}_2 \cdot x\text{H}_2\text{O}$  ( $\geq 99.0\%$ , Fluka) ( $\text{SiO}_2\%$  = 92.06%) as a source for silicon dioxide. The mixture was homogenized by grinding in a ball mill and then it was heated in a conic glassy carbon crucible (diameter = 45 mm, bottom = 41 mm, height = 168 mm, 3 mm wall thickness; SIGRADUR G type T, HTW Hochtemperatur-Werkstoffe GmbH) at a rate of 300 °C/h up to 1250 °C to achieve melting while  $\text{CO}_2$  was expelled. An argon flow was applied to prevent oxidation of the crucible. The final temperature of 1250 °C was maintained for 1 h.

Step 2. Basic magnesium carbonate,  $\text{MgCO}_3 \cdot \text{Mg}(\text{OH})_2 \cdot x \text{H}_2\text{O}$  (42.07 % MgO, Acros) and silicic acid hydrate,  $\text{SiO}_2 \cdot x\text{H}_2\text{O}$  ( $\geq 99.0\%$ , Fluka) were used as additional sources for MgO and  $\text{SiO}_2$ . Mixtures of basic magnesium carbonate and silicic acid hydrate ( $M^*$ ) with molar ratios of MgO/ $\text{SiO}_2$  appropriate for each type of Li-hect<sub>x</sub> were heated to 900 °C for 1 h at a heating rate of 300 °C/h to achieve decarboxylation and dehydration.

**Step 3.** The synthetic glass  $\text{Li}_2\text{O}-2\text{SiO}_2$  was combined with the devolatilized mixture  $M^*$  and an additional amount of  $\text{MgF}_2$  (> 97%, Fluka) to meet the desired total compositions of  $[\text{Li}_x]^{\text{inter}}[\text{Mg}_{3-x}\text{Li}_x]^{\text{oct}}[\text{Si}_4]^{\text{tet}}\text{O}_{10}\text{F}_2$  ( $x = 0.4, 0.6, 0.8, \text{ and } 1.0$ ). The mixture was homogenized by grinding in a ball mill for 30 minutes. The fine powder was directly transferred into the conic glassy carbon crucible described in step 1 and then heated in a high radio-frequency induction furnace. The temperature was rapidly increased to 800 °C, maintained there for 5 min, before it was ramped rapidly to 1350 °C at which temperature the sample was held for 10 min. The melt was then quenched by switching off the power supply and the melt was allowed to cool to room temperature. Again, the melting steps were performed under an argon stream to prevent the oxidation of the crucible. The synthetic Li-hect<sub>x</sub> obtained was suspended in 200 ml of water, stirred for 24 h before being filtered, resuspended in water, freeze-dried, and stored in ambient condition.

**Powder X-ray diffraction.** PXRD patterns of pristine Li-hect<sub>x</sub> as received from the melt but after equilibration at ambient conditions (30 % relative humidity (r.h.)) were recorded in transmission mode on a STOE Stadi P powder diffractometer using  $\text{Cu K}\alpha_1$  radiation. To minimize texture, the samples were placed in a Lindemann glass capillary.

To study the swelling properties, freeze-dried Li-hect<sub>x</sub> powders were used. PXRD patterns were recorded in a temperature-humidity chamber (Anton Paar temperature humidity chamber driven by a VTI corp. RH-200 humidity generator) mounted on a PANalytical Xpert Pro equipped with an X'Celerator Scientific RTMS detector ( $\text{Cu K}\alpha$  radiation, Bragg-Brentano geometry). Patterns with an incremental decrease of 5 % r.h. were taken at 25 °C and ambient pressure starting at 100 % r.h. The samples were equilibrated at least 30 min at each level of r.h. prior the measurement.

**Atomic Force Microscopy.** Topographical images of the Li-hect<sub>1.0</sub> were recorded using a MFP3D™ Atomic Force Microscopy (Asylum Research, Santa Barbara, California) equipped with silicon cantilevers (silicon tip, type NSC15/AIBS,  $\mu\text{mash}$ , Tallin, Estonia). A few drops of a diluted suspension were dropped onto a freshly cleaved mica sheet and the sample was dried slowly under ambient conditions. The scan rate was 1 Hz.

**Chemical Analysis** of the synthesized Li-hect<sub>x</sub> was done by inductively coupled plasma atomic emission spectrometry (ICP-AES) (Thermo ICAP 6500) and atomic absorption spectroscopy (AAS) (Perkin-Elmer 2380). In order to be able to distinguish between octahedral and interlayer Li the synthetic Li-hect<sub>x</sub> were ion exchanged (see determination of



cation exchange capacity) with Tris(ethylenediamine)-cobalt (III) chloride ( $\text{Co(en)}_3\text{Cl}_3 \cdot 3\text{H}_2\text{O}$ ; ABCR GmbH & Co. KG) prior to analysis. For determination of  $\text{Co}^{3+}$  and  $\text{Li}^+$  6 mg of the samples were dissolved with acids (2 mL HCl, 1 mL HF, and 1 mL  $\text{HNO}_3$ ) under pressure at  $180^\circ\text{C}$ , cobalt was detected by ICP-AES and lithium by AAS. For both,  $\text{Mg}^{2+}$  and  $\text{Si}^{4+}$  analysis 4 mg of the samples were fused with 0.5 g of a mixture of sodium carbonate and sodium tetraborate (2:1). The melt was then dissolved in a mixture of 2 mL of  $\text{HNO}_3$  and 1 mL HCl and the concentrations were determined via ICP-AES.

**Cation exchange capacity (CEC);** The CEC was determined colorimetrically as described by Ammann et. al.<sup>29</sup> applying the intensively coloured complex cation tris(ethylenediamine)cobalt(III) chloride ( $[\text{Co(en)}_3]^{3+}$ ) which shows a high selectivity for clays and is readily exchanged for interlayer Li cations. For CEC determination Lots of 0.2 g of washed synthetic Li-hect<sub>x</sub> were dried at  $110^\circ\text{C}$  for 24 h and weight before being dispersed in 100 mL distilled water (pH adjusted to 7) overnight. 10 mL of the homogeneous suspensions were then transferred into a 25 mL centrifuge tube and 10 mL  $[\text{Co(en)}_3]^{3+}$  were added. The samples were shaken for 24 h and then centrifuged, 3 mL of supernatant were transferred into cuvettes and the absorptions were measured using monochromatic light with  $\lambda = 466\text{ nm}$ .

**Particle size distributions (PSD)** were obtained from aqueous dispersions on a Retsch Horiba LA-950 SLS instrument. A measurement routine called “mica in water” supplied by the manufacturer (Horiba) was applied. micas are natural clays with similar lateral extensions as the synthetic hectorites studied here. The routine determines transmission rates and optimizes the concentration of the suspensions. SEM images were taken on a LEO 1530 FE-SEM at an operation voltage of 5 kV using in-lens detection modes. Specimens were prepared from pristine synthetic Li-hect<sub>x</sub> without washing. The samples were sputtered with a 2nm platinum layer prior the measurements.

### 3. Result and discussion

**3.1 Synthesis of Li-hect<sub>x</sub>** In Figure 2 PXRD patterns of synthetic Li-hect<sub>x</sub> with variable layer charge are shown. Since some possible side-phases might be soluble, for PXRD Li-hect<sub>x</sub> were used as obtained in the synthesis. The samples were exposed to ambient r.h. ( $20^\circ\text{C}$  and r.h.= 30%), but were not washed at all. Regardless of the layer charge, under these conditions all materials adopted uniformly the state of one layer hydrate (1 WL:  $d_{001} = 12\text{ \AA}$ ). Although the diffractogram was recorded in transmission mode and with non-textured samples, by far

the most intense reflections could be attributed to basal reflections. The  $00l$ -series was rational indicating a uniform intracrystalline reactivity which in turn is agreement with a homogenous charge density. In the light of the well-known segregation problem discussed above, the good homogeneity was somewhat surprising. Apparently, high-frequency induction heating provides effective homogenisation of the melts by convection. The 001 peaks were narrow and sharp indicating thick tactoids and again militating against possible random interstratifications caused by charge heterogeneity.

As indicated by the  $\lambda$ -shape of the  $02/11$ -band at  $20\text{--}23^\circ 2\theta$ , the layer stackings of all  $\text{Li-heckt}_x$  were turbostratic. Although the diffractograms were dominated by hectorite peaks, the materials clearly also contained some trace amounts of impurities. The main side-phase observed by PXRD is  $\text{Li}_2\text{SiO}_3$  while formation of protoamphibole could be reduced to very low levels (denoted with P in Figure 2). Going to nominal layer charges above 0.6 suppressed formation of protoamphibole below detection limit while with  $x=1.0$  p.f.u. other crystalline side-phases,  $\text{Li}_2\text{Si}_2\text{O}_5$  and cristobalite, appeared. The nature of starting material, highly efficient mixing of starting materials, and reaction time turned out to be critical parameters for the synthesis that needed to be optimized. For instance, more side-products appeared with extended reaction times at  $1350^\circ\text{C}$ .

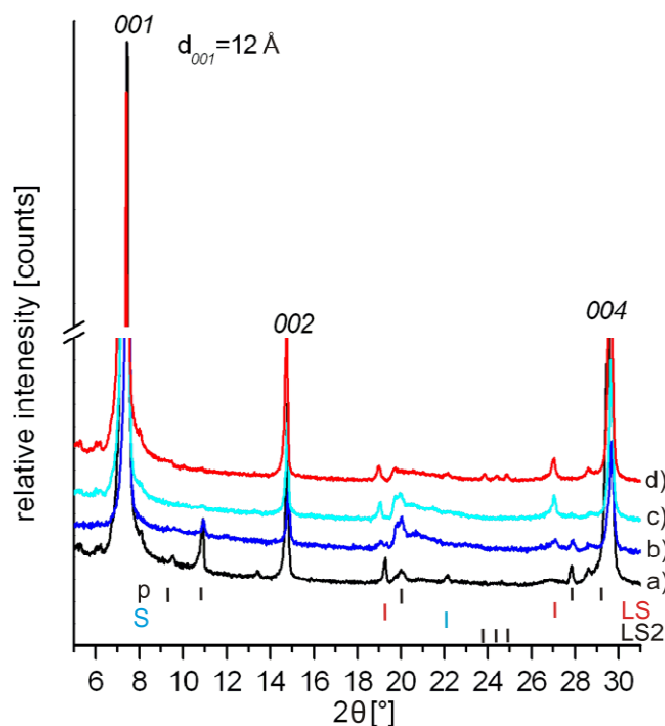


**Figure 2.** PXRD profiles of synthetic  $\text{Li-heckt}_x$ ,  $[\text{Li}_x]^{\text{inter}}[\text{Mg}_{3-x}\text{Li}_x]^{\text{oct}}[\text{Si}_4]^{\text{tet}}\text{O}_{10}\text{F}_2$  (a:  $x=0.4$ ; b:  $x=0.6$ ; c:  $x=0.8$ ; d:  $x=1.0$ ). Basal reflections are indexed; the basal spacing of  $12\text{ \AA}$

corresponds to the one-layer hydrate. Ticks indicate side-phases (LS:  $\text{Li}_2\text{SiO}_3$  [01-070-0330]<sup>29</sup>; LS2:  $\text{Li}_2\text{Si}_2\text{O}_5$  [01-082-2396]<sup>30</sup>; S:cristobalite [01-071-0785]<sup>31</sup>; P: protoamphibole [00-013-0409]<sup>26</sup>).

In particular, kind and amount of side-products was crucially dependant on the composition of the initial melts. In the ternary phase diagram of the system  $\text{Li}_2\text{O-MgO-SiO}_2$ , the protoamphibole composition is close to the  $\text{MgO-SiO}_2$ -line while vice versa, lithium containing layered silicates are close to the  $\text{Li}_2\text{O-SiO}_2$ -line. Consequently, the protoamphibole content is expected to decrease with increasing Li-concentration, as was actually confirmed in our experiments. In this line, in order to repress protoamphibole production, we sought to apply the maximum amount of  $\text{Li}_2\text{O-2SiO}_2$  glass in combination with the minimum amount of  $\text{MgO}$  which are still in line with the desired composition, while, following Eitel et al., all fluoride was introduced to the mixture via  $\text{MgF}_2$ .<sup>28</sup> Moreover,  $\text{LiF}$  is the compound with the highest partial pressure in the gas phase in equilibrium with the melt. Depending on reaction time and temperature generally a significant amount of  $\text{LiF}$  will consequently be volatilized in an open crucible system. Therefore, the loss of  $\text{LiF}$  during synthesis had to be taken into account by starting with a surplus of  $\text{LiF}$  as compared to the desired stoichiometry. This surplus was, however, not supplied as  $\text{LiF}$  but rather as combination of  $\text{Li}_2\text{O-2SiO}_2$  glass and  $\text{MgF}_2$ . For example, the synthesis of one mole of  $[\text{Li}_{0.6}]^{\text{inter}}[\text{Mg}_{2.4}\text{Li}_{0.6}]^{\text{oct}}[\text{Si}_4]^{\text{tet}}\text{O}_{10}\text{F}_2$  as described above would require one mole of  $\text{MgF}_2$  and 1.4 mole of  $\text{MgO}$ . To take the volatilisation of  $\text{LiF}$  into account, however, 1.5 mole of  $\text{MgF}_2$ , 0.9 mole of  $\text{MgO}$ , in combination with 1.1 mol  $\text{Li}_2\text{O-2SiO}_2$  were weight in, allowing for the loss of one mole  $\text{LiF}$  built in situ during synthesis.

### 3.2. Chemical composition

Despite having to counterbalance the loss of volatiles, the chemical compositions of obtained  $\text{Li-lect}_x$  given in Table 1 were in reasonable agreement with the formulas of the desired layered silicates. Please note that besides insoluble crystalline side phases seen in the PXRD; some glassy side-products are likely to be formed by quenching these silicate melts. During washing and cation exchange with  $[\text{Co}(\text{en})_3]^{3+}$  soluble components might be leached to some degree. Such leaching effects are expected to be most pronounced for the Li-content. In Table 1 we refrained from converting the element ratios into layered silicate formulae because this would neglect the fact that the products are not phase pure and the formulae would be in error. For comparison we rather listed expected element ratios as calculated applying the

desired formulae (cited in parenthesis) while in the text the different samples are referred to by their nominal stoichiometry.

**Table 1.** Chemical compositions of washed synthetic Li-hect<sub>x</sub> as determined via AAS and ICP-AES (after cation exchange with Co(en)<sub>3</sub>Cl<sub>3</sub>·3H<sub>2</sub>O).

sample	Mg wt%	Li wt%	Si wt%	Co wt%
Li-hect <sub>0.4</sub>	15.45 (15.48)	1.63 (0.68)	25.00 (27.52)	1.30 (1.93)
Li-hect <sub>0.6</sub>	14.55 (13.86)	1.72 (0.99)	25.60 (26.70)	1.45 (2.80)
Li-hect <sub>0.8</sub>	13.35 (12.35)	1.01 (1.28)	24.35 (25.93)	2.26 (3.54)
Li-hect <sub>1.0</sub>	12.15 (10.91)	1.04 (1.56)	25.95 (25.21)	2.41 (4.41)

**3.3. Cation exchange capacity (CEC)** Deviations from the nominal formula as seen in the chemical analysis will of course also greatly influence the CEC. Table 2 lists the experimentally observed CECs together with expected values as calculated applying the desired formulae. The pronounced discrepancies between experimental and calculated CECs again were attributed to both, crystalline and possible amorphous impurities. Moreover, additionally a minor contribution might originate from the influence of layer edges that represent stoichiometric defects. There are numerous methods available for the determination of the CEC,<sup>32-34</sup> the most convenient being colorimetric methods applying cationic dyes with high extinction coefficients. Please note that we could not use the standard complex cation, [Cu(trien)]<sup>2+</sup>, since according to Ammann et. al.<sup>34</sup> [Cu(trien)]<sup>2+</sup> is limited to medium and low layer charge for steric reasons. We therefore rather used [Co(en)<sub>3</sub>]<sup>3+</sup> as dye that due to its higher charge is capable of also matching higher layer charge densities in a monolayer arrangement. Although CECs deviated significantly from nominal values (Table 2) the absolute values nevertheless consistently increased with nominal layer charge. The CEC of Li-hect<sub>0.6</sub> is close to the value reported for the Corning hectorite (122 meq/100g) for which a formula of [Li<sub>0.56</sub>]<sup>inter</sup>[Mg<sub>2.44</sub>Li<sub>0.56</sub>]<sup>oct</sup>[Si<sub>4</sub>]<sup>tet</sup>O<sub>10</sub>F<sub>2</sub>, has been given. As described in the patent US 4339540, the Corning material was made in a similar approach: After grinding the raw material in a ball mill, the mixture was melted at 1450 °C for 5 h without stirring. Then the melt was allowed to crystallize at 700 °C within 4 h. The product was purified by immersing the crystallized material in water while stirring, to remove soluble impurities by washing. Unfortunately, the patent gives no information what means had been taken to limit and or counterbalance the loss of Li by volatilization. Given the rather long reaction times, the effect must have been pronounced.

The maximum CEC of 185 meq/100 g observed for Li-hect<sub>1.0</sub> is among the highest reported CEC in the literature for swelling 2:1 layered silicates. For comparison, a commercial Na-fluorotetrasilicic mica (nominal layer charge  $x = 1.0$  p.f.u) with an ideal formula of NaMg<sub>2.5</sub>Si<sub>4</sub>O<sub>10</sub>F<sub>2</sub> (COOP Chemicals Co. Ltd., Somasif ME-100) was reported to have a CEC of around 120 meq/100g.<sup>35</sup>

**Table 2.** CECs of synthetic Li-hect<sub>x</sub>.

Samples	Li-hect <sub>0.4</sub>	Li-hect <sub>0.6</sub>	Li-hect <sub>0.8</sub>	Li-hect <sub>1.0</sub>
CEC <sub>exp.</sub> (meq/100g)	70	118	130	185
CEC <sub>calc.</sub> (meq/100g)	106	159	213	268

**3.4. Hydration behaviour** Since our ultimate goal was to obtain high aspect ratio nanoplatelets by spontaneous delamination of Li-hect<sub>x</sub> in water; their intracrystalline reactivity was investigated in some detail by studying hydration in situ in a humidity chamber. Figure 3 illustrates the evolution of the basal spacings ( $d$ -values of the 001-reflection) of Li-hect<sub>x</sub> as a function of r.h. recorded at 25°C. It is commonly accepted that intracrystalline reactivity is diminished with increasing layer charge. Besides the coulomb attraction between interlayer species and silicate lamellae, the state of hydration is, however, determined by a second as important factor, the hydration enthalpy of the interlayer cation. Both factors will increase with layer charge, because the hydration enthalpy will scale with the number of interlayer cations. With interlayer cations having high hydration enthalpies like Li<sup>+</sup> it is therefore a priori not clear which of the two factors is going to win and whether hydration will decrease as commonly assumed or rather increase with increasing layer charge.

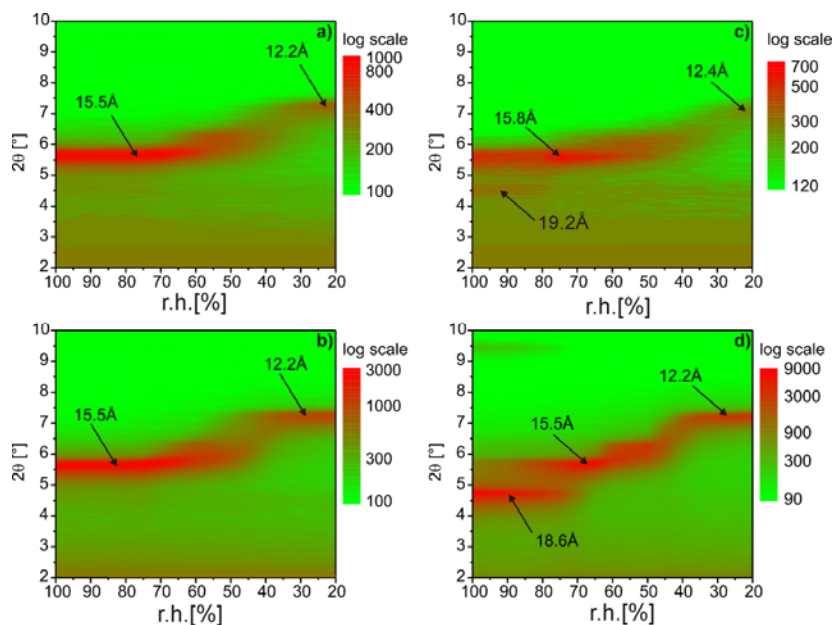


**Figure 3.** Water desorption experiments of freeze-dried Li-hect<sub>x</sub> a)  $x=0.4$ , b)  $x=0.6$ , c)  $x=0.8$  and d)  $x=1.0$ ) at 25 °C as monitored in a humidity chamber via in-situ PXRD. The  $2\theta$ -range, where the 001-reflection of the different hydrates is expected, is recorded as function of the relative humidity while diffraction intensities are given as colour code. Arrows mark the  $d$ -values for one-, two-, and three-layer hydrates.

Generally, the transition between the different states of hydration for all synthetic materials was rather sharp and occurred in steps at well defined r.h. (Figure 3). The absence of randomly interstratified intermediates, as frequently observed for natural montmorillonites,<sup>36</sup> indicated a uniform intracrystalline reactivity which in turn supported a homogenous charge density.

Interestingly, only the material with the highest layer charge Li-hect<sub>1.0</sub> adopted the 3 WL state of hydration above 80 % r.h. ( $d=18.6 \text{ \AA}$ ) (Figure 3d). Even with prolonged equilibration times at 100 % r. h., the 3WL-hydrate could not be achieved for the three materials with lower charge densities (For completeness, we note that for Li-hect<sub>0.8</sub> barely visible traces of 3WL-hydrate were observed (Figure 3c)). The maximum hydration state achieved for Li-hect<sub>0.4-0.8</sub> was the 2WL-hydrate ( $d=15.5 \text{ \AA}$ ) (Figure 3a-c). At ambient conditions (r.h. < 40 %) all materials adopted the 1WL-hydrate ( $d\approx 12 \text{ \AA}$ ). Moreover, comparing Li-hect<sub>0.6</sub> with Li-hect<sub>0.8</sub>, the latter showed the higher swelling power as indicated by the fact that the transition from the 1WL- to the 2WL-hydrate was observed at lower r.h. These results prove that for Li-

hect the swelling power indeed increases with the number of interlayer cations due to the high hydration enthalpy of the small lithium cation.

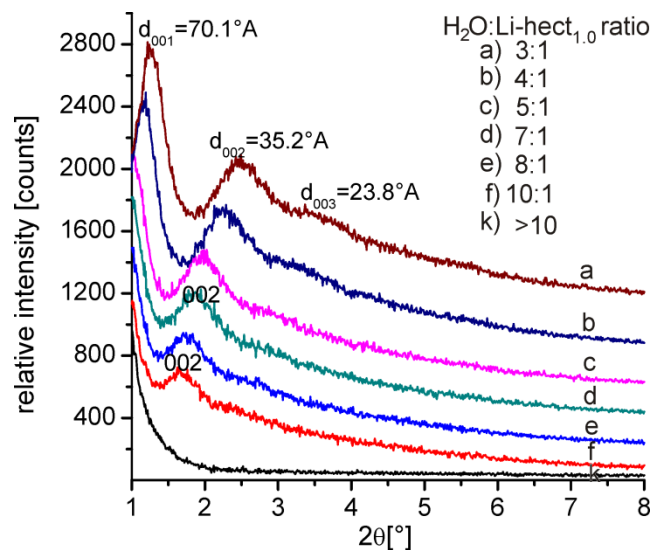


**Figure 4.** Swelling of Li-heck<sub>1,0</sub> at higher water activities. PXRD patterns of varying H<sub>2</sub>O:Li-heck<sub>1,0</sub> ratios are shown.

To extend the swelling studies for the most reactive hectorite to higher water activities, freeze-dried Li-heck<sub>1,0</sub> was mixed with varying amounts of water. Figure 4 shows PXRD patterns of these H<sub>2</sub>O:Li-heck<sub>1,0</sub>-mixtures. With increasing amount of water available in the mixtures, the *00l* peaks were shifted to lower diffraction angle (higher *d*-values). This gradual shift of *d*-values with increasing water activity available, indicated, that Li-heck<sub>1,0</sub> might show osmotic swelling when suspended in an excess of water.

Similar to what has been reported by Tamura et al.,<sup>37</sup> even the highly hydrated states showed an integral series of *00l* reflections. The *d*<sub>00*l*</sub> series for the mixture with a ratio of water to Li-heck<sub>x</sub> (H<sub>2</sub>O:Li-heck<sub>1,0</sub>) of 3:1 was quite rational (*d*<sub>001</sub> = 70.1 Å, *d*<sub>002</sub> = 35.2 Å, and *d*<sub>003</sub> = 23.8 Å). With ratios of H<sub>2</sub>O:Li-heck<sub>1,0</sub> of 5:1 and higher the 001 peak is out of the 2θ-range that can be measured, but the 002 peak continued to be shifted to higher *d*-values with increasing amounts of water available (for 5:1: *d*<sub>002</sub> = 44 Å).

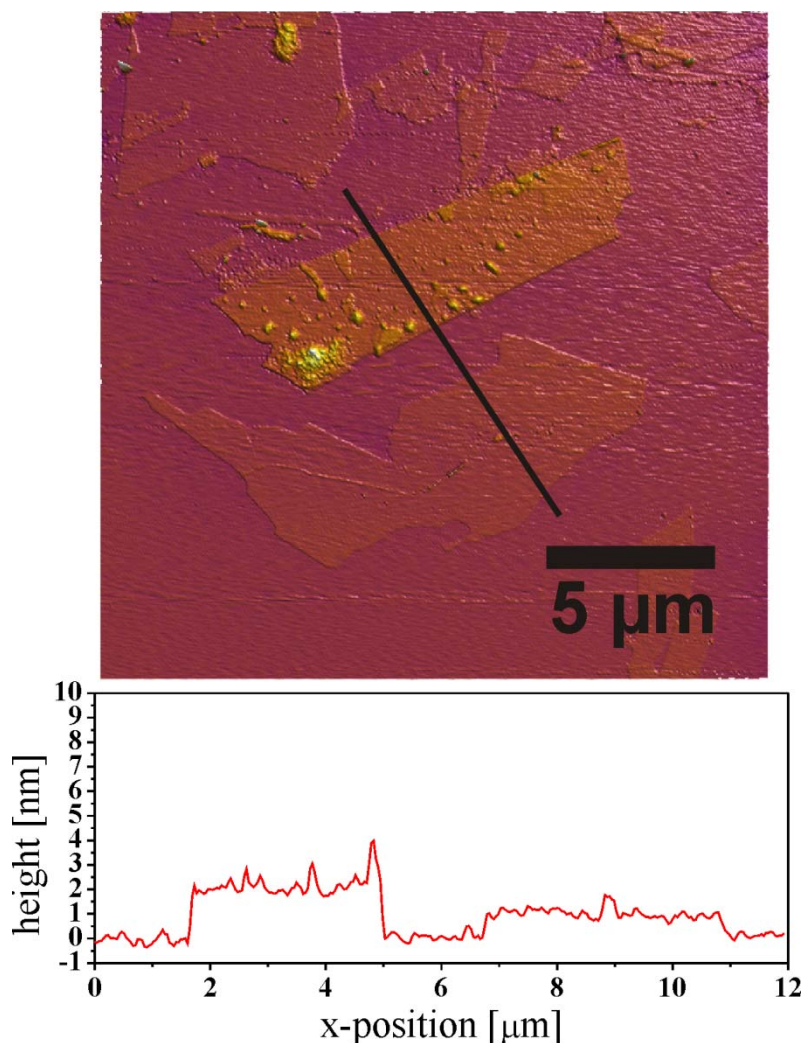


**Figure 5.** AFM image (20 μm × 20 μm scan) of a typical sample of synthetic Li-hect<sub>1.0</sub>.

For H<sub>2</sub>O:Li-hect<sub>1.0</sub>– ratios > 10 basal reflections could no longer be observed, indicating that the tactoids might have delaminated. AFM images were in line with this interpretation of the PXRD pattern as mostly delaminated platelets could be seen after suspending Li-hect<sub>1.0</sub> in deionized water (Figure 5) (please see also Fig S1 in supporting information). Beginning exfoliation/delamination might have already been indicated with ratios of H<sub>2</sub>O:Li-hect<sub>1.0</sub> < 10 by the much broadened basal reflections as compared to the 1WL-hydrate (Figure 2) that has not been in contact with liquid water. For completely delaminated fluorohectorite a specific surface area of 800 m<sup>2</sup>.g<sup>-1</sup> would be expected. It is, however, well known that high vacuum conditions required in N<sub>2</sub>-physisorption experiments induce massive re-aggregation into band-like structures and only a minor part of the potential surface is accessible for the probe gas. In line with this, we measured a BET-surface area as low as 12.3 m<sup>2</sup>.g<sup>-1</sup> for a freeze dried sample of Li-hect<sub>1.0</sub>.<sup>38</sup>



**3.5. Particle size distribution.** Aspect ratios are not only determined by the thickness of tactoids but of course also by their diameter (Figure 1c). Usually the diameter of tactoids of layered silicates increases with increasing layer charge p.f.u.<sup>38,39</sup> The synthetic Li-hect<sub>x</sub> clearly followed this trend. As indicated by SLS measurements (Table 3 and Figure 6), a correlation was observed between median particle size and layer charge. SEM images of the materials confirmed this trend (Figure 7). The SLS measurements were performed in aqueous dispersions; the PSDs therefore are representative for the bulk material. Moreover, it has been shown by Goossens<sup>40</sup> that the lateral extensions of tactoids correlate well with the hydrodynamical radius obtained from SLS. Considering the observed median values of 20 to 40  $\mu\text{m}$  and assuming complete delamination by osmotic swelling, average aspect ratios of these hectorites are certainly significantly above 1000 and may range up to more than 10000 as confirmed by the AFM-images of a typical sample shown in Figure 5.

**Table 3.** Median particle sizes of synthetic Li-hect<sub>x</sub> as measured by SLS.

Sample	Li-hect <sub>0.4</sub>	Li-hect <sub>0.6</sub>	Li-hect <sub>0.8</sub>	Li-hect <sub>1.0</sub>
d <sub>50%</sub> Particle size $\mu\text{m}$ (SLS)	19	27	30	48

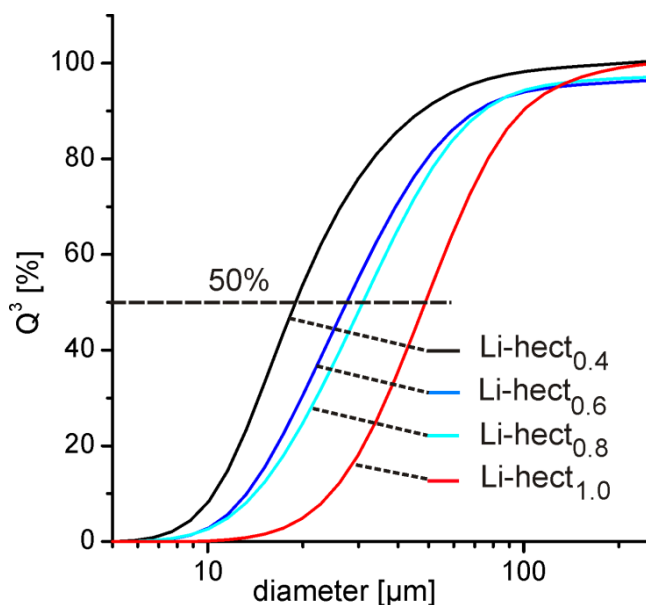


**Figure 6.** Particle size distributions of the Li-hect<sub>x</sub> as analyzed by SLS.

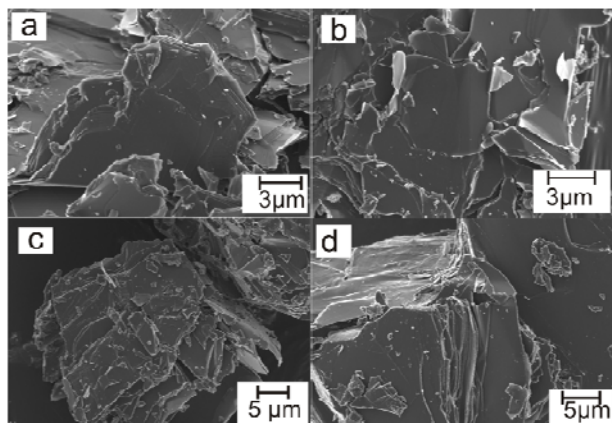


**Figure 7.** SEM images of pristine Li-hect<sub>x</sub> as obtained by synthesis (a: x = 0.4; b: x = 0.6; c: x = 0.8; d: x = 1.0).

#### 4. Conclusion

Melt-synthesis yielded Li-hect<sub>x</sub> of variable layer charge. Luckily and somewhat counter intuitively, both tactoid diameter and intracrystalline reactivity increased concomitantly with increasing layer charge. This way hectorites with huge tactoid diameters were obtained ( $d_{50\%} = 48 \mu\text{m}$ ) that spontaneously delaminated by osmotic swelling when immersed into deionized water. Nano-platelets consisting of a singular 2:1 lamella of approximately 1 nm thickness and a diameter of more than 40  $\mu\text{m}$  could thus easily be obtained. These unprecedented huge aspect ratio fillers promise great potential for flame retardants and barrier application. Proof of concept papers on barrier properties and flame retardancy have already been published.<sup>2,42,43</sup>

#### Acknowledgements

This work was financially supported by the Deutsche Forschungsgemeinschaft (SFB 840) and the University of Aleppo (Syria).

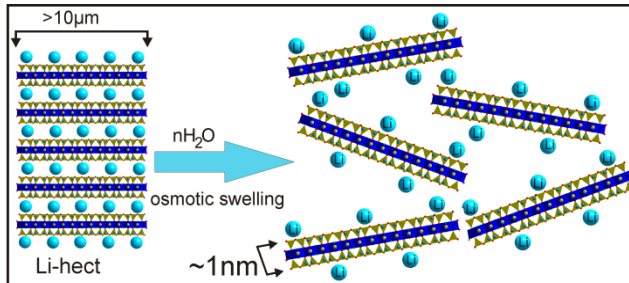
#### References

- 1 K. Tamura, S. Yokoyama, C. S. Pascua and H. Yamada, *Chem. Mater.*, 2008, 20, 2242-2246.
- 2 M. W. Möller, T. Lunkenbein, H. Kalo, M. Schieder, D. A. Kunz and J. Brey, *Adv. Mater.*, 2010, 22, 5245-5249.
- 3 T. Cao, P. D. Fasulo and W. R. Rodgers, *Appl. Clay Sci.*, 2010, 49, 21-28.

- 4 A. Baumgartner, K. Sattler, J. Thun and J. Breu, *Angew. Chem. Int. Ed.*, 2008, 47, 1640-1644.
- 5 A. Baumgartner, F. E. Wagner, M. Herling and J. Breu, *Microporous and Mesoporous Mater.*, 2009, 123, 253-259.
- 6 Y. Umemura, A. Yamagishi, R. Schoonheydt, A. Persoons and F. De Schryver, *Langmuir*, 2001, 17, 449-455.
- 7 I. Dekany, L. Turi and Z. Kiraly, *Appl. Clay Sci.*, 1999, 15, 221-239.
- 8 M. W. Riley, P. S. Fedkiw and S. A. Khan, *J. Electrochem. Soc.*, 2003, 150, A933-A941.
- 9 M. W. Möller, U. A. Handge, D. A. Kunz, T. Lunkenbein, V. Altstadt and J. Breu, *Acc Nano*, 2010, 4, 717-724.
- 10 J. E. F. C. Gardolinski and G. Lagaly, *Clay Miner.*, 2005, 40, 537-546.
- 11 K. S. Triantafyllidis, P. C. LeBaron, I. Park and T. J. Pinnavaia, *Chem. Mater.*, 2006, 18, 4393-4398.
- 12 H. Tetsuka, T. Ebina, H. Nanjo and F. Mizukami, *J. Mater. Chem.*, 2007, 17, 3545-3550.
- 13 I. Berend, J. M. Cases, M. Francois, J. P. Uriot, L. Michot, A. Masion and F. Thomas, *Clays Clay Miner.*, 1995, 43, 324-336.
- 14 A. Berghout, D. Tunega and A. Zaoui, *Clays Clay Miner.*, 2010, 58, 174-187.
- 15 H. Kalo, M. W. Möller, M. Ziadeh, D. Dolej and J. Breu, *Appl. Clay Sci.*, 2010, 48, 39-45.
- 16 J. Breu, W. Seidl, A. J. Stoll, K. G. Lange and T. U. Probst, *Chem. Mater.*, 2001, 13, 4213-4220.
- 17 S. Taruta, T. Ichinose, T. Yamaguchi and K. Kitajima, *J. Non-Cryst. Solids*, 2006, 352, 5556-5563.
- 18 M. K. Murthy and F. A. Hummel, *J. Am. Ceram. Soc.*, 1955, 38, 55-63.
- 19 B. O. Mysen, *Annu. Rev. Earth Planet. Sci.*, 1983, 11, 75-97.
- 20 P. Hudon and D. R. Baker, *J. Non-Cryst. Solids*, 2002, 303, 299-345.
- 21 V. McGahay and M. Tomozawa, *J. Non-Cryst. Solids*, 1989, 109, 27-34.
- 22 F. C. Kracek, *J. Am. Chem. Soc.*, 1939, 61, 2863-2877.

- 23 R. Ota, T. Wakasugi, W. Kawamura, B. Tuchiya and J. Fukunaga, *J. Non-Cryst. Solids*, 1995, 188, 136-146.
- 24 D. R. Baker and E. B. Watson, *J. Non-Cryst. Solids*, 1988, 102, 62-70.
- 25 K. Matusita, N. Osawa, M. Koide, R. Sato and T. Komatsu, *J. Non-Cryst. Solids*, 1994, 177, 216-220.
- 26 G. V. Gibbs, F. D. Bloss and H. R. Shell, *Amer. Mineral.*, 1960, 45, 974-989.
- 27 R. M. Barrer and D. L. Jones, *J. Chem. Soc. A*, 1970, 1531-1537.
- 28 W. Eitel, R. A. Hatch and M. V. Denny, *J. Am. Ceram. Soc.*, 1953, 36, 341-348.
- 29 L. Ammann, F. Bergaya and G. Lagaly, *Clay Miner.*, 2005, 40, 441-453.
- 30 K. F. Hesse, *Acta Cryst. B*, 1977, 33, 901-902.
- 31 B. H. W. S. de Jong, P. G. G. Slaats, H. T. J. Supèr, N. Veldman and A. L. Spek, *J. Non-Cryst. Solids*, 1994, 176, 164-171.
- 32 W. A. Dollase, *Z. Kristallogr.*, 1965, 121, 369-&.
- 33 R. Dohrmann, *Appl. Clay Sci.*, 2006, 34, 31-37.
- 34 R. Dohrmann and S. Kaufhold, *Clays Clay Miner.*, 2009, 57, 338-352.
- 35 L. A. Utracki, M. Sepehr and E. Boccaleri, *Polym. Adv. Technol.*, 2007, 18, 1-37.
- 36 K. Devineau, I. Bihannic, L. Michot, F. Villieras, F. Masrouri, O. Cuisinier, G. Fragneto and N. Michau, *Appl. Clay Sci.*, 2006, 31, 76-84.
- 37 K. Tamura, T. Sasaki, H. Yamada and H. Nakazawa, *Langmuir*, 1999, 15, 5509-5512.
- 38 F. Bergaya, B.K.G. Theng and G. Lagaly, *Handbook of Clay Science*, Elsevier, Amsterdam, 2006, vol 1.
- 39 S. Taruta, R. Obara, N. Takusagawa and K. Kitajima, *J. Mater. Sci.*, 2005, 40, 5597-5602.
- 40 A. Meunier, *Clay Miner.*, 2006, 41, 551-566.
- 41 D. Goossens, *Sedimentology*, 2008, 55, 65-96.
- 42 M. R. Schütz, H. Kalo, T. Lunkenbein, J. Breu and C. A. Wilkie, *Polymer*, 2011, 52, 3288-3294.
- 43 M. W. Möller, D. A. Kunz, T. Lunkenbein, S. Sommer, A. Nennemann and J. Breu, *Adv. Mater.*, 2012, 24, 2142-2147.

**TOC:** By a novel melt synthesis hectorites with very large diameters were obtained that spontaneously delaminate when immersed into water. These nano-platelets with unprecedented huge aspect ratio ( $> 10000$ ) promise great potential as fillers for flame retardants and barrier applications.



Supporting Information:

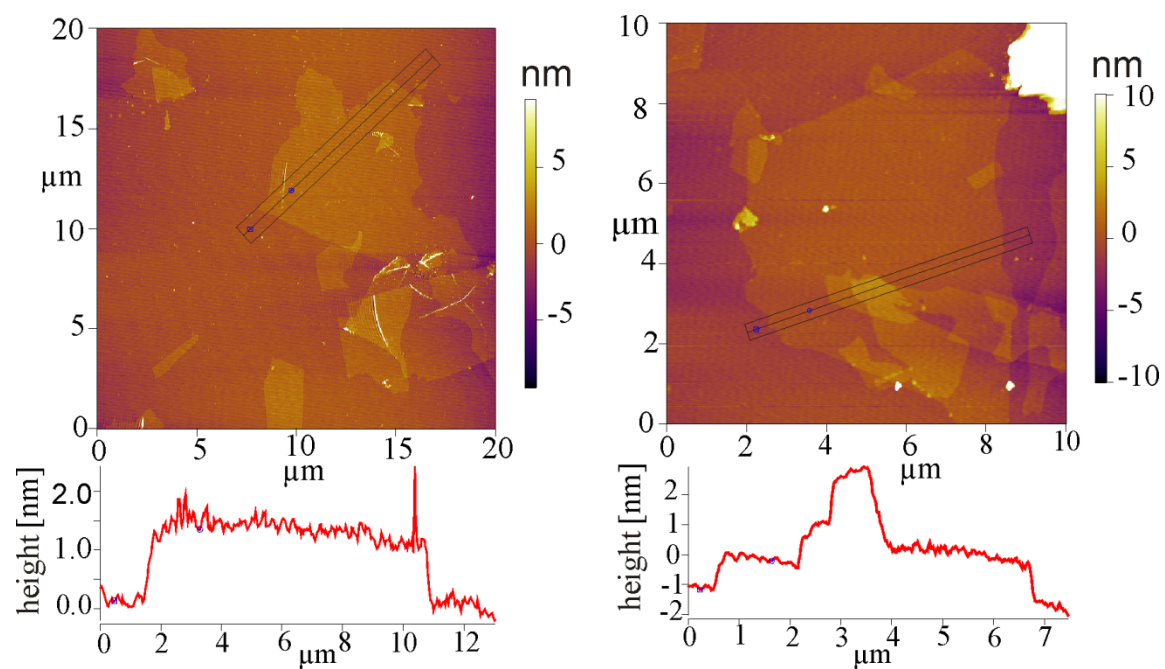


**Fig. S1** AFM image of different samples of synthetic Li-hect1.0

# Appendix 4

## **Synthesis and Single Crystal Structure Refinement of Hydrate Sodium Brittle Mica**

Hussein Kalo, Wolfgang Milius, Michael Bräu and Josef Breu\*

Department of Inorganic chemistry I, University of Bayreuth, D-95440 Bayreuth, Germany

Run title: crystal structure of hydrate Sodium-Fluorohectorite

Corresponding author:

Prof. Dr. Josef Breu

Universitätsstr. 30

95440 Bayreuth

Germany

\* E-mail address: josef.breu@uni-bayreuth.de

Submitted to journal of Solid State Chemistry

## Synthesis and Single Crystal Structure Refinement of the One-layer Hydrate of Sodium Brittle Mica

Hussein Kalo<sup>a</sup>, Wolfgang Milius<sup>a</sup>, Michael Bräu<sup>b</sup>, Josef Breu<sup>a</sup> \*

<sup>a</sup>Lehrstuhl für Anorganische Chemie I, University of Bayreuth, D-95440 Bayreuth, Germany

<sup>b</sup>BASF Construction Chemicals GmbH, 83308 Trostberg, Germany

\* josef.breu@uni-bayreuth.de

\* Corresponding author: Prof. Dr. Josef Breu, Phone: 0049921552531 Fax: 0049921552788

E-mail: [Josef.Breu@uni-bayreuth.de](mailto:Josef.Breu@uni-bayreuth.de)

### Abstract

A sodium brittle mica with the ideal composition  $[\text{Na}_4]^{\text{inter}}[\text{Mg}_6]^{\text{oct}}[\text{Si}_4\text{Al}_4]^{\text{tet}}\text{O}_{20}\text{F}_4$  was synthesized via melt synthesis in a gas tight crucible. This mica is unusual inasmuch as the known mica structure holds only room for two interlayer cations per unit cell and inasmuch as it readily hydrates despite the high layer charge while ordinary micas and brittle micas are non-swelling. The crystal structure of one-layer hydrate sodium brittle mica was determined and refined from single crystal X-ray data. Interlayer cations reside at the center of the distorted hexagonal cavities and are coordinated by the three inner basal oxygen atoms. The coordination of the interlayer cation is completed by three interlayer water molecules residing at the center of the interlayer region. The relative position of adjacent 2:1-layers thus is fixed by these octahedrally coordinated interlayer cations. Pseudo-symmetry leads to extensive twinning. In total 5 twin operations generate the same environment for the interlayer species and are energetically degenerate.

**Keyword:** Sodium brittle mica, twinning, stacking disorder, swelling mica.



## 1. Introduction

The degree of swelling of 2:1 layer silicates is mainly determined by the hydration enthalpy of the interlayer cation [1]. Only the smectite and vermiculite family with moderate layer charge are hydrated and interlayer cations can be readily exchanged. The cation exchange capacities (CEC) for these swelling materials typically vary in a range from 80 to 180 milliequivalents per 100 gram [2-4]. More recently, a sodium brittle mica with ideal composition  $[\text{Na}_4]^{\text{inter}}[\text{Mg}_6]^{\text{oct}}[\text{Si}_4\text{Al}_4]^{\text{tet}}\text{O}_{20}(\text{OH})_4$ , named Na4-mica, attracted a lot of interest. Despite the very high layer charge, this material was found to readily swell with water and complete cation exchange could be achieved [5-10]. Due to the high CEC (theoretically 468 meq/100g) applications like radioactive cation fixation or removal of heavy metal cations from waste water were proposed [11-14]. Furthermore, Na4-mica was pillared and nanoparticles were grown in the interlayer [15-17].

Despite the swelling properties of this material the structure is puzzling because double the number of cations as compared to mica or brittle mica has to be accommodated in the interlayer space. Different synthetic routes have been established, however, they all produce small particle sizes ( $< 5 \mu\text{m}$ ) and moreover, turbostratically disordered materials [6,7,11]. Consequently no reliable structure is available up to date. In 1987 Gregorkiewitz and Rausellcolom [18] recorded PXRD data, precession photographs, and electron diffraction data for  $[\text{Na}_4]^{\text{inter}}[\text{Mg}_{6.0}\text{Ti}_{0.05}]^{\text{oct}}[\text{Fe}_{0.1}\text{Si}_{4.5}\text{Al}_{3.4}]^{\text{tet}}\text{O}_{20.7}\text{F}_{3.3}$  which they obtained from reacting augite in NaF-MgF<sub>2</sub> melts at 1080°C. They were able to determine unit cell parameters for both zero-layer and one-layer hydrate. Based on a one-dimensional Fourier analysis of the 00/ series and by comparing the observed intensities of the 02/0-2/ and the 11/1-1/ reciprocal lattice rows with calculated intensities obtained by geometric relations for mica-type layers, they proposed a model for the arrangement of interlayer cations and interlayer water and stacking modes. The “crystals” investigated by Gregorkiewitz and Rausellcolom, however, showed only sharp reflections for  $k = 3n$ , whereas all other reflections were found to be diffuse forming streaks parallel to  $c^*$  and consequently no least square refinement of the structural model could be performed.

In the light of the interesting properties of Na4-mica we thought to synthesize larger crystals with less disorder that would enable us to solve and refine the structure by single crystal data. Melt synthesis of the fluoro-analogues has previously yielded single crystals of swelling smectites [2,3,19-21]. In that line, a sodium brittle fluoro-mica with ideal composition of  $[\text{Na}_4]^{\text{inter}}[\text{Mg}_6]^{\text{oct}}[\text{Si}_4\text{Al}_4]^{\text{tet}}\text{O}_{20}\text{F}_4$  (Na4-F-mica) was synthesized in a gas tight molybdenum

crucible and the crystal structure of its one-layer hydrate was determined and refined from single crystal X-ray data.

## 2. Materials and Methods

Na4-F-mica was synthesized via melt synthesis [3,19,22]. The high purity reagents (in total ~4 g)  $\alpha$ -Al<sub>2</sub>O<sub>3</sub> (Chempure, 99.99%), MgF<sub>2</sub> (Chempur, 99.99%), MgO (Alfa Aesar 99.95 %), and Na<sub>2</sub>O-2SiO<sub>2</sub> were weighed into a molybdenum crucible in an Ar atmosphere in accordance with a stoichiometric composition of [Na<sub>4</sub>]<sup>inter</sup>[Mg<sub>6</sub>]<sup>oct</sup>[Si<sub>4</sub>Al<sub>4</sub>]<sup>tet</sup>O<sub>20</sub>F<sub>4</sub> (target composition). Na<sub>2</sub>O-2SiO<sub>2</sub> glass has been produced by melting Na<sub>2</sub>CO<sub>3</sub> (Aldrich, 99.9%) and SiO<sub>2</sub> (Merck, fine granular, calcined) in a 1:2 molar ratio at 1050 °C for 10 h to ensure complete release of carbon dioxide. The molybdenum crucible was sealed so as to be gas tight using the procedure described elsewhere [23]. The crucible was heated in a graphite furnace (Graphit HT-1900, Linn High Therm) for the synthesis. To prevent inhomogeneity of the material owing to gravity segregation in the melt, the crucible was positioned horizontally in the furnace and rotated at 50 rpm. The crucible was heated from room temperature (RT) to 1750 °C (20 °C min<sup>-1</sup>), left at 1750 °C for 1 h, cooled to 1250 °C with a cooling rate of 50 °C min<sup>-1</sup>, left to cool from 1250 °C to 800 °C at a rate of 1.5 °C min<sup>-1</sup> without rotation, and then quenched by switching off the power. The crucible was opened under Ar atmosphere and the synthetic Na4-F-mica was stored in a Glovebox.

Powder X-ray diffraction (PXRD) patterns of zero-, and one-layer hydrate of synthetic Na4-F-mica were recorded using a STOE Stadi P powder diffractometer (transmission geometry, CuK $\alpha$ <sub>1</sub> radiation  $\lambda = 1.54059$  Å), Ge monochromator, linear position sensitive detector). The measurement was done in sealed glass capillaries in order to fix the relative humidity (r.h.) and to minimize texture effects. For zero-layer hydrate Na4-F-mica, the capillary was filled and closed in the Glovebox. For the one-layer hydrate the synthetic Na4-F-mica was exposed to water vapour at 43% r.h. (above K<sub>2</sub>CO<sub>3</sub> saturated solution). The equilibrated sample was quickly transferred into a capillary which was then sealed with grease for PXRD measuring.

The single crystal X-ray data of one-layer hydrate of synthetic Na4-F-mica were collected for selected crystals showing a minimum of diffuse streaks. In order to minimize dynamics of interlayer water and to fix the water content, data were collected at 173 K on a STOE IPDS I diffractometer with graphite monochromated MoK $\alpha$ <sub>1</sub> radiation ( $\lambda = 0.71073$  Å) using a crystal 0.25 mm x 0.25 mm x 0.02. Prior to mounting, the single crystals were equilibrated at appropriate r.h. as described above for the PXRD measurements.

The diffraction pattern could be indexed with a C-centered monoclinic lattice but systematically for all individuals investigated some non-indexed reflections remained along  $c^*$  indicating twinning. Moreover, diffuse scattering was observed for reflections with  $k \neq 3n$  indicating the presence of  $\pm b/3$  stacking faults. Careful inspection of the diffraction data allowed to index all reflections by six twin domains that are related by the following twinning operations:

Domain 1, 3 and 5 are related by a 3-fold rotation axis  $\parallel [001]$  e.g.  $\begin{pmatrix} 1/2 & -1/2 & 0 \\ -3/2 & -1/2 & 0 \\ -1/2 & 1/6 & -1 \end{pmatrix}$

while domains 1 and 2, 3 and 4, 5 and 6 are related by a 2-fold rotation axis  $\parallel [001]$  e.g.

$$\begin{pmatrix} -1 & 0 & 0 \\ 0 & -1 & 0 \\ 2/3 & 0 & 1 \end{pmatrix}$$

The structures solution and refinement were carried out applying SHELXTL 5.1 (Bruker AXS) [24]. The atom position were refined using the HKLF 4 file format while for the final refinement the HKLF 5 file type was used taking all domains into account. The data in HKLF 5 format were created by integrating the domain showing the highest intensities in the reflection pattern and followed by checking each reflection for potential overlap with the other domains. By this procedure a total of 1933 reflections have been processed while 116 reflections have contributions of all six domains, 165 reflections have contribution of domain 1, 3 and 5, and 157 reflections have contributions of 1 and 2. The final refinement results in volume contributions of 40.6 (0.1), 2.4 (0.1), 42.2 (0.1), 2.8 (0.1), 12.0 (0.1), and 0.0 (0.1). Further details of the data collection and structure refinement are given in Table 1. All crystals investigated were systematically twinned. For instance a second crystal investigated showed volume contributions of 35.2 (0.2), 5.1 (0.2), 37.5 (0.2), 6.4 (0.2), 15.3 (0.1), and 0.5 (0.2).

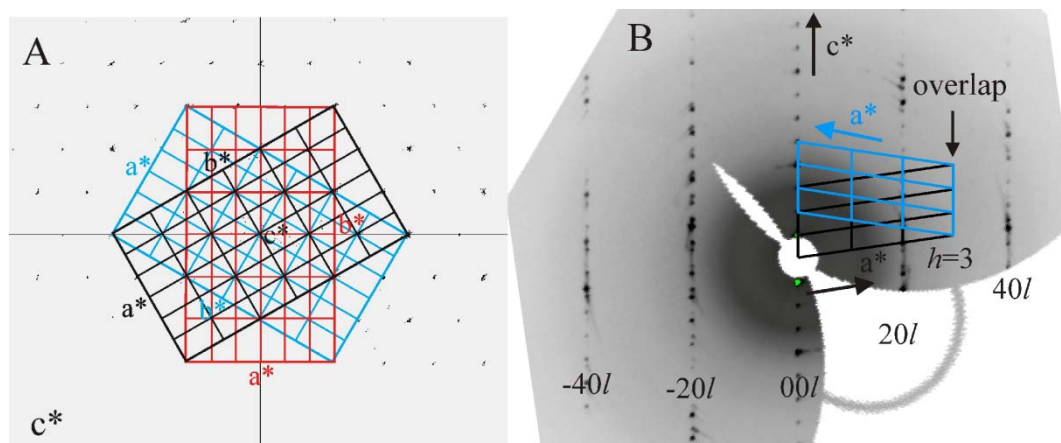


**Fig. 1** A; Cut's through the reconstructed reciprocal space. (A) *hk0* showing the three domains 1 (blue), 3 (red), and 5 (black) that are related by the 3-fold rotation axis  $\parallel [001]$ . (B) *h0l* exemplarily showing how each of these three domains is related to a corresponding domain by a 2-fold rotation axis  $\parallel [001]$ , where the 2-fold twin domains is completely overlap with  $h=3n$ .

The composition of the synthetic Na<sub>4</sub>-F-mica was determined by (WDX) with acceleration voltage 15 kV, and a beam spot diameter of 1  $\mu\text{m}$  on a Joel JXA 8200 spectrometer, which was calibrated against certified mineral standards (Si - andradite  $\text{Ca}_3\text{Fe}_2\text{Si}_3\text{O}_{12}$ , O -  $\text{SiO}_2$ , F - fluorite  $\text{CaF}_2$ , Na - albite  $\text{NaAlSi}_3\text{O}_8$ , Al- Spinel  $\text{MgAl}_2\text{O}_4$ , Mg- synthetic Enstatit  $\text{Mg}_2[\text{Si}_2\text{O}_6]$ ). The counting time was 20 s at the peak position and 10 s on each side of the peak position. The very same crystal that has been used for structure refinement (Table 1) was fixed in resin on a glass slide and coated with carbon. The composition of the synthetic layered silicate was normalized to  $\text{Mg}_6$  per formula unit. Additionally, the  $\text{Na}^+$ ,  $\text{Mg}^{2+}$ , and  $\text{Al}^{3+}$  content of the bulk material was confirmed independently by inductively coupled plasma atomic emission spectroscopy (ICP-AES). Two samples of about 20 mg of dry synthetic Na<sub>4</sub>-F-mica were weighed into a clean Teflon flask of 150 mL volume. After addition of 1.5 mL 30 wt. % HCl (Merck), 0.5 mL of 85 wt. %  $\text{H}_3\text{PO}_4$  (Merck), 0.5 mL 65 wt. %  $\text{HNO}_3$  (Merck) and 1 mL of 48 wt. %  $\text{HBF}_4$  (Merck) the sample was digested in a MLS 1200 Mega microwave digestion apparatus for 6.5 min and heated at 600W (MLS GmbH, Mikrowellen-Labor-Systeme, Leutkirch, Germany). The closed sample container was cooled to room temperature and the clear solution was diluted to 100 mL in a volumetric flask and analyzed.

The water content of one-layer hydrated of Na<sub>4</sub>-F-mica was determined gravimetrically. Approximately 100 mg of equilibrated one-layer hydrated samples were dried at 250  $^\circ\text{C}$  at reduced pressure ( $2.0 \cdot 10^{-2}$  mbar) for 24 h. The weight loss during drying was attributed to

interlayer water. The cation exchange capacity (CEC) of synthetic Na<sub>4</sub>-F-mica was determined by the potassium chloride method. A 0.2 g of synthetic Na<sub>4</sub>-F-mica was suspended in 25 mL of distilled water and 1 M potassium chloride solution was added. The mixture was shaken for 48h and then centrifuged, and the supernatant solution was collected. To ensure complete exchange of sodium, the cation exchange was repeated four more times. The Na<sup>+</sup> content of the collected solutions was determined by Atomic Absorption Spectroscopy (AAS). SEM pictures are taken on a LEO 1530 FE-SEM at an operation voltage of 2 kV using in-lens detection modes.

### 3. Results and Discussions

#### 3.1. Synthesis of Na<sub>4</sub>-F-mica

Fig. 2 shows the PXRD pattern of zero-, and one-layer hydrate of synthetic Na<sub>4</sub>-F-mica. Two crystalline impurities could be identified: magnesium orthosilicate (Mg<sub>2</sub>SiO<sub>4</sub>) [25] and sodium aluminum silicate Na<sub>6</sub>Al<sub>4</sub>Si<sub>4</sub>O<sub>17</sub> [26]. Indexing of both diffractograms was straight forward and gave the following unit cell parameters:  $a=5.3322 \text{ \AA}$ ,  $b=9.2477 \text{ \AA}$ ,  $c=10.0621 \text{ \AA}$ ,  $\beta=99.717^\circ$  and  $a=5.3248 \text{ \AA}$ ,  $b=9.2688 \text{ \AA}$ ,  $c=12.1597 \text{ \AA}$ ,  $\beta=99.054^\circ$  for zero-, and one-layer hydrate, respectively. The parameters are in close agreement with what had been published by Gregorkiewitz and Rausellcolom [18]:  $a=5.34 \text{ \AA}$ ,  $b=9.24 \text{ \AA}$ ,  $c=9.97 \text{ \AA}$ ,  $\beta=100.3^\circ$  and  $a=5.35 \text{ \AA}$ ,  $b=9.24 \text{ \AA}$ ,  $c=12.32 \text{ \AA}$ ,  $\beta=98.5$  for zero-, and one-layer hydrate, respectively.

Good quality crystals with little diffuse scattering could quite easily be found for the one-layer hydrate allowing for structure refinements. Screening several “single crystals” of the zero-layer hydrate, however, showed massive diffuse scattering suggesting that extended planar disorder might have prevented successful structure refinements, much similar to what has been reported by Gregorkiewitz and Rausellcolom [18]. Obviously the stacking order could be improved significantly with hydration suggesting that the interlayer water helped to bridge the interlayer space in a more defined way and thus fixing the phase of adjacent 2:1-silicate layers. Despite the planar defects, the zero-layer hydrate of Na<sub>4</sub>-F-mica nevertheless showed uniform intracrystalline reactivity. At a relative humidity of 43 % a rational 00l series with a basal spacing of  $d_{001}=12.1 \text{ \AA}$  was observed. Neither was residual intensity at the positions of the zero-layer hydrate nor was any signs of random interstratifications found indicating a uniform one-layer hydrate of synthetic Na<sub>4</sub>-F-mica. Further hydration steps of synthetic Na<sub>4</sub>-F-mica were not accessible (see discussion in crystal structure part).

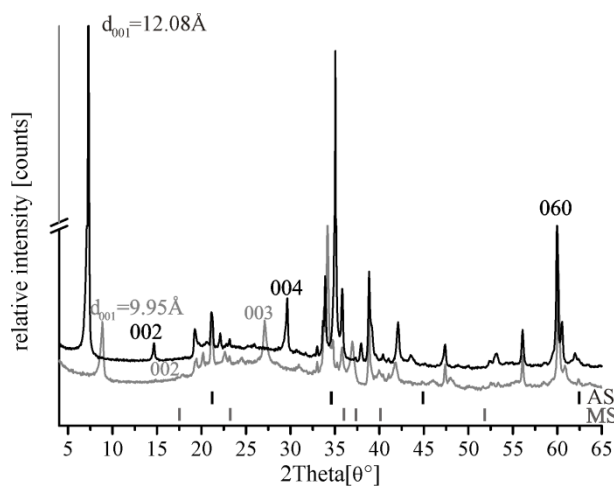


**Fig. 2** PXR D of zero- and one- layer hydrate of Na<sub>4</sub>-F-mica. The one-layer water hydrate was measured at a relative humidity of 43%. Ticks indicate the impurity phases: AS: Sodium aluminum silicate Na<sub>6</sub>Al<sub>4</sub>Si<sub>4</sub>O<sub>17</sub>, MS: Magnesium silicate Mg<sub>2</sub>SiO<sub>4</sub>.

The average chemical composition of synthetic Na<sub>4</sub>-F-mica as determined by WDX for three different crystal [Na<sub>3.3</sub>]<sup>inter</sup>[Mg<sub>6</sub>]<sup>oct</sup>[Si<sub>4.7</sub>Al<sub>3.3</sub>]<sup>tet</sup>O<sub>20</sub>F<sub>4</sub>. Using ICP-AES the ratio of Na<sup>+</sup> : Al<sup>3+</sup> : Mg<sup>2+</sup> was found to be 3.3 : 6 : 3.3. The CEC of synthetic Na<sub>4</sub>-F-mica as determined via Na<sup>+</sup> in the supernatant after K<sup>+</sup> exchange was 2.40 meq.g<sup>-1</sup>. SEM micrographs showed that melt synthesis of Na<sub>4</sub>-F-mica not only yielded highly crystalline but also coarse grained material (Fig. 3), contrary to established synthesis routes that reported particle sizes too small to pick single crystals (~5 μm) [5,6]. The water content as determined gravimetrically was H<sub>2</sub>O:Na= 1.6, a ratio in close agreement with what has been reported by Kodama et. al. (1.5) [27]. Furthermore, this ratio was confirmed by the occupation factors obtained in the structure refinement (see discussion below).

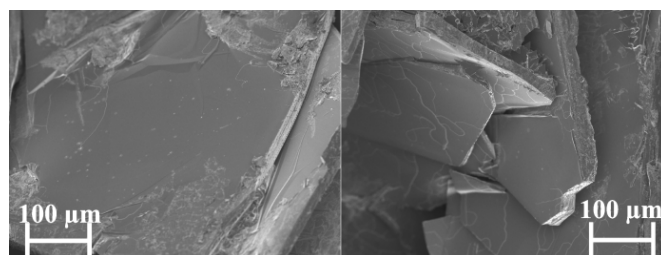


**Fig. 3** SEM images of synthetic Na<sub>4</sub>-F-mica.

### 3.2. Single crystal structure refinement

Crystallographic data, experimental details of the structure refinement, and details of the single crystal structure refinement of one-layer water hydrate of synthetic Na<sub>4</sub>-F-mica are included in Table 1. Although some diffuse intensity was visible in reciprocal space, a

standard single crystal refinement program was applied that is not capable of handling diffuse (non-Bragg) scattering. Diffuse scattering had to be ignored but refinement was performed against the complete data set.

A comprehensive description of the structure of hydrated phases of layered silicates has to deliver information about the coordination of interlayer cations, the relative position/phase relationship of adjacent 2:1-layer (interlayer displacement) [28], and the “interaction” pattern between the interlayer species (cations and water) and the basal oxygen atoms comprising the interlayer. For Na<sub>4</sub>-F-mica initial structural models cannot be deduced from known mica structure because it is not obvious where the additional interlayer cations would fit in. Certainly, the extra interlayer cations will have a crucial influence the distortion of tetrahedral sheet of sodium brittle mica and relative position of upper and lower tetrahedral sheet.

To reduce the complexity of structure solution and to increase the precision of the structure refinement, we sought to synthesize a well ordered Na<sub>4</sub>-F-mica. Furthermore, the synthesis was optimized in order to yield large crystals Fig. 3 by applying high melting procedures and decreasing the cooling rate (as described in experimental section). Fortunately, for this synthetic Na<sub>4</sub>-F-mica stacking disorder and thus diffuse scattering are indeed reduced to a level that allows a full crystal structure refinement applying all *hkl* reflections delivering full structural details for the one-layer hydrate. Although the structure could be solved using the diffraction of the data of the main a stable and reliable refinement was possible only after having identified all twins triggered by the high pseudo symmetry of the interlayer.

Gregorkiewitz and Rausellcolom [18] had already noticed that absences are consistent with the assumption of a twin of two individuals with a 1M cell and rotation of 120° between them. They, however, missed the second type of twinning operations based on the 2-fold rotation axis. Moreover, they noticed that Laue symmetry  $2/m$  is violated which they interpreted reduced symmetry (1Tc) instead of the monoclinic polytype (1M). As Löwenstein's rule would require an at least locally ordered distribution for an approximately 1:1 ratio of Al : Si, we reduced the symmetry to  $C 2$  applying such an ordered model. Taking into account Löwenstein's principle of avoidance of Al-O-Al geometries, the Si<sup>4+</sup> and Al<sup>3+</sup> substitution in the tetrahedral sheet was therefore assumed to be arranged in an ordered manner allowing each Al<sup>3+</sup>-tetrahedral to be surrounded by three Si<sup>4+</sup>-tetrahedral and vice versa when the Si : Al ratio is 1:1 [29,30]. An ordered arrangement would be expected to be corroborated by Si-O being significantly shorter than Al-O distances (1.63 and 1.78 Å, respectively). We see smaller differences in these distances in our refinement which we

attributed to be related to twinning because twin operations interrelate  $\text{Al}^{3+}$  and  $\text{Si}^{4+}$  sites. Additionally, the real composition showed a  $\text{Al}^{3+} : \text{Si}^{4+}$ -ratio  $< 1 : 1$  end hence some  $\text{Si}^{4+}$  must reside on  $\text{Al}^{3+}$  -sites. Alternatively, the ordering might be long range and the X-ray beam might be averaging over the ordered domains. The average observed Si-O and Al-O distance were 1.67 and 1.72 Å, respectively and clearly support an ordered tetrahedral sheet.

Taking into account all six twin domains the refinement of the one-layer hydrate of Na4-F-mica was straight forward. Atomic displacement parameters (ADP) of all heavy atoms including the interlayer cations and the oxygen atoms of interlayer water could even be refined anisotropically. This underlines the good quality of the data sets. Occupancies of interlayer cations and water were freely refined. The water content as obtained by the refinement is in good agreed with values determined by gravimetric analysis. From the occupation factors obtained in the refinement the following compositions could be calculated:

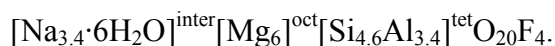




**Table 1.** Crystallographic data and experimental details of the structure refinement of one-layer water hydrate of synthetic Na<sub>4</sub>-F-mica.

Crystal data	
	Formula unit [Na <sub>3.4</sub> ] <sup>inter</sup> [Mg <sub>6</sub> ] <sup>oct</sup> [Si <sub>4.6</sub> Al <sub>3.4</sub> ] <sup>tet</sup> O <sub>20</sub> F <sub>4</sub> ·6H <sub>2</sub> O
	Formula weight (anhydrous) = 822.54 g/mol
	MoK $\alpha$ radiation ( $\lambda = 0.71073 \text{ \AA}$ ) graphite monochromator
	T = 173 K
	a = 5.3520(11) $\text{\AA}$
	b = 9.2700(19) $\text{\AA}$
	c = 12.145(2) $\text{\AA}$
	$\beta = 98.35(3)^\circ$
	V = 596.1(2) $\text{\AA}^3$
	Monoclinic. C2 (No. 5)
	Z = 2
	Plate colorless
	0.2 mm x 0.2 mm x 0.05 mm
Data collection	
	STOE IPDS I diffractometer
	Completeness of 2theta= 0.89
	1825 measured reflections
	720 merged reflections
	307 reflections with $I > 2\sigma(I)$
	R <sub>int</sub> = 0.087
	$\theta_{\text{max}} = 25.33^\circ$
	$\theta_{\text{min}} = 3.39^\circ$
	$h = -6 \rightarrow 6$
	$k = -11 \rightarrow 10$
	$l = -14 \rightarrow 14$
Refinement SHELXTL	
	Refinement on $F^2$
	$R[F^2 > 2\sigma(F^2)] = 0.083$
	$wR(F^2) = 0.219$
	S = 1.31
	$w = 1/[\sigma^2(F_o^2) + (0.10000P)^2 + 10.000P]$ where $P = (F_o^2 + 2 F_c^2)/3$
	$\Delta \rho_{\text{max}} = 1.691 \text{ e\AA}^{-3}$
	$\Delta \rho_{\text{min}} = -1.140 \text{ e\AA}^{-3}$
	117 refined parameters

### 3.3. Structure of one-layer hydrate of Na<sub>4</sub>-F-mica

The structure of one-layer hydrate Na<sub>4</sub>-F-mica projected along [100] is shown in Fig. 4. As suggested by Gregorkiewitz and Rausellcolom [18], the interlayer water was found to be located in the middle of the interlayer space. Sodium interlayer cations were displaced from the center of the interlayer space towards the lower and upper tetrahedral sheet and on each side were located above the center of the distorted hexagonal cavity (Fig. 6).

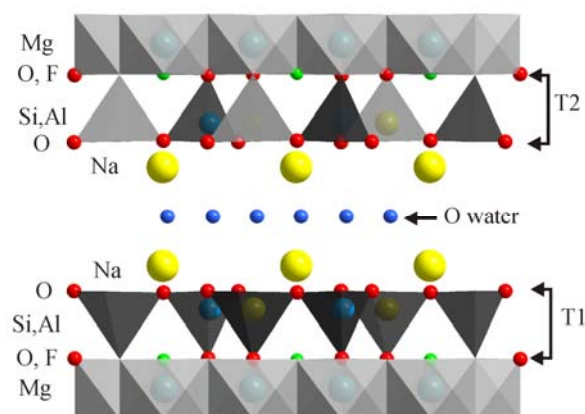


**Fig. 4** Refined structure of one-layer hydrate of Na<sub>4</sub>-F-mica viewed along [100].

The relative position of the lower and the upper tetrahedral sheet was, however, crucially different from the structure proposed by Gregorkiewitz and Rausellcolom (compare Fig. 5 with Fig. 7 in ref. [18]). This is of course not surprising because the interlayer displacement cannot be determined reliably if massive disorder is present. Because of the limited quality of the crystals available to Gregorkiewitz and Rausellcolom the suggested interlayer displacement is erroneous. Unfortunately, this also affects details of the coordination of interlayer cations, and the “interaction” pattern between the interlayer species (cations and water) and the basal oxygen atoms comprising the interlayer. While Gregorkiewitz and Rausellcolom proposed the displacement to be  $+b/3$ , we found the lower tetrahedral sheet in relation to the upper tetrahedral sheet being shifted along [100] by approximately  $+a/2$ . As pointed out by Gregorkiewitz and Rausellcolom, having to accommodate 4 interlayer cations per unit cell excludes a face-to-face stacking of the hexagonal cavities of the tetrahedral sheets. Rather, adjacent layers must be displaced and consequently each hexagonal cavity becomes an independent site large enough to host a relatively small Na<sup>+</sup>. While both, shifts of  $+b/3$  and  $+a/2$  create four Na<sup>+</sup> sites per unit cell, the coordination environment created for the interlayer cation will be different.

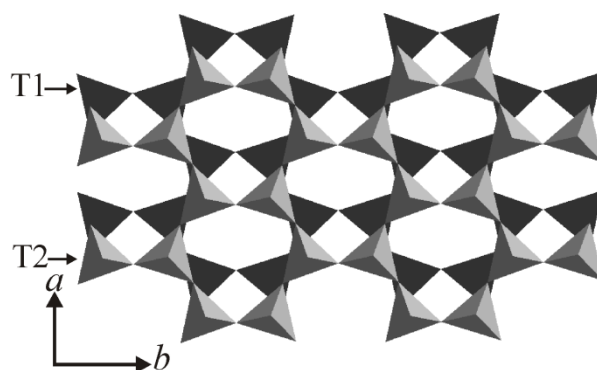


**Fig. 5** Relative position of upper and lower tetrahedral sheet comprising the interlayer space as viewed along  $c^*$  (please compare **Fig. 4** for assignment of T1 and T2).

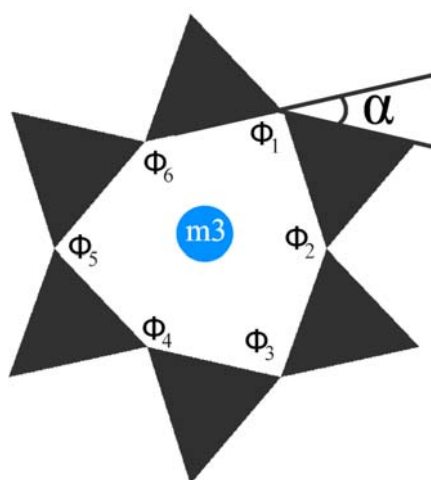


**Fig. 6** Structure of the hexagonal cavity of six connected tetrahedra showing the location of the  $\text{Na}^+$  interlayer cation (m3). The tetrahedron rotation angle ( $\alpha$ ) was calculated applying the

$$\text{equation: } \alpha = \frac{1}{6} \sum_{i=1}^6 |120^\circ - \Phi_i|, \alpha = 24^\circ.$$

As previously observed for non-swollen brittle mica, the hexagonal cavity of Na4-F-mica was found to be severely distorted (Fig. 6). This distortion of the hexagonal cavity is related to the pronounced misfit between the octahedral and the tetrahedral sheet and also reflects the field strength of the interlayer cation [31]. The  $\alpha$  angle of tetrahedron rotation was calculated to be  $\alpha \sim 24^\circ$ , while the model suggested by Gregorkiewitz and Rausellcolom gives only  $\alpha = 14^\circ$  [18]. The sodium cations are located in the m3 position above the center of the distorted hexagonal cavity.

The sodium interlayer cations are coordinated to three basal oxygen atoms of the tetrahedral sheet ( $\text{O}_b$ ) on one side and on the other side they are coordinated to three oxygen atoms ( $\text{O}_w$ ) of intercalated water. The distance between  $\text{Na}^+$  and the three coordinated inner basal oxygen atoms of the tetrahedral sheet is  $\sim 2.50 \text{ \AA}$ , while due to the distortion the remaining three

oxygen atoms of the same hexagonal cavity are significantly further away ( $\sim 3.2$  Å). The distance between  $\text{Na}^+$  and the three oxygen atoms of water is  $\sim 2.57$  Å, where the distance of  $\text{O}_w\text{-O}_w$  is 3.1 Å (Fig. 7A). The interlayer  $\text{Na}^+$  are thus coordinated by three planes of oxygen atoms, basal oxygens of lower and upper tetrahedral sheet and the interlayer water. Two sheets of isolated  $[\text{Na}(\text{O}_b)_3(\text{O}_w)_3]$  octahedra (blue and yellow in Fig. 7B) at different z-values are created, which are connected by shared water molecules. Blue and yellow each share one edge and one corner which gives a ratio of sodium : water of 1:1.5 which in turn corresponds to 5.1 water molecules per unit cell of Na4-F-mica (the sodium content is 3.4 mole per unit cell). This is in good agreement with the water content as determined gravimetrically (5.28 mole water per unit cell). Although the interlayer displacement is different the mixed  $\text{O}_w/\text{O}_b$  coordination of the interlayer cation in some respects resembles motifs found for the one-layer hydrate of a highly charged Na-hectorite [32]. While these highly charged hectorites like vermiculites readily hydrate to the two-layer hydrate state at higher r.h., this was not observed for synthetic Na4-F-mica. This can certainly be related to the much higher Coulomb attraction. But it might also be related to crystal chemically reasons. In the two-layer hydrate of hectorites and vermiculites, the sodium cations in the central plane of the interlayer space. If one would have to pack four sodium cations per unit cell into one plane, the  $\text{Na}^+ - \text{Na}^+$  distance would be much too short (3 Å).

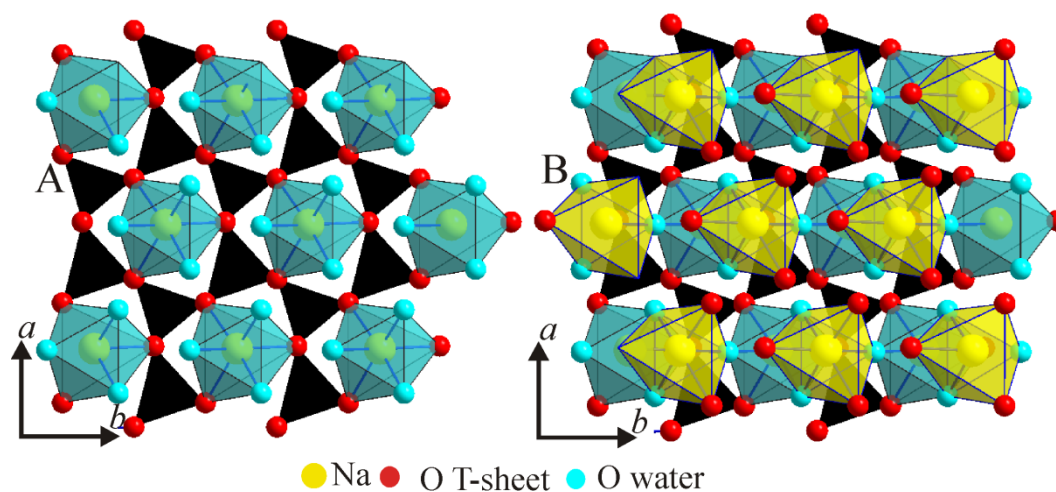


**Fig. 7** Position of interlayer sodium cations, oxygens of the interlayer water and oxygens of the tetrahedral sheet along projection [001]. A) the lower octahedral sheet of  $[\text{Na}(\text{O}_b)_3(\text{O}_w)_3]$  (cyan color) and B) the lower and the upper octahedral sheet of  $[\text{Na}(\text{O}_b)_3(\text{O}_w)_3]$  (yellow color).

### 3.4. Stacking faults in one-layer hydrate Na<sub>4</sub>-F-mica

As has been pointed out in the literature, stacking faults may significantly vary properties and in consequence applications of clays [33,34]. Clearly, scanning the reciprocal lattice space of the one-layer hydrate of Na<sub>4</sub>-F-mica revealed that the structure has some stacking faults on top of twinning. As observed by Gregorkiewitz and Rausellcolom [18] reflections with  $k=3n$  are sharp whereas all other  $hk$ -bands showed some diffuse intensity parallel to  $c^*$  (Fig. 8). This pattern in reciprocal space is well known with micas and indicates a certain degree of  $\pm b/3$  stacking disorder in the one-layer hydrate of Na<sub>4</sub>-F-mica. As shown in Fig. 8, shifts of the upper layer by  $\pm b/3$  create the same environment for the interlayer cations suggesting that random shifts of that type will generate energetically degenerate modes of stacking. This degeneracy in turn is responsible for the stacking disorder observed. Moreover, since only some  $hk$ -rods are affected by the disorder while others only show sharp Bragg reflections, suggesting that the disorder patterns are commensurate with the lattice, even the domains of one-layer-hydrate of Na<sub>4</sub>-F-mica that suffer of disorder are not turbostratically disordered but still have a semi-ordered structure. The unusual high pseudo-symmetry reflected in several degenerate alternative stackings generating similar coordination of interlayer species that give rise to twinning and disorder is “probing the limits of the concept “crystal” as it was recently stated in a paper by Gerisch and Ruck [35].

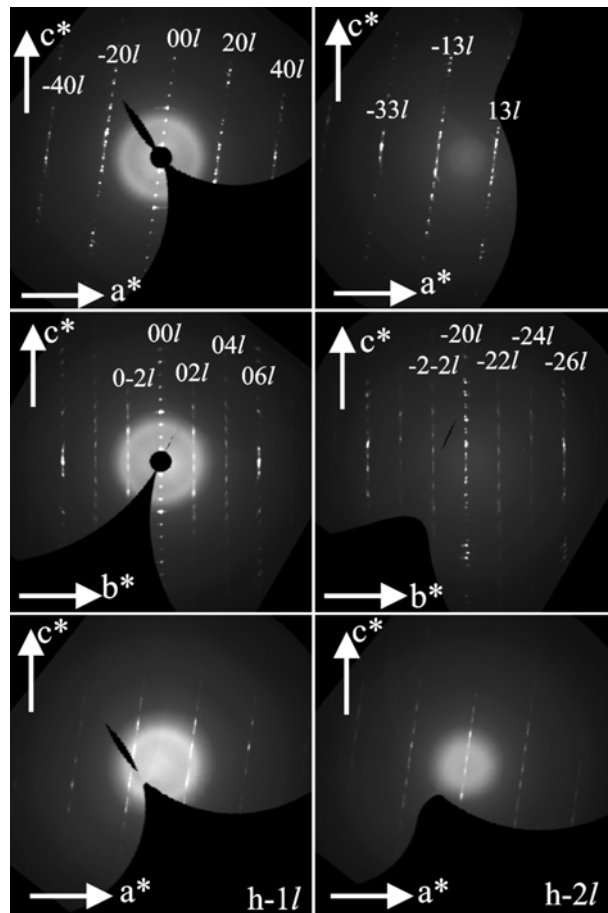


**Fig. 8** Selected reciprocal lattice planes of the one-layer hydrate of synthetic Na<sub>4</sub>-F-mica created using the X-area software from STOE.

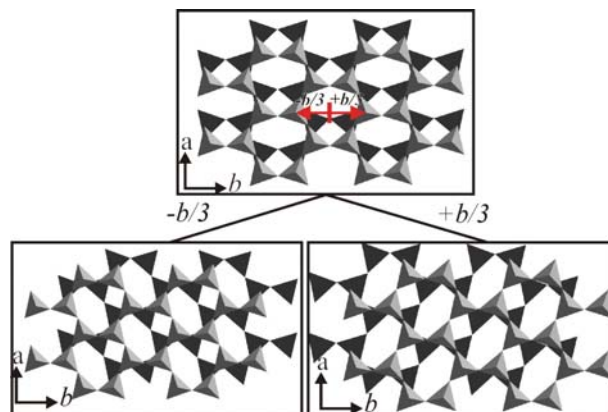


**Fig.9** Illustration of energetically degenerate stacking modes for semi-ordered one-layer hydrate of Na<sub>4</sub>-F-mica explaining the observed diffuse scattering.  $\pm b/3$  shifts of the upper tetrahedral sheet (grey) relative to lower tetrahedral sheet (black) provide a similar environment for interlayer species.

#### 4. Conclusion

Na4-F-mica with the ideal composition  $[\text{Na}_4]^{\text{inter}}[\text{Mg}_6]^{\text{oct}}[\text{Si}_4\text{Al}_4]^{\text{tet}}\text{O}_{20}\text{F}_4$  was synthesized in a gas tight crucible via melt synthesis and the crystal structure of the one-layer hydrate was refined by single crystal data. The applied procedure yielded highly crystalline material and uniform intercrystalline reactivity as synthetic Na4-F-mica is completely hydrated with one layer of water. Structurally the most puzzling feature of Na4-F-mica is its high layer charge which must be compensated by ideally four interlayer cations per unit cell. Consequently, the structure must differ from the classical face-to-face arrangement of hexagonal cavities found in ordinary micas and brittle micas. The four sites for interlayer cations are rather generated by shifting the lower tetrahedral sheet in relation to the upper tetrahedral sheet along [100] by approximately  $+a/2$ . The interlayer water resides at the central plane of the interlayer space, while interlayer cations are arranged in two planes displaced from the middle of the interlayer space toward the upper and the lower tetrahedral sheet. The oxygen atoms of intercalated water bridge the upper and lower interlayer sodium cations. The high pseudo-symmetry of the distorted hexagonal cavity explains the systematic twinning of the crystals.

#### Acknowledgments

The authors thank the Bayerisches Geoinstitut, Bayreuth, Germany, for the WDX measurement. This work was supported financially by the graduate school ‘Structure, Reactivity and Properties of Oxide Materials’ within the Elitenetzwerk Bayern, the Deutsche Forschungsgemeinschaft (SFB 840), and the University of Aleppo.

References

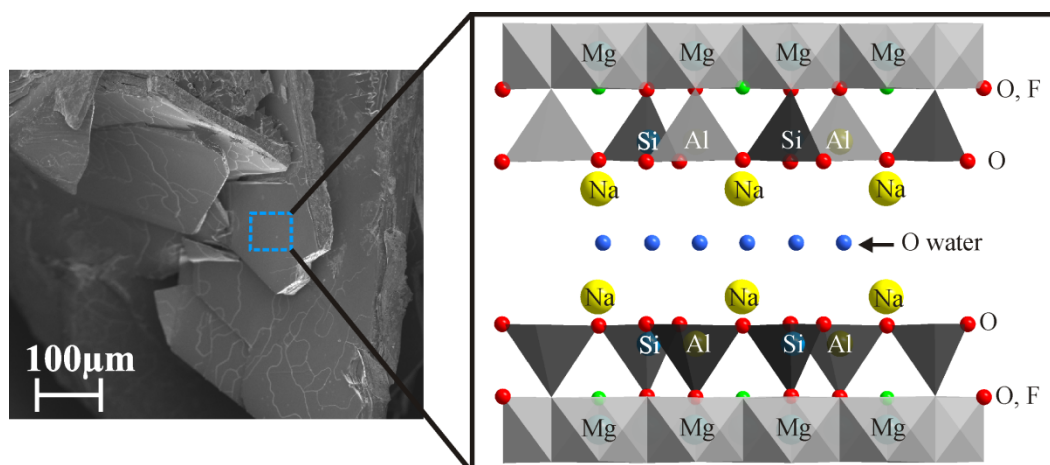
- [1] M.W. Möller, U.A. Handge, D.A. Kunz, T. Lunkenbein, V. Altstadt and J. Breu, *Acs Nano* 4 (2010) 717-724.
- [2] J. Breu, W. Seidl, A.J. Stoll, K.G. Lange and T.U. Probst, *Chem. Mater.* 13 (2001) 4213-4220.
- [3] H. Kalo, M.W. Möller, M. Ziadeh, D. Dolej and J. Breu, *Appl. Clay Sci.* 48 (2010) 39-45.
- [4] T. Kodama, Y. Harada, M. Ueda, K. Shimizu, K. Shuto, S. Komarneni, W. Hoffbauer and H. Schneider, *J. Mater. Chem.* 11 (2001) 1222-1227.
- [5] M.D. Alba, M.A. Castro, M. Naranjo, M.M. Orta, E. Pavon and M.C. Pazos, *J. Phys. Chem. C* 115 (2011) 20084-20090.
- [6] M. Park, D.H. Lee, C.L. Choi, S.S. Kim, K.S. Kim and J. Choi, *Chem. Mater.* 14 (2002) 2582-2589.
- [7] M.D. Alba, M.A. Castro, M. Naranjo and E. Pavon, *Chem. Mater.* 18 (2006) 2867-2872.
- [8] S. Taruta, T. Kaga, T. Yamaguchi and K. Kitajima, *Mat. Sci. Eng. B* 173 (2010) 271-274.
- [9] S. Komarneni, R. Ravella and M. Park, *J. Mater. Chem.* 15 (2005) 4241-4245.
- [10] H. Bedeleian, A. Maicaneanu, S. Burca and M. Stanca, *Clay Miner.* 44 (2009) 487-495.
- [11] T. Kodama and S. Komarneni, *J. Mater. Chem.* 9 (1999) 533-539.
- [12] W.J. Paulus, S. Komarneni and R. Roy, *Nature* 357 (1992) 571-573.
- [13] T. Tatsuya and S. Komarneni, *J. Mater. Chem.* 9 (1999) 2475-2479.
- [14] M.F. Brigatti, S. Colonna, D. Malferrari, L. Medici and L. Poppi, *Appl. Clay Sci.* 28 (2005) 1-8.
- [15] Y.D. Noh and S. Komarneni, *Environ. Sci. Technol.* 45 (2011) 6954-6960.
- [16] T. Kodama, S. Komarneni, W. Hoffbauer and H. Schneider, *J. Mater. Chem.* 10 (2000) 1649-1653.



- [17] K. Shimizu, Y. Nakamuro, R. Yamanaka, T. Hatamachi and T. Kodama, *Microporous and Mesoporous Mater.* 95 (2006) 135-140.
- [18] M. Gregorkiewitz and J.A. Rausellcolom, *Amer. Mineral.* 72 (1987) 515-527.
- [19] M. Stöcker, L. Seyfarth, D. Hirsemann, J. Senker and J. Breu, *Appl. Clay Sci.* 48 (2010) 146-153.
- [20] W. Seidl and J. Breu, *Z. Kristallogr.* 220 (2005) 169-176.
- [21] A. Baumgartner, K. Sattler, J. Thun and J. Breu, *Angew. Chem. Int. Ed.* 47 (2008) 1640-1644.
- [22] K. Kitajima, F. Koyama and N. Takusagawa, *Bull. Chem. Soc. Jpn.* 58 (1985) 1325-1326.
- [23] J. Breu, W. Seidl, A.J. Stoll, K.G. Lange and T.U. Probst, *Chem. Mater.* 13 (2001) 4213-4220.
- [24] G. Sheldrick, *Acta Cryst. A* 64 (2008) 112-122.
- [25] W.H. Baur, *Amer. Mineral.* 57 (1972) 709-&.
- [26] W. Borchert and K. Jürgen, *Contrib. Mineral. Petr.* 1 (1947) 17-30.
- [27] T. Kodama, M. Ueda, Y. Nakamuro, K.i. Shimizu and S. Komarneni, *Langmuir* 20 (2004) 4920-4925.
- [28] S. Guggenheim, J.M. Adams, F. Bergaya, M.F. Brigatti, V.A. Drits, M.L.L. Formoso, E. Galan, T. Kogure, H. Stanjek and J.W. Stucki, *Clays Clay Miner.* 57 (2009) 134-135.
- [29] R. Langner, M. Fechtelkord, A. Garcia, E.J. Palin and J. Lopez-Solano, *Amer. Mineral.* 97 (2012) 341-352.
- [30] W. Löwenstein, *Amer. Mineral.* 39 (1954) 92-96.
- [31] M.F. Brigatti and S. Guggenheim, *Rev. Mineral. Geochem.* 46 (2002) 1-97.
- [32] H. Kalo, W. Milius, J. Breu, Single Crystal Structure Refinement of One- and Two-layer Hydrate of Sodium-Fluorohectorite, paper will published soon in RSC Advance.
- [33] A. Plancon, *Clay Miner.* 36 (2001) 1-14.
- [34] T. Kogure, J. Elzea-Kogel, C.T. Johnston and D.L. Bish, *Clays Clay Miner.* 58 (2010) 62-71.

[35] A. Gerisch and M. Ruck, *Z. Kristallogr.* 226 (2011) 613-618.

Graphical abstract:



Highlights:

- ▶ Melt synthesis yielded coarse grained sodium brittle mica which showed little disorder. ▶
- Sodium brittle mica hydrated completely to the state of one-layer hydrate. ▶
- Structure of one-layer hydrate of sodium brittle mica could therefore be determined and refined. ▶
- Arrangement of upper and lower tetrahedral sheet encompassing interlayer cation were clarified.

Hussein Kalo  
Köllstr. 5  
95447 Bayreuth  
Phone: 00499211612301  
Mobile:004917664131900  
[huseinkalo@gmail.com](mailto:husseinkalo@gmail.com)

**Personal Data**

Data of birth	04.06.1975
Place of birth	Aleppo\Syria
Family Status	Married
Nationality	Syrian

**Study**

03/ 2007 – present	PhD student at department of inorganic chemistry I –university of Bayreuth. Title: „ <i>Melt Synthesis, Structural, Characterization and Scaling of Swelling 2:1-Layer Silicate Materials</i> ”
05/2004 - 05/2006	Lecturer in Chemistry Department at the Faculty of Science and Civil Engineering – university of Aleppo
11/2001 - 12/2003	M.Sc. Applied chemistry – faculty of science – university of Aleppo Title of project: “manufacturing of Silica refractory from Syrian sand”
09/2001 - 06/2000	diploma in applied Chemistry – faculty of science – University of Aleppo
09/1996 - 06/2000	Bachelor in applied Chemistry – faculty of science – University of Aleppo
09/1995 - 06/1996	Syrian Baccalaureate , scientific section -Aleppo - Syria

**7. Publication List:**

**The following publications are enclosed in this PhD thesis:**

- 1- **Hussein Kalo**, Wolfgang Milius and Josef Breu, Single Crystal Structure Refinement of One- and Two-layer Hydrate of Sodium-Fluorohectorite. Journal of RSC Advance, DOI: 10.1039/C2RA20457F.
- 2- **Hussein Kalo**, Michael W. Möller, Mazen Ziadeh, David Dolejš and Josef Breu, Large scale melt-synthesis in an open crucible of Na-fluorohectorite with superb charge homogeneity and particle size. Applied Clay Science, 2010, 48, 1-2, 1-290.
- 3- **Hussein Kalo**, Michael W. Möller, Daniel A. Kunz and Josef Breu, How to Maximize the Aspect Ratio of Clay Nanoplatelets. Nanoscale, DOI: 10.1039/C2NR31322G.
- 4- **Hussein Kalo**, Wolfgang Milius, Michael Bräu and Josef Breu, Synthesis and single crystal structure of hydrate sodium brittle mica, Hussein Kalo, Manuscript submitted to Journal of Solid State Chemistry.
- 5- Möller, M.W., Lunkenbein, T., **Kalo, H.**, Schieder, M., Kunz, D.A. and Breu, J. (2010) Barrier Properties of Synthetic Clay with a Kilo-Aspect Ratio. Advanced Materials, **22**, 5245-5249.
- 6- Möller, M.W., Lunkenbein, T., **Kalo, H.**, Schieder, M., Kunz, D.A. and Breu, J. (2010) Kilo Aspect Ratio clay platelets. Zeitschrift für anorganische und allgemeine Chemie. 2010, 636, 2113.
- 7- Schütz, M.R., **Kalo, H.**, Lunkenbein, T., Breu, J. and Wilkie, C.A. (2011a) Intumescent-like behavior of polystyrene synthetic clay nanocomposites. Polymer, **52**, 3288-3294.
- 8- Schütz, M.R., **Kalo, H.**, Lunkenbein, T., Groschel, A.H., Muller, A.H.E., Wilkie, C.A. and Breu, J. (2011b) Shear stiff, surface modified, mica-like nanoplatelets: a novel filler for polymer nanocomposites. Journal of Materials Chemistry, **21**, 12110-12116.
- 9- Mazen Ziadeh, Bettina Chwalka, **Hussein Kalo**, Michael R. Schütz, Josef Breu, A Facile Approach for Producing High Aspect Ratio Fluorohectorite Nanoplatelets by Utilizing a Stirred Media Mill. Submit to Clay Minerals.
- 10- Markus M. Herling, **Hussein Kalo**, Sebastian Seibt, Rainer Schobert, Josef Breu, Tailoring the Pore Sizes of microporous pillared interlayered clays. Manuscript will submit to microporous and mesoporous materials.

## Publication List

---

### Patent:

- 1- WO/2010/034408A1, synthetic Phyllosilicates Not Capable of swelling for Polymer Phyllosilicate Nanocomposite. Nennemann Arno, Bahnmüller Stefan, Breu Josef, Möller Michael, **Kalo Hussein**.
- 2- WO/2011/089089A1, Method for producing Phyllosilicate Platelet having a High Aspect Ratio Breu Josef, Möller Michael, **Kalo Hussein**, Nennemann Arno.

**8. Erklärung**

Hiermit versichere ich, die vorliegende Arbeit selbstständig verfasst und keine anderen als die von mir angegebenen Quellen und Hilfsmittel benutzt zu haben.

Ferner erkläre ich, dass ich weder an der Universität Bayreuth, noch an einer anderen Hochschule versucht habe, eine Dissertation einzureichen, oder mich einer Promotionsprüfung zu unterziehen.

Bayreuth den, 8/10/2012

---

Hussein kalo